PhD PROCEEDINGS

ANNUAL ISSUES OF THE DOCTORAL SCHOOL

FACULTY OF INFORMATION TECHNOLOGY & BIONICS

2025

PhD PROCEEDINGS

ANNUAL ISSUES OF THE DOCTORAL SCHOOL

FACULTY OF INFORMATION TECHNOLOGY & BIONICS
PÁZMÁNY PÉTER CATHOLIC UNIVERSITY

PhD PROCEEDINGS

ANNUAL ISSUES OF THE DOCTORAL SCHOOL

FACULTY OF INFORMATION TECHNOLOGY & BIONICS

2025

PÁZMÁNY 1635 since

PÁZMÁNY UNIVERSITY *e*PRESS
BUDAPEST, 2025

HU ISSN 2064-7271

Kiadja a Pázmány Egyetem eKiadó
Budapest, 2025

Felelős kiadó
Rev. Mons. Dr. Kuminetz Géza
a Pázmány Péter Katolikus Egyetem rektora

Cover image by Ábel Petik: *High-resolution 3D mapping of cat visual cortex using functional ultrasound imaging. A, Illustration of the stimulation used for elevation retinotopy mapping. B, Visualization of the sagittal imaging planes. C, Multi-plane elevation retinotopy map. Colormap explanation shown in A. Shading based on response magnitude. Scale bars 2 mm. A: anterior, P: posterior D, Activation of the visual cortex in response to flickering checkerboards with increasing spatial frequencies. Voxels showing a significant increase in their activity are shaded in dark red. Lower right: plot of the number of significantly active voxels as a function of the spatial frequency of the checkerboard pattern. Scale bars 2 mm.*

Contents

Introduction

It is our pleasure to publish this Annual Proceedings again to demonstrate the genuine multidisciplinary research done at the Jedlik Laboratories by young talents working in the Roska Tamás Doctoral School of Sciences and Technology of the Faculty of Information Technology and Bionics at Pázmány Péter Catholic University. The scientific results of our PhD students outline the main recent research directions in which our faculty is engaged. We also appreciate the support of the supervisors and consultants, as well as that of the five collaborating National Research Laboratories of the Hungarian Research Network, Semmelweis University and the University of Pannonia. The collaborative work with the partner universities, especially Katolieke Universiteit Leuven, Politecnico di Torino, Technische Universität München, University of California at Berkeley, University of Notre Dame, Universidad de Sevilla, Università di Catania, Université de Bordeaux and Universidad Autónoma de Madrid is gratefully acknowledged.

We acknowledge the support of numerous institutes, organizations and companies:

- Hungarian Research Network (HUN-REN),
- National Research, Development and Innovation Office (NKFIH),
- Hungarian Academy of Sciences (MTA),
- EKÖP Programme, Ministry of Culture and Innovation, Hungarian Government,
- EKÖP-KDP Programme, Ministry of Culture and Innovation, Hungarian Government,
- Gedeon Richter Co.,
- NVIDIA Ltd.,
- Verizon Computer Vision Center of Excellence (CV CoE), Budapest,
- MorphoLogic Ltd., Budapest,
- AnaFocus Ltd., Seville,

and several other companies and individuals.

Needless to say, the resources and support of the Pázmány Péter Catholic University are gratefully acknowledged.

Budapest, June 2025.

GÁBOR PRÓSZÉKY
Chairman of the Board of the Doctoral School

GÁBOR SZEDERKÉNYI
Head of the Doctoral School

PROGRAM 1
BIONICS, BIO-INSPIRED WAVE COMPUTERS, NEUROMORPHIC MODELS

Heads: Tamás FREUND, Zsolt LIPOSITS, Sándor PONGOR

Detecting infant cries in noisy NICU recordings

Ákos ANTAL
(Supervisors: Péter FÖLDESY, Péter MIHAJLIK)
Pázmány Péter Catholic University, Faculty of Information Technology and Bionics
50/a Práter street, 1083 Budapest, Hungary
antal.akos@itk.ppke.hu

***Abstract*—Preterm infants primarily communicate their emotional and physiological states through crying, which serves as a critical indicator of pain. If left unaddressed, such pain may contribute to long-term health complications. Neonatal Intensive Care Units (NICUs) often experience staffing shortages, leading to delayed responses to infant cries. This paper investigates the potential of leveraging advanced technologies to detect infant cries in the NICU environment, and therefore reduce response times of medical staff. Recent breakthroughs in deep learning and self-supervised learning have revolutionized audio and speech representation, enabling extraction of rich features directly from raw audio signals. Analyzing infant cries presents a challenging yet promising application for these techniques.**

***Keywords*-cry detection, audio processing, preterm infant comfort**

I. Introduction

Preterm infants express their needs, emotions, and stress predominantly through crying, which is a primary signal of pain. Untreated pain in preterm infants can adversely affect their long-term health outcomes. In many Neonatal Intensive Care Units (NICUs), limited staffing often results in delayed responses to crying infants. To support research on the developmental impact of preterm pain and to enable quicker caregiver interventions, automated cry detection technology should be integrated into NICU monitoring systems, analogous to existing vital sign monitors.

Over the past decade, advances in deep learning and self-supervised training have transformed audio and speech representation learning [1], [2]. These methods allow machines to extract semantically meaningful features from raw audio, driving progress in speech recognition and healthcare diagnostics. Infant cry analysis is a particularly challenging domain where representation learning holds significant promise.

II. Methods

For this study, a subset of self-collected audio recordings was segmented and annotated using Praat software [3]. Prior to annotation, a spectral subtraction-based noise reduction filter was applied to enhance the clarity of infant crying sounds, facilitating more accurate labeling. Each audio segment was manually classified into one of three categories: *crying*, *intermediate*, or *background*. The *intermediate* class included infant vocalizations not clearly identifiable as crying, as well as ambiguous segments. Annotations were performed with millisecond-level precision to ensure fine temporal resolution.

Because background samples were more abundant, a subset of the CryCeleb2023 dataset [4], which contains relatively noise-free infant crying expiration sounds, was incorporated to balance the dataset. This study evaluates the effectiveness of pretrained self-supervised models for detecting cries in noisy NICU audio recordings.

Figure I illustrates the schematic of the cry detection setup. A Raspberry Pi microcomputer collects audio data from a MEMS microphone and transmits it to the dedicated cry detection system. An audio representation model extracts features from the signal, which are then fed into a classifier. The classifier outputs the probability that a given signal corresponds to an infant cry. These probabilities can be used to alert medical staff and to monitor crying episodes over extended periods.

References

[1] A. Baevski, H. Zhou, A. Mohamed, and M. Auli, "wav2vec 2.0: A framework for self-supervised learning of speech representations," *Advances in Neural Information Processing Systems*, vol. 2020-December, 6 2020.
[2] W. Hsu, B. Bolte, Y. H. Tsai, K. Lakhotia, R. Salakhutdinov, and A. Mohamed, "HuBERT: Self-supervised speech representation learning by masked prediction of hidden units," *CoRR*, vol. abs/2106.07447, 2021.
[3] P. Boersma and D. Weenink, "Praat: doing phonetics by computer [computer program]," 2025. Version 6.4.27, retrieved 27 January 2025.
[4] D. Budaghyan, C. C. Onu, A. Gorin, C. Subakan, and D. Precup, "CryCeleb: A speaker verification dataset based on infant cry sounds," *preprint arXiv:2305.00969*, 2023.

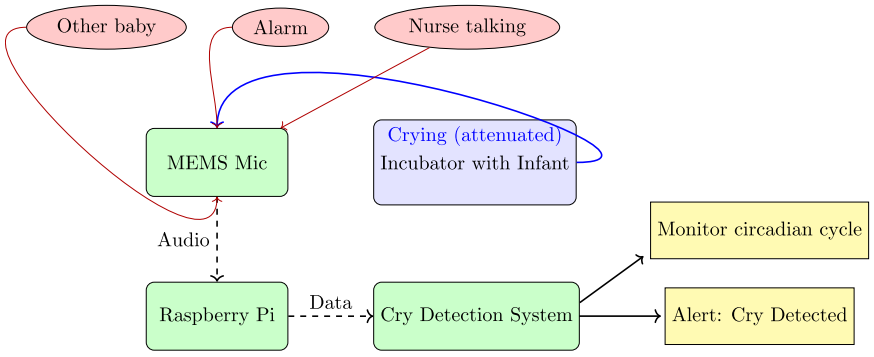

Fig. 1. Schematic of the cry detection setup in the NICU. A MEMS microphone connected to a Raspberry Pi records ambient sounds through the closed incubator. The audio stream includes infant cries and ambient hospital noise, used to train robust cry detection models.

Á. ANTAL, "Detecting infant cries in noisy NICU recordings" in *PhD Proceedings – Annual Issues of the Doctoral School, Faculty of Information Technology and Bionics, Pázmány Péter Catholic University – 2025.* G. Prószéky, G. Szederkényi Eds. Budapest: Pázmány University ePress, 2025, pp. 11–11.

Single-unit response latencies to infrared stimulation revealed via high-density electrophysiological recordings

Zsófia BALOGH-LANTOS
(Supervisors: Kristóf IVÁN, Ágoston Csaba HORVÁTH)
Pázmány Péter Catholic University, Faculty of Information Technology and Bionics
50/a Práter street, 1083 Budapest, Hungary
lantos.zsofia@itk.ppke.hu

***Abstract*—Infrared neural stimulation (INS) is a technique that uses temperature modulation of brain tissue to influence neuronal activity. However, the detailed biophysical mechanisms involved are still unclear. To investigate these effects, we examined the impact of pulsed and continuous-wave INS on cortical neurons in anesthetized rats using high-density laminar electrode arrays for recording. Our analysis revealed that INS elicits distinct, frequency- and mode-dependent temporal patterns in temperature dynamics and neuronal firing. These results highlight the critical role of timing in shaping neural responses.**

***Keywords*-infrared neuromodulation; electrophysiology; spike detection; temporal dynamics**

I. Introduction

The significant number of people affected by neurological disorders such as Parkinson's disease and epilepsy highlights the urgent need for effective treatments [1]. Infrared neural stimulation uses infrared (IR) light to raise the temperature of neural tissue locally, which can inhibit or trigger neuronal firing. Although various biophysical and molecular explanations for INS have been proposed, a thorough understanding requires integrating detailed theoretical frameworks with experimental evidence.

II. Methods

This study examined how tissue temperature influences neuronal activity in anesthetized rats. Neural responses to both pulsed and continuous infrared stimulation were recorded using a Neuropixels probe [2]. IR light was applied in alternating ON and OFF cycles to induce peak temperature elevations followed by return to baseline. Spike detection was performed with Kilosort [3], an automated algorithm that processes raw electrophysiological recordings to identify spikes and extract precise waveforms. Next, manual curation was carried out to isolate single-unit activity clusters. Data analysis was conducted using custom MATLAB scripts, which computed both average and relative firing rates of all identified neurons. To assess neuronal response timing across stimulation frequencies, we also measured rise and fall times.

Figure 1 illustrates firing rate changes from a representative animal. Each row corresponds to a different neuron, and the colors indicate varying levels of firing activity.

III. Results and discussion

Depending on the stimulation mode, infrared stimulation produced distinct neuronal effects: pulsed IR mainly increased firing rates, while continuous wave IR primarily led to suppression. The rise time of firing rate changes increased with higher stimulation frequencies, and it was notably longer during continuous wave (CW) stimulation than during pulsed stimulation. Conversely, fall times were generally shorter than rise times and remained consistent across frequencies. Importantly, no significant differences in temporal dynamics were observed between interneurons and principal cells, indicating consistent response timing across key cortical neuron types. Together, these results suggest that infrared stimulation can modulate cortical activity with temporal precision and reversibility, supporting its potential as a safe and effective neuromodulation strategy.

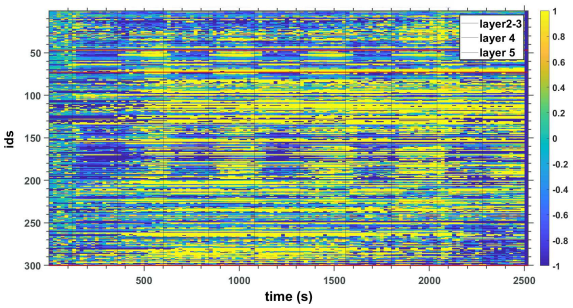

Fig. 1. Example color map showing firing rate changes across single units during infrared stimulation. Each row represents one neuron, with color indicating relative activity levels over time.

IV. Acknowledgement

The author is grateful for the funding of the National Development and Innovation Office (grants NKFIH FK 134403 and TKP2021-EGA-42), the support of the Hungarian Brain Research Program (grants NAP2022-I-8/2022 and NAP2022-I-2/2022), and support by the EKÖP-24-3 University Research Scholarship Program of the Ministry for Culture and Innovation from the source of the National Research, Development and Innovation Fund.

References

[1] Z. Fekete, Á. C. Horváth, and A. Zátonyi, "Infrared neuromodulation: a neuroengineering perspective," *Journal of Neural Engineering*, vol. 17, no. 5, p. 051003, 2020.

[2] N. A. Steinmetz, C. Aydin, A. Lebedeva, M. Okun, M. Pachitariu, M. Bauza, M. Beau, J. Bhagat, C. Böhm, M. Broux, *et al.*, "Neuropixels 2.0: A miniaturized high-density probe for stable, long-term brain recordings," *Science*, vol. 372, no. 6539, p. eabf4588, 2021.

[3] M. Pachitariu, N. A. Steinmetz, S. N. Kadir, M. Carandini, and K. D. Harris, "Fast and accurate spike sorting of high-channel count probes with kilosort," *Advances in neural information processing systems*, vol. 29, 2016.

Zs. BALOGH-LANTOS, "Single-unit response latencies to infrared stimulation revealed via high-density electrophysiological recordings" in *PhD Proceedings – Annual Issues of the Doctoral School, Faculty of Information Technology and Bionics, Pázmány Péter Catholic University – 2025.* G. Prószéky, G. Szederkényi Eds. Budapest: Pázmány University ePress, 2025, pp. 12–12.

Exploring diffusion-driven variations in extracellular vesicles from cancer patients using microfluidic systems

Gréta Lilla BÁNYAI
(Supervisor: Tamás Márton GARAY)
Pázmány Péter Catholic University, Faculty of Information Technology and Bionics
50/a Práter street, 1083 Budapest, Hungary
banyai.greta.lilla@itk.ppke.hu

***Abstract*—Extracellular vesicles (EVs) are nanoscale carriers of molecular information, emerging as promising cancer biomarkers. In this study, plasma-derived EVs from patients with pancreatic, prostate, and metastatic colon cancers were analyzed using a simplified microfluidic platform that profiles the diffusion behavior of fluorescently labeled EVs under laminar flow. While conventional assays (protein, lipid, size) revealed no major differences, flow-based fluorescence patterns showed distinct, cancer-type-specific diffusion profiles. Pancreatic and prostate EVs exhibited reproducible behaviors, whereas colon cancer samples were more heterogeneous. These findings demonstrate the potential of microfluidic diffusion profiling to detect subtle biophysical variations in EV populations not captured by standard methods.**

***Keywords*-extracellular vesicles, plasma-derived EVs, microfluidics, diffusion profiling**

I. Introduction

Extracellular vesicles are membrane-enclosed particles released by nearly all cell types. They carry bioactive cargo, including proteins, lipids, RNAs, and sometimes DNA, that reflects the origin and state of the parent cell, and influences vesicle properties such as density and size. EVs are often grouped by size into small (< 200 nm) and large (> 200 nm) categories [1].

Through their cargo, EVs mediate intercellular communication both locally and over long distances. In addition to acting on neighboring cells, they can enter circulation and influence remote tissues via the bloodstream or lymphatic system [2]. In cancer, tumor-derived EVs play roles in immune modulation, angiogenesis, and metastatic niche formation, supporting disease progression [3].

Microfluidics enables precise fluid handling under laminar flow due to low Reynolds numbers. In straight microchannels, EV displacement occurs primarily via diffusion, which depends on particle size, shape, and density [4]. Recent studies have demonstrated that even simple, diffusion-based microchannel designs can separate EVs label-free by exploiting these physical differences [5], providing a scalable and sensitive tool for analyzing EV heterogeneity.

II. Methods

Plasma EVs were isolated via differential centrifugation and size-exclusion chromatography (SEC). Protein and lipid contents were measured using Qubit and SPV assays, while particle size and concentration were determined by nanoparticle tracking analysis (NTA).

For microfluidic analysis, EVs were fluorescently labeled with Atto-488 NHS ester, purified via an additional SEC step, and introduced into a custom straight-channel PDMS device with three inlets. Fluorescence images were captured at multiple channel positions and processed with a custom MATLAB script to derive normalized diffusion profiles.

III. Results and conclusion

Bulk parameters, such as protein, lipid content, and particle size, did not differ significantly among EVs from pancreatic, prostate, or colon cancer patients. In contrast, microfluidic diffusion analysis revealed distinct, cancer-type-specific patterns. EVs from pancreatic and prostate cancer showed consistent, reproducible diffusion profiles. Colon cancer samples, however, exhibited marked heterogeneity, with profiles either resembling the other groups or appearing intermediate.

These findings suggest that diffusion profiling captures subtle biophysical differences among EV populations that traditional assays may miss. The variability observed in colon cancer may reflect not just tumor-derived vesicle traits but systemic physiological changes affecting EV biogenesis or processing. In contrast, the uniform profiles seen in pancreatic and prostate cancers likely indicate more consistent disease-associated systemic responses.

IV. Acknowledgements

This research was supported by the National Research, Development and Innovation Office grant TKP2021-EGA-42. The author of this study received support from the EKÖP-24-3-II-PPKE-129 grant.

References

[1] C. Théry, K. W. Witwer, E. Aikawa, M. J. Alcaraz, J. D. Anderson, R. Andriantsitohaina, A. Antoniou, T. Arab, F. Archer, G. K. Atkin-Smith, and et al., "Minimal information for studies of extracellular vesicles 2023 (MISEV2023): A position statement of the international society for extracellular vesicles and update of the MISEV2018 guidelines," *Journal of Extracellular Vesicles*, vol. 12, no. 2, p. e12404, 2023.

[2] G. Raposo and W. Stoorvogel, "Extracellular vesicles: Exosomes, microvesicles, and friends," *The Journal of Cell Biology*, vol. 200, no. 4, pp. 373–383, 2013.

[3] A. Becker, B. K. Thakur, J. M. Weiss, H. S. Kim, H. Peinado, and D. Lyden, "Extracellular vesicles in cancer: Cell-to-cell mediators of metastasis," *Cancer Cell*, vol. 30, no. 6, pp. 836–848, 2016.

[4] H. A. Stone, A. D. Stroock, and A. Ajdari, "Engineering flows in small devices: Microfluidics toward a lab-on-a-chip," *Annual Review of Fluid Mechanics*, vol. 36, pp. 381–411, 2004.

[5] Y. Meng, Y. Zhang, M. Bühler, S. Wang, M. Asghari, A. Stürchler, B. Mateescu, T. Weiss, S. Stavrakis, and A. J. deMello, "Direct isolation of small extracellular vesicles from human blood using viscoelastic microfluidics," *Science Advances*, vol. 9, no. 40, p. eadi5296, 2023.

G. BÁNYAI, "Exploring diffusion-driven variations in extracellular vesicles from cancer patients using microfluidic systems" in *PhD Proceedings – Annual Issues of the Doctoral School, Faculty of Information Technology and Bionics, Pázmány Péter Catholic University – 2025.* G. Prószéky, G. Szederkényi Eds. Budapest: Pázmány University ePress, 2025, pp. 13–13.

Exploring the links between grapevine physiology and the composition and functionality of grapevine microbiome in the context of drought stress

Ramóna BIRÓ-KOVÁCS
(Supervisors: Zsolt ZSÓFI, Balázs LIGETI)
Pázmány Péter Catholic University, Faculty of Information Technology and Bionics
50/a Práter street, 1083 Budapest, Hungary
biro-kovacs.ramona@itk.ppke.hu

Abstract*—This study investigates the physiological responses of grapevine rootstock-scion combinations to drought stress, focusing on gas exchange and photosynthetic performance. Using controlled drought treatments, we compared Richter 110 and Teleki 5C rootstocks grafted with Furmint. Our findings show that Richter 110 exhibits superior drought resilience and recovery, maintaining higher CO_2 assimilation and stomatal conductance. These results highlight the importance of rootstock selection in climate-resilient viticulture and support the integration of physiological and molecular data for improved vineyard management.** ***Keywords: drought stress, Vitis vinifera, rootstock, photosynthesis, water deficit

I. Introduction

Grapevine is one of the oldest cultivated plants and holds significant cultural and economic value, especially in Hungary. Climate change—particularly rising temperatures and increasing drought frequency—poses a growing threat to the sustainability of viticulture. Water availability is a key environmental factor influencing grapevine physiology, especially processes like photosynthesis and stomatal regulation[1], [2]. Drought stress triggers both short-term and long-term responses in the plant, such as stomatal closure, reduced growth, and metabolic adjustments. In prolonged stress, plants prioritize root growth and deplete carbohydrate reserves, leading to reduced vigor and yield. Understanding rootstock-scion interactions is crucial for developing effective strategies to enhance grapevine resilience to environmental challenges [3], [4].

II. Objectives

This study aimed to investigate how grapevine rootstock-scion combinations with differing drought tolerance respond to water deficiency, with a focus on photosynthetic performance. By analyzing light and CO_2 response curves, the research provides insights into grapevine stress adaptation and strategies to sustain yield and quality under climate change.

III. Methodology

The drought stress experiment was conducted at the Eszterházy Vineyard in Eger using two rootstocks, Richter 110 and Teleki 5C, grafted with the Furmint scion. Plants were subjected to moderate drought and compared to well-watered controls over six weeks, followed by a 24-hour rehydration phase. Photosynthetic responses were measured using a CIRAS-4 system, focusing on light response, CO_2 response, and A/Ci curves. Measurements were taken under controlled environmental conditions to evaluate how each rootstock responded to drought and recovery in terms of gas exchange and photosynthetic activity.

IV. Results

Physiological measurements revealed that *Richter 110* exhibited significantly better photosynthetic performance and recovery under drought conditions compared to *Teleki 5C*. This was consistently supported by CO_2 response curves, light response measurements, and A/C_i analyses, all indicating higher net assimilation rates and stomatal conductance in *Richter 110*, particularly after rehydration. In contrast, *Teleki 5C* showed reduced photosynthetic capacity and limited recovery, suggesting stronger physiological constraints. These findings underscore the superior drought resilience of *Richter 110* and highlight the importance of rootstock selection in sustaining grapevine productivity under water-limited conditions.

V. Conclusion

This study highlights the critical role of rootstock-scion interactions in grapevine responses to drought stress, with Richter 110 showing superior photosynthetic efficiency and recovery compared to Teleki 5C. The results underscore the importance of selecting drought-resilient rootstocks like Richter 110 to sustain viticulture under climate change. Integrating physiological data with molecular approaches offers a promising path toward adaptive vineyard management in Hungary and globally.

Acknowledgment

This research was supported by the NKFIH Thematic Research Excellence Program (TKP2021-NKTA-16) and the EKÖP-24 University Research Fellowship Program. Special thanks to Dr. Zsolt Zsófi and Dr. Balázs Ligeti for their valuable guidance and support throughout the project.

References

[1] B. D. Mckersie, Y. Y. Leshem, B. D. Mckersie, and Y. Y. Leshem, "Chilling stress," *Stress and stress coping in cultivated plants*, pp. 79–103, 1994.

[2] J. Araus, G. Slafer, M. Reynolds, and C. Royo, "Plant breeding and drought in C3 cereals: what should we breed for?" *Annals of botany*, vol. 89, no. 7, pp. 925–940, 2002.

[3] F. Tardieu, "Drought perception by plants do cells of droughted plants experience water stress?" *Plant growth regulation*, vol. 20, pp. 93–104, 1996.

[4] R. G. Shaffer, T. Sampalo, J. Pinkerton, and M. Vasconcelos, "Grapevine rootstocks for Oregon vineyards," Oregon State University Extension Service, Corvallis, Oregon, USA, Tech. Rep. EM 8882, 2004.

R. BIRÓ-KOVÁCS, "Grapevine photosynthetic response to drought stress as influenced by rootstock-scion combinations" in *PhD Proceedings – Annual Issues of the Doctoral School, Faculty of Information Technology and Bionics, Pázmány Péter Catholic University – 2025.* G. Prószéky, G. Szederkényi Eds. Budapest: Pázmány University ePress, 2025, pp. 14–14.

Reinforcement learning to study the effects of tactile sensors in different simulated environments

Eszter BIRTALAN
(Supervisor: Miklós KOLLER)
Pázmány Péter Catholic University, Faculty of Information Technology and Bionics
50/a Práter street, 1083 Budapest, Hungary
birtalan.eszter@itk.ppke.hu

***Abstract*—This study explores the impact of tactile sensor configurations on reinforcement learning (RL) performance in robotic grasping tasks using a 3D hand model. We employed two distinct environments to minimize biases from specific algorithms, hand models, or simulators. Initially, Proximal Policy Optimization (PPO) was used in a PyBullet-based setup. To validate our findings, a second environment utilized Deep Deterministic Policy Gradient (DDPG) with Hindsight Experience Replay (HER). We found certain characteristics of learning to be present across the different setups, such as higher performance of simulations with tactile data towards the end of the simulation, and similar performance of configurations with vastly differing amounts of sensors.**

***Keywords*-reinforcement learning; proximal policy optimization; deep deterministic policy gradient; hindsight experience replay; tactile sensors; robotic grasping; prosthetic hand**

I. Introduction

With the rapidly expanding demand for robotics, hardware and software innovations are continuously rising in this field, made partly possible by improvements in machine learning, including reinforcement learning (RL). This type of learning has been widely used in complex tasks such as grasping and object manipulation. Two commonly used RL algorithms are PPO and DDPG with HER [1]. PPO is great to use when heavy exploration is needed and stabilizes learning by limiting large policy updates. In contrast, DDPG is an off-policy algorithm, where exploration is defined by stochastic noise, and HER allows learning from failed attempts. Including tactile data in training improves performance in object manipulation and grasping tasks [2]. Our goal was to assess the effect of different touch sensor configurations using a 3D hand model. We ensured results were not specific to a single setup by selecting multiple environments and learning algorithms.

II. Methods

We chose the two most commonly used simulators: PyBullet and MuJoCo. The 6 different configurations of the tactile sensors were the same in both setups, aimed to evaluate the effect of both sensor location and density. Control configurations have an equal amount of sensor output as their respective sensorized counterparts; however, all values are set to zero to ensure identical observation dimensions. The task in both cases was to lift object into the air. Performance is measured by the ratio of successful to all episodes. In PyBullet, we used the Modular Prosthetic Limb and a PPO algorithm. Possible actions included moving in 3D space and bending the fingers along a given trajectory. Each training instance was repeated 5 times for each configuration, both for the sensorized and control groups. In MuJoCo, the hand model used in this setup was the Shadow Hand, with a combination of DDPG+HER [2] algorithms controlling it. Control actions included moving in 3D space, bending the fingers and the wrist. Later, arm rotation was also allowed. The initially used object in this setup was a cube, and training was repeated 10 times to produce results. Simulations in this setup were repeated using 19 CPU cores, multiprocessing, and parallelized environments.

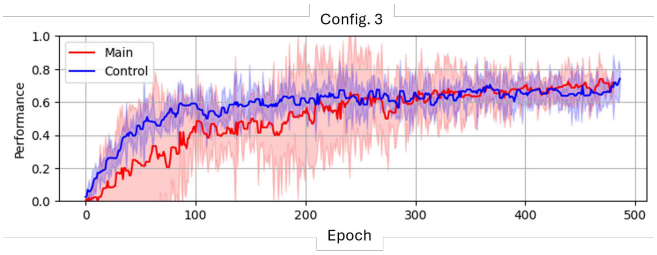

Fig. 1. Results from the PyBullet environment. The missing central sensor caused a significant performance drop in the main (sensorized, red) group.

III. Results

The results from both environments showed that while configurations with multiple sensors initially seem beneficial, equipping hand models with too many sensors was redundant. The absence of a central sensor significantly impacted performance in the PyBullet environment 1, while it had no such effect in MuJoCo. Simulations performed with a single CPU core configuration showed that the main group (with tactile information) outperformed the control group (without tactile data) in the second half of the training for 3 out of the 6 configurations in PyBullet and 2 out of 6 configurations in MuJoCo. Simulations performed with a 19-CPU-core configuration vastly outperform both PPO and the single-core DDPG+HER.

Acknowledgements

Project no. 2023-2.1.2-KDP-2023-00011 has been implemented with the support provided by the Ministry of Innovation and Technology of Hungary from the National Research, Development and Innovation Fund, based on the grant award certificate issued by the National Research, Development and Innovation Office.

References

[1] Al-Hamadani MNA, Fadhel MA, Alzubaidi L, Balazs H. Reinforcement Learning Algorithms and Applications in Healthcare and Robotics: A Comprehensive and Systematic Review. Sensors (Basel). 2024 Apr 11;24(8):2461. doi: 10.3390/s24082461.

[2] Melnik A, Lach L, Plappert M, Korthals T, Haschke R, Ritter H. Using Tactile Sensing to Improve the Sample Efficiency and Performance of Deep Deterministic Policy Gradients for Simulated In-Hand Manipulation Tasks. Front Robot AI. 2021 Jun 29;8:538773. doi: 10.3389/frobt.2021.538773.

E. BIRTALAN, "Reinforcement learning to study the effects of tactile sensors in different simulated environments" in *PhD Proceedings – Annual Issues of the Doctoral School, Faculty of Information Technology and Bionics, Pázmány Péter Catholic University – 2025.* G. Prószéky, G. Szederkényi Eds. Budapest: Pázmány University ePress, 2025, pp. 15–15.

A method for hippocampal place field detection using in vivo calcium imaging data in mice

Martin BLAZSEK
(Supervisors: Judit MAKARA, Balázs UJFALUSSY)
Pázmány Péter Catholic University, Faculty of Information Technology and Bionics
50/a Práter street, 1083 Budapest, Hungary
blazsek.martin.janos@itk.ppke.hu

***Abstract*—Hippocampal place cells and their respective place fields are known to be key components in the mental representation of the environment. However, the mechanisms underlying the evolution of spatial representation within the hippocampus are yet to be fully understood. The detection of place fields is the first step towards understanding their properties. Here I describe an algorithm for the detection of place fields in *in vivo* two-photon Ca^{2+} imaging recordings.**

***Keywords*-two-photon microscopy, calcium imaging, hippocampus, place fields**

I. Introduction

The hippocampus plays a key role in spatial navigation [1]. Place cells are excitatory cells in the hippocampus with activity selective to spatial locations referred to as place fields (PF). A plasticity mechanism underlying the evolution of spatial representation in the hippocampal CA1 has been described, called behavioral timescale synaptic plasticity (BTSP). PFs formed through BTSP exhibit a strong initial burst, followed by a backward shifting of the spatial center of the PF, serving as signatures of BTSP-formed PFs.

This summary describes a method for detecting PFs in 2P Ca^{2+} recordings of hippocampal CA1 place cells. It was developed in collaboration with Máté Sümegi (Research Group of Cellular Neurophysiology, Institute of Experimental Medicine, Budapest). Our results have recently been published in the journal eLife as a reviewed preprint, and it is currently under revision [2]. My contributions involve the classification and subsequent analysis of PF properties regarding their formation.

II. Experimental paradigm, data preprocessing

Head-restrained mice were placed on a 8 m long belt and trained to navigate a virtual environment with 6 visual landmarks. The animals were double transgenic for the fluorescent calcium indicator GCaMP6s and Cre-dependent td-Tomato. The software *Suite2p* was used to perform preprocessing of raw recordings: motion correction, detection of cells and spike inference.

III. Spatio-temporal detection of PFs

The spatial location of PFs were detected the following way:

1) Tuning curves in odd and even laps were correlated, and low correlation cells were discarded.
2) Skaggs information was evaluated [3] and cells with low information content were discarded.
3) Peak detection was performed; peaks with significant local Skaggs information are classified as PFs.

The temporal formation and end of PFs were determined the following way:

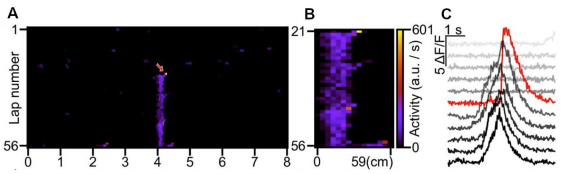

Fig. 1. Example PF. (A) Spiking activity of cell as a function of spatial bins and laps. Red arrow indicates PF formation. (B) Activity matrix of detected PF: formation lap at no. 21, end lap at no. 56. (C) Normalized fluorescence traces for the 5 laps preceding formation (lighter grey), formation lap (red), and 5 laps succeeding formation lap (darker gray). Figure adapted from [2].

1) Filtering based on proportion of active laps and spike thresholds were applied.
2) The formation lap of a PF is defined as the first lap with significant spatially tuned activity within the spatial bounds of the PF.
3) The end of a PF was determined by finding the first set of 5 consec. laps with no activity.

IV. Classification and analysis of PFs

PFs formed early during the recording session were excluded, as well as PFs with unreliable lap-by-lap activity. Three features were evaluated on the rest (stable, newly formed PFs):

1) **Initial backward shift**: shortly after formation, the COM of the PF negatively shifts
2) **High formation gain**: formation activity is stronger than subsequent activity
3) **No drifting**: the already formed place field does not show a *continuous* backward drift

If all three of these criteria are met, we classify the PF as BTSP-formed. An example for a BTSP-formed place field can be seen in Fig. 1.

V. Acknowledgements

This work was supported by the European Research Council (ERC-CoG 771849), the Hungarian National Brain Research Program (NAP3.0), the International Research Scholar Program of the Howard Hughes Medical Institute (55008740) and the National Research, Development and Innovation Office, Hungary (K-124824).

References

[1] J. O'Keefe, L. Nadel, The hippocampus as a cognitive map. (Oxford University Press, 1978)
[2] M. Sümegi, G. Oláh, I. Lukács, M. Blazsek, J. Makara, Z. Nusser, Diverse calcium dynamics underlie place field formation in hippocampal CA1 pyramidal cells (eLife, 2024)
[3] W. Skaggs, B. Mcnaughton, K. Gothard, An information-theoretic approach to deciphering the hippocampal code (Adv. Neural Inf. Process Syst., 1992)

M. BLAZSEK, "A method for hippocampal place field detection using in vivo calcium imaging data in mice" in *PhD Proceedings – Annual Issues of the Doctoral School, Faculty of Information Technology and Bionics, Pázmány Péter Catholic University – 2025.* G. Prószéky, G. Szederkényi Eds. Budapest: Pázmány University ePress, 2025, pp. 16–16.

LiDAR-based gait recognition: a survey of methods and opportunities for advancement

Balázs Márk BÓDIS
(Supervisor: Csaba BENEDEK)
Pázmány Péter Catholic University, Faculty of Information Technology and Bionics
50/a Práter street, 1083 Budapest, Hungary
bodis.balazs.mark@itk.ppke.hu

***Abstract*—Lidar-based gait recognition excels due to its 3D spatial data, overcoming limitations of 2D camera systems [1], [2]. However, many methods still project 3D point clouds to 2D, losing inherent 3D information [3]. Effectively handling spatio-temporal information in an end-to-end manner remains a challenge, leading to complex feature extraction [2]. This work critically evaluates these shortcomings and proposes a novel end-to-end 3D point cloud sequence processing pipeline with a custom neural network designed to directly learn spatio-temporal gait features.**

I. Introduction

Gait analysis is a promising non-contact biometric for identification in surveillance and security [4]. While 2D camera-based methods are limited by factors like lighting and viewpoint [1], 3D Lidar-based gait recognition has gained attention. The task involves identifying individuals from the unique spatio-temporal patterns of their walking motion captured as 3D point cloud sequences [5]. The goal is to extract robust features invariant to walking variations, clothing for an accurate identification.

II. Related work

Yamada et al. [4] pioneered deep learning for Lidar gait recognition using LSTMs to analyze temporal data. However, they processed 3D point clouds as depth images and their experiments, however, were conducted under controlled conditions with a fixed sensor distance and viewpoint.

Shen et al. [1] contributed the SUSTech1k dataset for more comprehensive Lidar gait evaluation, featuring multiple viewpoints and appearance variations within a 5-10 meter range. They also used depth images (multiple views) with a 2D CNN and horizontal pooling for feature extraction, trained with triplet and BCE loss.

Ahn et al. [5] tackled long-range Lidar gait recognition across different viewpoints and distances. They used multi-scale point cloud processing and extracted features from estimated side and back views, fusing them with an attention mechanism within a convolutional network to achieve improved robustness.

Han et al. [2] introduced HMRNet, the state-of-the-art method on the SUSTech1k and their newly proposed FreeGait datasets, which are leading 3D Lidar gait datasets. Their pipeline involves extracting dense body structure from range views and undistorted geometric/motion features using a motion-aware feature embedding (MAFE) from point clouds. An adaptive cross-representation mapping module (ACM) then hierarchically fuses these features. Finally, a gait-saliency feature enhancement (GSFE) module highlights key gait information for identification. FreeGait, while having fewer probe samples and views per identity compared to SUSTech1k, includes a larger number of individuals and greater overall variability.

Zhang et al. [3] introduced GaitCloud, emphasizing a true 3D gait representation through voxelization of Lidar point clouds to avoid information loss and viewpoint issues associated with 2D depth image projections. While their method, utilizing 2D and 3D convolutional steps and Horizontal Convolutional Pooling, excels in capturing spatial features, its temporal aggregation is relatively basic, indicating a stronger focus on spatial rather than complex spatio-temporal modeling. Although GaitCloud outperformed the similarly sized baseline model from [1], it did not achieve the same level of performance as the state-of-the-art HMRNet proposed in [2], which is significantly more complex.

III. Conclusion

A significant direction for future research lies in developing a unified spatio-temporal representation that integrates the strengths of approaches like Lidargait (temporal modeling) and GaitCloud (3D spatial representation). Constructing an end-to-end network capable of directly processing such a 3D temporal representation holds the potential to create lightweight and highly effective Lidar gait recognition models. While transformer networks have been explored for Lidar gait recognition, their application often treats the data as a sequence of 2D-like representations, thus not fully leveraging the inherent 3D structure of the point clouds.

IV. Acknowledgements

The author is grateful to HUN-REN SZTAKI, particularly to Csaba Benedek for the opportunity to work on this topic.

References

[1] C. Shen, C. Fan, W. Wu, R. Wang, G. Q. Huang, and S. Yu, "LidarGait: Benchmarking 3D gait recognition with point clouds," in *Proceedings of the IEEE/CVF Conference on Computer Vision and Pattern Recognition (CVPR)*, June 2023, pp. 1054–1063.

[2] X. Han, Y. Ren, P. Cong, Y. Sun, J. Wang, L. Xu, and Y. Ma, "Gait recognition in large-scale free environment via single LiDAR," 2024. [Online]. Available: https://arxiv.org/abs/2211.12371

[3] S. Zhang, H. Awano, and T. Sato, "Gaitcloud: Leveraging spatial-temporal information for LiDAR-based gait recognition with a true-3D gait representation," in *2025 IEEE/CVF Winter Conference on Applications of Computer Vision (WACV)*. IEEE Computer Society, Mar. 2025, pp. 2849–2858. [Online]. Available: https://doi.ieeecomputersociety.org/10.1109/WACV61041.2025.00282

[4] H. Yamada, J. Ahn, O. M. Mozos, Y. Iwashita, and R. K. and, "Gait-based person identification using 3D LiDAR and long short-term memory deep networks," *Advanced Robotics*, vol. 34, no. 18, pp. 1201–1211, 2020. [Online]. Available: https://doi.org/10.1080/01691864.2020.1793812

[5] J. Ahn, K. Nakashima, K. Yoshino, Y. Iwashita, and R. Kurazume, "Learning viewpoint-invariant features for LiDAR-Based gait recognition," *IEEE Access*, vol. 11, pp. 129 749–129 762, 2023.

B. BÓDIS, "LiDAR-based gait recognition: a survey of methods and opportunities for advancement" in *PhD Proceedings – Annual Issues of the Doctoral School, Faculty of Information Technology and Bionics, Pázmány Péter Catholic University – 2025.* G. Prószéky, G. Szederkényi Eds. Budapest: Pázmány University ePress, 2025, pp. 17–17.

Immune marker and C-reactive protein dynamics in modulated electro-hyperthermia treatment of advanced pancreatic cancer

Nikolett Kitti DOBOS
(Supervisor: Tamás Márton GARAY)
Pázmány Péter Catholic University, Faculty of Information Technology and Bionics
50/a Práter street, 1083 Budapest, Hungary
dobos.nikolett.kitti@itk.ppke.hu

***Abstract*—Pancreatic ductal adenocarcinoma (PDAC) has a poor prognosis. This retrospective study on 73 PDAC patients investigated adjunctive modulated electro-hyperthermia (mEHT) with chemotherapy. Immune markers (CRP, WBC, NLR, GLR) were monitored at baseline, mid-, and post-treatment. Post-treatment elevations in these markers were associated with shorter survival. Increased mEHT treatment frequency in the first six months improved outcomes. Monitoring immune markers during mEHT treatment can aid prognostication; early, intensive mEHT therapy showed survival benefits.**

***Keywords*-pancreatic ductal adenocarcinoma; modulated electro-hyperthermia; C-reactive protein; immune marker**

I. Introduction

Pancreatic ductal adenocarcinoma (PDAC) is highly lethal [1]. Modulated electro-hyperthermia (mEHT), an adjunct therapy inducing immunogenic cell death [2], was studied. We investigated systemic immune markers, including C-reactive protein (CRP), white blood cell count (WBC), neutrophil-to-lymphocyte ratio (NLR), and granulocyte-to-lymphocyte ratio (GLR) in 73 PDAC patients receiving mEHT therapy with chemotherapy to identify prognostic patterns.

II. Methods

Retrospectively, 73 advanced PDAC patients received chemotherapy and mEHT treatment (2–3x/week, 60-150W). Blood samples for WBC, CRP, NLR [3], and GLR [4] were collected at baseline, mid-, and post-mEHT treatment. Overall survival (OS) from first session was recorded. Statistical methods were employed, including linear mixed-effects models and Cox regression, and the significance threshold was set to $p<0.05$.

III. Results

Patients (N=73, mean age 64.6 years) received mean 35.8 mEHT cycles. Immune markers were stable mid-treatment but CRP, WBC, NLR, and GLR significantly elevated post-treatment (Fig. 1). Median OS from the start of the therapy was 8.15 months. Higher post-treatment CRP (>6.20 mg/L), NLR (>7.78), GLR (>3.30), and WBC ($> 8.65 \times 10^9$/L) strongly predicted worse OS (all HR>2, $p<0.003$). More mEHT treatments in the first 6 months were associated with improved survival (HR=0.9376, p=0.0001), a benefit lost after 6 months.

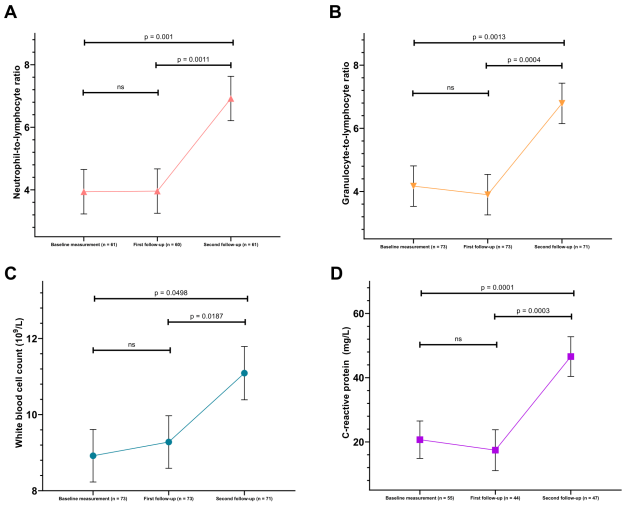

Fig. 1. Immune markers (A) NLR, (B) GLR, (C) WBC, (D) CRP (mean±SE) at baseline, mid-, and post-mEHT therapy (LME model; p-values shown).

IV. Summary

Post-treatment CRP, NLR, GLR, and WBC are novel prognostic markers for PDAC with mEHT treatment. Their late elevation, despite initial stability, may reflect diminishing mEHT treatment efficacy or disease progression. Increased treatment frequency in the first 6 months significantly improved survival, indicating a critical treatment window. Limitations include retrospective design and cohort size. Monitoring these markers could aid personalized mEHT therapy.

Acknowledgement

Supported by National Research, Development and Innovation Office of Hungary (NVKP16-1-2016-0042).

References

[1] F. Bray et al., *Global cancer statistics 2022: GLOBOCAN estimates of incidence and mortality worldwide for 36 cancers in 185 countries*, CA: A Cancer Journal for Clinicians, Volume 74, Pages 229-263, 2024.
[2] A.M. Szász et al., *Review of the Clinical Evidences of Modulated Electro-Hyperthermia (mEHT) Method: An Update for the Practicing Oncologist*, Frontiers in Oncology, Volume 9, 2019.
[3] Y. Zhou et al., *Prognostic role of the neutrophil-to-lymphocyte ratio in pancreatic cancer: A meta-analysis containing 8252 patients*, Clinica Chimica Acta, Volume 479, Pages 181-189, 2018.
[4] H. Liu et al., *The granulocyte/lymphocyte ratio as an independent predictor of tumour growth, metastasis and progression: Its clinical applications*, Molecular Medicine Reports, Volume 1, Pages 699-704, 2008.

N. DOBOS, "Immune marker and C-reactive protein dynamics in modulated electro-hyperthermia treatment of advanced pancreatic cancer" in *PhD Proceedings – Annual Issues of the Doctoral School, Faculty of Information Technology and Bionics, Pázmány Péter Catholic University – 2025.* G. Prószéky, G. Szederkényi Eds. Budapest: Pázmány University ePress, 2025, pp. 18–18.

Population activity and cellular firing in the human epileptic hippocampal formation, in-vitro

Nour ESSAM
(Supervisors: Lucia WITTNER)
Pázmány Péter Catholic University, Faculty of Information Technology and Bionics
50/a Práter street, 1083 Budapest, Hungary
essam.fawzy.ahmed.aly.nour@itk.ppke.hu

***Abstract*—Epilepsy of the temporal lobe is one of the most common forms of epilepsies, as the temporal lobe, and most specifically the hippocampus is the most epileptogenic region of the brain. It is characterized by recurrent seizures that lead to changes in neurological functions due to the excessive synchronized neuronal activity in the brain. Electrophysiological methods are key to understanding epileptic activtity**

***Keywords*-epilepsy; hippocampal formation; synchoronous activity; in-vitro**

I. Introduction

Epilepsy is one of the most common neurological disorders that is characterized by impulsive seizures which occur due to the imbalance between excitatory and inhibitory neuronal firing with a prevalence of excitation, along with high amplitude synchronous activity [1]. Approximately 30 percent of temporal lobe epileptic patients experience pharmacoresistant epilepsy, which refers to epilepsy that lasts despite undergoing multiple trials of available anti-seizure medications [2]. The hippocampal formation is the most prone structure to epileptic seizures, it is the primary structure to be affected in case of neuropsychiatric disorders [3]. Our study aimed to investigate the electrophysiological characteristics of epilepsy in the subiculum and the CA2 region of the hippocampus.

II. Methods

Extracellular multiple-channel recordings were conducted (1) to investigate the spontaneous population activity (SPA) - which is characterized by both excitatory and inhibitory signaling - within the CA2 region and the subiculum region, aiming to correlate cellular firing with synchronous population events. Specific neuronal staining was performed to characterize the neuron death and synaptic reorganization associated with epilepsy.

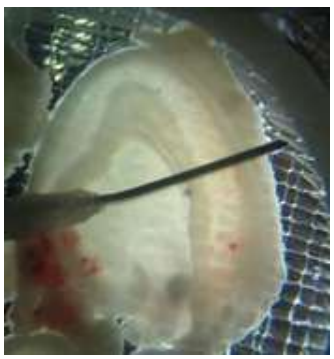

Fig. 1. The inside of the in vitro recording system, where the brain slice is placed on a net that is supplied with artificial cerebrospinal fluid (ACSF), the electrode orientation to the slice (an example). Photo made by N.E.

From the electrophysiological recordings we could analyze the local field potential gradient, current source density and multiple unit activity. Additionally spike sorting was performed using different software to help our understanding of the population activity in the epileptic hippocampal formation. Different neuronal types like intrinsically bursting and regular spiking pyramidal cells and inhibitory neurons were classified based on their action potential shape and their autocorrelogram, and the firing rate and the burstiness index were determined.

III. Results

SPA was detected in both regions, subiculum and CA2. SPAs were defined by their occurrence across multiple channels as recurring population bursts, marked by local field potential fluctuations, and elevated neuronal firing. A total of 133 neurons were identified in recordings with SPA, while 165 neurons were clustered in recordings without SPA (no-SPA). Neurons from the no-SPA recordings exhibited a higher firing rate (6.1 ± 4.4 Hz vs. 2.4 ± 2.9 Hz) and greater burstiness index (17.6 ± 22.9 vs. 10.7 ± 20.9) compared to those located near SPA. However, the firing rates of interneurons did not differ significantly between the two groups.

IV. Discussion

This study represents one step towards understanding the electrophysiological properties of the hippocampal formation in epilepsy, highlighting differences between regions and potential implications for epileptogenesis. It is important to mention that these initial neuronal clustering results represent less than half of the total dataset collected and therefore, the final findings may differ.

References

[1] D. Thurman, E. Beghi, C. Begley, A. Berg, J. Buchhalter, D. Hesdorffer, W. Hauser, L. Kazis, R. Kobau, B. Kroner, D. Labiner, K. Liow, G. Logroscino, M. Medina, C. Newton, K. Parko, A. Paschal, P.-M. Preux, and S. Wiebe, "Standards for epidemiologic studies and surveillance of epilepsy," *Epilepsia*, vol. 52 Suppl 7, pp. 2–26, 09 2011.

[2] M.-C. Hsiao, P.-N. Yu, D. Song, C. Liu, C. Heck, D. Millett, and T. Berger, "An in vitro seizure model from human hippocampal slices using multi-electrode arrays.," *Journal of neuroscience methods*, vol. 244, 09 2014.

[3] K. Anand and V. Dhikav, "Hippocampus in health and disease: An overview," *Annals of Indian Academy of Neurology*, vol. 15, pp. 239–46, 10 2012.

N. ESSAM, "Population activity and cellular firing in the human epileptic hippocampal formation, in-vitro" in *PhD Proceedings – Annual Issues of the Doctoral School, Faculty of Information Technology and Bionics, Pázmány Péter Catholic University – 2025.* G. Prószéky, G. Szederkényi Eds. Budapest: Pázmány University ePress, 2025, pp. 19–19.

Investigation of the Homer1:Shank3 interaction

Fanni FARKAS
(Supervisor: Zoltán GÁSPÁRI)
Pázmány Péter Catholic University, Faculty of Information Technology and Bionics
50/a Práter street, 1083 Budapest, Hungary
farkas.fanni@itk.ppke.hu

***Abstract*—The human brain has billions of neurons which connects each other through synapses. One of the most common type is the excitatory glutamaterg synapse. Under the postsynaptic membrane, a dense protein network, called the potsynaptic denstiy (PSD) is found. Protein:protein interactions are crucial in PSD for information transfer, therefore alterations in this regions or mutation in its constituent proteins can cause several severe diseases. To investigate selected protein:protein interactions in the PSD, NMR spectroscopy and partner binding studies can be used. My aim was to apply such methods to characterize the interaction between the postsynaptic scaffold proteins Homer1 and Shank3.**

***Keywords*-PSD; Homer1; EVH1; NMR; interaction; NMR titration**

I. Introduction

The postsynaptic density (PSD) is dynamically changing structure, a protein dense network found beneath the postsynaptic membrane of neurons in glutamatergic synapses. PSD plays an important role in memory formation, learning, and various cognitive functions [1]. Some neurodegenerative and neurodevelopmental diseases were associated with alterations in the PSD, interaction errors, and protein mutations or abnormalities, such as autism spectrum disorder or Alzheimer's disease [2]. PSD includes several types of proteins, including signalling enzymes, receptors, scaffold proteins, etc. Homer and Shank proteins are two of the main organizers of the core structure of PSD. They form an interaction with each other, as the EVH1 domain of Homer1 protein connects to Shank [3]. To investigate the structure of EVH1 domain and its point mutation variants, NMR spectroscopy is one of the most suitable methods which is currently available. SAXS and CD measurements can add important additional aspects. NMR titration experiments can be used to monitor the interaction of EVH1 variants with partner peptides. For functional investigations, biolayer interferometry and thermal shift assays can be used.

II. Methods

First of all, a protocol is needed to be set up for protein production and purification. Wild-type and two mutant (M65I and S97L) versions of the EVH1 domain of Homer1 protein were produced, for this BL21 *E. coli* cells were used. For Bio-layer Interferometry, Thermal Shift Assay and for SAXS measurement unlabeled version of the proteins were produced, which means that cells were grown in LB media. For NMR titration with Shank3 peptide ^{15}N isotope labeled- and for NMR resonance assignment, ^{13}C, ^{15}N isotope labeled EVH1 domains were used. To produce these labeled proteins, M9 minimal media was used with the additional isotopes. After protein production was induced in the cells, the cell walls needs to be broken to make proteins available, for this ultrasonic homogenization was used. For all the above mentioned techniques, the same purification steps were performed; first the Immobilized Metal Affinity Chromatography (IMAC) using the nickel column, followed by the Ion Exchange Chromatography (IEC) using the S column. The final purification step was the Size Exclusion Chromatography (SEC) which was used not only for purification but also to change the buffer to contain minimal additives (20 mM NaCl, 50 mM NaPi, pH 7.4). To verify the results, SDS-PAGE was performed which confirmed the successful production and purification of the proteins.

III. Results

The production and purification protocol was successfully set up for the Homer1 EVH1 domain. The sample was created for different structural and functional measurements. Unlabelled and isotopically labelled WT, M65I and S97L proteins were successfully purified. For NMR, a highly concentrated sample was sent to the University of Debrecen. For resonance assignment, a series of spectra were recorded. SAXS measurement was performed in Brno (Czech Republic), results are under analysis. To determine structural changes based on Shank3 peptide binding, NMR titration was performed. For functional analysis Bio-layer Interferometry and Thermal Shift Assay were performed. Early results are very promising, but further analysis are needed.

Acknowledgements

I would like to sincerely thank Dr. Zoltan Gaspari and Dr. Balint Peterfia for their invaluable guidance and unwavering support throughout my research journey. I am deeply appreciative of your time, patience, and encouragement, all of which have been instrumental in the success of this study. This work was supported by the Hungarian National Research, Development and Innovation Office (NKFIH) (grants, OTKA K 137947, TKP2021-EGA-42, and 2021-4.1.2-NEMZ_KI-2022-00027).

References

[1] M. Sheng and C. C. Hoogenraad, "The postsynaptic architecture of excitatory synapses: a more quantitative view," *Annu. Rev. Biochem.*, vol. 76, no. 1, pp. 823–847, 2007.

[2] T. Kaizuka and T. Takumi, "JB special review—neuronal functions and disorders postsynaptic density proteins and their involvement in," *J. Biochem*, vol. 163, no. 6, pp. 447–455, 2018.

[3] K. Irie, T. Nakatsu, K. Mitsuoka, A. Miyazawa, K. Sobue, Y. Hiroaki, T. Doi, Y. Fujiyoshi, and H. Kato, "Crystal structure of the Homer 1 family conserved region reveals the interaction between the EVH1 domain and own proline-rich motif," *Journal of molecular biology*, vol. 318, no. 4, pp. 1117–1126, 2002.

F. FARKAS, "Investigation of the Homer1:Shank3 interaction" in *PhD Proceedings – Annual Issues of the Doctoral School, Faculty of Information Technology and Bionics, Pázmány Péter Catholic University – 2025.* G. Prószéky, G. Szederkényi Eds. Budapest: Pázmány University ePress, 2025, pp. 20–20.

Investigation of the molecular mechanisms of postsynaptic plasticity using detailed, optimized computational models

Gábor FARKAS
(Supervisor: Szabolcs KÁLI)
Pázmány Péter Catholic University, Faculty of Information Technology and Bionics
50/a Práter street, 1083 Budapest, Hungary
farkas.gabor@itk.ppke.hu

***Abstract*—The biochemical mechanisms of long-term potentiation (LTP) and long-term depression (LTD) were studied using detailed, experimental data-driven computational models. Several experimental data were incorporated regarding the resting state of AMPA receptors, free calcium level, and different induction protocol-induced changes in synaptic strength. The resulting models were used to explain the underlying molecular mechanisms of a wide set of hippocampal postsynaptic plasticity-related experimental data.**

***Keywords*-postsynaptic plasticity, LTP, LTD, molecular mechanisms, AMPA receptors**

I. Introduction

A sophisticated network of intracellular signaling pathways in the spine heads of postsynaptic dendrites remarkably takes part in shaping synaptic plasticity - the cellular-level basis of learning and information storage in the brain. Using computational tools to investigate networks of biochemical cascades is a well-established research method. Furthermore, many different kinds of experimental data, e.g., electrophysiological recordings and various biochemical measurements are described in the scientific literature that can be incorporated in a detailed computational model. Fitting the model to different experimental data by optimizing the model parameters potentially results in models that can be used to study the mechanisms shaping synaptic plasticity.

II. Methods

A computational model of synaptic plasticity-related intracellular signaling pathways (CaMKII, PKA, and PKC cascades) was created based on the model described in [1]. The model was used to fit various experimental data collected from articles in which different induction protocols and pharmacological interventions were used to study hippocampal Schaffer collateral LTP and LTD. The model simulations were run using the reaction-diffusion submodule of the NEURON simulator [2]. The Neuroptimus optimization software tool [3] was used to optimize the model parameters. High-performance supercomputers provided by the Neuroscience Gateway (NSG) [4] were utilized to perform the computationally heavy optimizations. Because the resulting models fit the experimental data sufficiently well, they were used in further investigations of the underlying molecular mechanisms.

III. Results

In addition to fitting the experimental data, we aimed to have a realistic, steady-state baseline by fitting quantitative

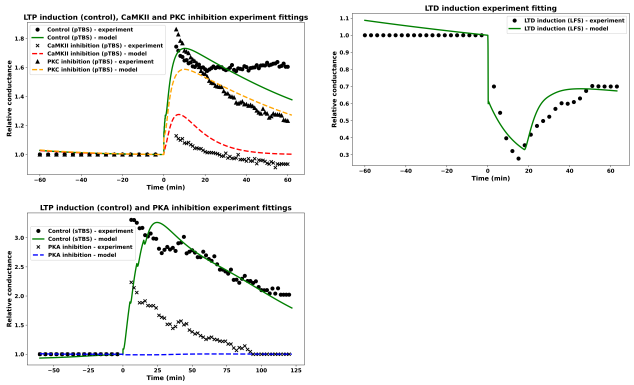

Fig. 1. Results of fitting models to different experimental data sets.

data regarding the resting state, such as intracellular calcium concentration (70 nM), ratio of GluR1 subunits phosphorylated at S845 (15%), fraction of GluR2 subunits bound to the membrane (45%), and ratio of GluR1 homomers (8-10%). By estimating these values, we can realistically model the resting state during which most AMPA tetramers are heteromers that have the greatest contribution to baseline synaptic conductance, supplemented by approximately 10% GluR1 homomers contributing a maximum 47% to baseline conductance. The resulting model fits to four different experimental data sets can be seen in Figure 1. The average of the resulting steady state values across 5 optimizations are:

- 84.9 nM, 18.2%, 38.6%, 10.4%;
- 55.7 nM, 17.5%, 7.3%, 10.5%;
- 61.5 nM, 25.6%, 38.3%, 0.3%

in the CaMKII and PKC inhibition experiment, in the PKA inhibition, and in the LTD induction experiments, respectively. Values were optimized during control experiments only.

References

[1] T. Mäki-Marttunen, K. T. Blackwell, I. Akkouh, A. Shadrin, M. Valstad, T. Elvsåshagen, M.-L. Linne, S. Djurovic, G. T. Einevoll, and O. A. Andreassen, "Genetic mechanisms for impaired synaptic plasticity in schizophrenia revealed by computational modeling," *Proceedings of the National Academy of Sciences*, 2024.

[2] R. Mcdougal, M. Hines, and W. Lytton, "Reaction-diffusion in the NEURON simulator," *Frontiers in Neuroinformatics*, 2013.

[3] M. Mohácsi, M. P. Török, S. Sáray, L. Tar, G. Farkas, and S. Káli, "Evaluation and comparison of methods for neuronal parameter optimization using the neuroptimus software framework," *PLOS Computational Biology*, 2024.

[4] S. Sivagnanam, A. Majumdar, K. Yoshimoto, V. Astakhov, A. Bandrowski, M. Martone, and N. Carnevale, "Introducing the neuroscience gateway," *CEUR Workshop Proceedings*, 2013.

G. FARKAS, "Investigation of the molecular mechanisms of postsynaptic plasticity using detailed, optimized computational models" in *PhD Proceedings – Annual Issues of the Doctoral School, Faculty of Information Technology and Bionics, Pázmány Péter Catholic University – 2025.* G. Prószéky, G. Szederkényi Eds. Budapest: Pázmány University ePress, 2025, pp. 21–21.

Genomic LMs generalization capability in phage identification tasks

Bendegúz FILYÓ
(Supervisor: Balázs LIGETI)
Pázmány Péter Catholic University, Faculty of Information Technology and Bionics
50/a Práter street, 1083 Budapest, Hungary
filyo.bendeguz@itk.ppke.hu

***Abstract*—Recent research unveils growing evidence on the importance of phages in the microbiome, yet their ecosystem remain poorly understood. Genomic Language Models (gLMs) have emerged as powerful AI tools capable of learning from unlabeled sequences and identifying context-dependent patterns in biological sequences. This study explores how fine-tuning hyperparameters, particularly sequence length and learning rate, influence these models' ability to generalize to unseen microbial data, establishing trends to guide future development.**

***Keywords*-Metagenomics, Genomic Language Model, Phage identification, Hyperparameter optimization**

I. Introduction

Microbial communities form complex ecosystems that fundamentally influence health, disease progression, and environmental processes. They consist of diverse bacterial, fungal, and viral species whose interactions create intricate networks, critical to their host environments. Despite their importance, our understanding of their functional behavior remains limited by the sheer complexity of these communities and their genetic diversity. Large-scale metagenomic sequencing has generated vast genomic datasets, yet significant annotation gaps persist, hampering biological interpretation. Genomic Language Models (gLMs) have emerged as a promising computational approach to address these challenges in microbiome research. This work investigates how core hyperparameters, affect the generalization performance of gLMs.

TABLE I
Models evaluated.

Name	Num params	Tokenization
NT-500m [1]	500m	Non-ovelapping k-mers
NT-50m	50m	Non-ovelapping k-mers
DNABERT-2 [2]	117m	Byte-Pair Encoding
ProkBERT Mini [3]	20m	Local Context-Aware
ProkBERT Mini Long	26m	Local Context-Aware

II. Data and Methods

Our goal was to evaluate the generalization properties of these foundational models. To do so, we created a dataset, we named Leave-Genera-Out (LeGO), which includes bacterial contigs and their associated phage contigs from species related to antimicrobial resistance. However, contigs from three bacterial genera and their corresponding phages were excluded to form the test set, ensuring that evaluation was performed on previously unseen data. We explored a small set of hyperparameters with grid search to find their effect on model performance, as well as to compare models. All models were trained for three epochs, with experiments exploring different learning rates (0.00005, 0.0001, 0.00001) and sequence lengths (256, 512, 1024, 2048).

III. Results

The table below presents test performance grouped by sequence length, using the best performing hyperparameters for each configuration. Prediction accuracy improved with longer sequences, likely due to the increased context available. Generally the lowest learning rate $5 * 10^{-6}$ yielded the best models, with the smoothest convergence. Nucleotide Transformer v2 500M achieved the highest overall performance, while ProkBERT models delivered comparable results despite having significantly fewer parameters.

TABLE II
Metrics of the fine-tuned models on the LeGO test set.

Ls	Model	MCC	Recall	Specificity	AUC
256	DNABERT-2-117M	0.42	0.69	0.73	0.79
	NT-500m	**0.60**	0.80	**0.80**	**0.88**
	NT-50m	0.52	**0.82**	0.70	0.84
	ProkBERT-mini	0.59	0.79	**0.80**	0.87
	ProkBERT-mini-long	0.59	0.80	0.79	0.87
512	DNABERT-2-117M	0.44	0.80	0.63	0.79
	NT-500m	**0.70**	**0.87**	0.83	**0.92**
	NT-50m	0.62	0.84	0.77	0.89
	ProkBERT-mini	0.68	0.83	**0.85**	0.91
	ProkBERT-mini-long	0.68	0.85	0.83	0.91
1024	DNABERT-2-117M	0.63	0.74	0.89	0.90
	NT-500m	**0.78**	**0.89**	0.89	**0.94**
	NT-50m	0.69	0.87	0.82	0.92
	ProkBERT-mini	0.75	0.84	**0.90**	0.93
	ProkBERT-mini-long	0.76	0.88	0.88	**0.94**
2048	DNABERT-2-117M	0.48	0.45	**0.96**	0.88
	NT-500m	**0.82**	**0.92**	0.90	**0.95**
	NT-50m	0.75	0.87	0.88	0.94
	ProkBERT-mini-long	0.78	0.87	0.90	0.94

Acknowledgements

We acknowledge the Digital Government Development and Project Management Ltd. for awarding us access to the Komondor HPC facility based in Hungary. The project was supported by the National Fund for Development, Research and Innovation (NKFIH), OTKA PD (138055) and 2020-1.2.3-EUREKA-2022-00023; Ministry of Innovation and Technology, NRDI Office within the framework of the National Laboratory for Artificial Intelligence (RRF-2.3.1-21-2022-00004). FB was supported by the National Laboratory for Artificial Intelligence Research Grant (RRF-2.3.1-21-2022-00004).

References

[1] H. Dalla-Torre, L. Gonzalez, J. Mendoza-Revilla, N. Lopez Carranza, A. H. Grzywaczewski, F. Oteri, C. Dallago, E. Trop, B. P. de Almeida, H. Sirelkhatim, G. Richard, M. Skwark, K. Beguir, M. Lopez, and T. Pierrot, "Nucleotide transformer: building and evaluating robust foundation models for human genomics," vol. 22, no. 2, pp. 287–297. Publisher: Nature Publishing Group.

[2] Z. Zhou, Y. Ji, W. Li, P. Dutta, R. Davuluri, and H. Liu, "DNABERT-2: Efficient foundation model and benchmark for multi-species genome."

[3] B. Ligeti, I. Szepesi-Nagy, B. Bodnár, N. Ligeti-Nagy, and J. Juhász, "ProkBERT family: genomic language models for microbiome applications," vol. 14, p. 1331233.

B. FILYÓ, "Genomic LMs generalization capability in phage identification tasks" in *PhD Proceedings – Annual Issues of the Doctoral School, Faculty of Information Technology and Bionics, Pázmány Péter Catholic University – 2025.* G. Prószéky, G. Szederkényi Eds. Budapest: Pázmány University ePress, 2025, pp. 22–22.

Flaccid muscle stimulation training for spinal cord injured patients – Preliminary study

Amelita FODOR
(Supervisor: József LACZKÓ)
Pázmány Péter Catholic University, Faculty of Information Technology and Bionics
50/a Práter street, 1083 Budapest, Hungary
fodor.amelita@itk.ppke.hu

***Abstract*—According to WHO data, more than 15 million people worldwide live with spinal cord injuries, and approximately one quarter of them suffer from lower motor neuron damage. This condition leads to rapid muscle atrophy, tissue remodeling, and metabolic difficulties, while therapeutic options remain limited. In recent decades, increasing research has focused on how to influence flaccid paralysis and its consequences. In my study, I treated patients with subacute spinal cord injury with electrotherapy twice a week, using individualized Long Pulse Width Stimulation (LPWS) parameters to achieve appropriate tetanic contractions. During training sessions, I measured excitability threshold of several muscles and duration of the session. My results showed a decreasing training trend and moderate variability in threshold values, suggesting that in the subacute phase, neural conduction and muscle excitability strongly depend on the spinal cord's recovery process and the tissue quality of the remaining muscles.**

***Keywords*-Flaccid paralyzes; spinal cord injury; muscle excitability; long pulse width stimulation**

I. Introduction

Spinal cord injury (SCI) causes severe functional impairments and triggers rapid muscle degeneration, especially during spinal shock phase. This transient state can last up to 7 months and involves the loss of motor, sensory, and autonomic functions below the injury level. Early intervention is critical to prevent secondary complications and support recovery. Paralysis following SCI can present as spastic or flaccid. In flaccid paralysis, acute axonal damage begins within minutes and leads to loss of nerve-muscle connection [1]. Muscle atrophy progresses over months, with up to 40% loss in mass within two years [2]. Long Pulse Width Stimulation (LPWS) has been proposed as a method to preserve or restore muscle function in denervated muscles. Although LPWS can take weeks to elicit visible contraction in chronic cases, studies show long-term improvements in muscle structure and volume [3]. The aim of our preliminary study was to investigate how denervated muscles can be stimulated during spinal shock.

II. Methods

Measurements were conducted at the Semmelweis University Rehabilitation Clinic with ethical approval, involving four spinal cord injured patients in the spinal shock phase. LPWS training was applied using a Stimulette R2X stimulator with individualized parameters based on strength-duration curves. The goal was to achieve effective muscle contraction with the shortest possible pulse width and moderate current intensity. Motor threshold values were recorded during each session, from which mean, standard deviation and coefficient of variation (CV) were calculated. Stimulation duration per muscle was adjusted based on fatigue, ranging from 2 to 20 minutes.

III. Results

Quadriceps muscles were stimulated in P1, P2, and P4, with P1 showing the lowest and P2 the highest average threshold currents, indicating varying excitability. P4 displayed the highest variability (CV: 35.2%), reflecting unstable muscle responses. Thresholds generally decreased over time, especially in P2 and P4, while P1 showed mixed trends. Tibialis Anterior stimulation in all four patients revealed that P3 required the lowest and P4 the highest currents, again suggesting individual differences in excitability. Variability was moderate, though P4's right side had the highest variability (CV: 19.4%), and all patients showed decreasing trends of excitability threshold. Triceps Surae stimulation in P3 and P4 also showed decreasing thresholds, with P4 having lower average currents but higher variability. The strongest improvement was seen in P3, while P4 showed a milder but consistent decline in threshold values.

IV. Conclusion

During spinal shock, motor thresholds generally decreased with regular LPWS, and patients responded faster than the expected 12-week adaptation period. Shorter pulse widths and lower currents were sufficient to achieve tetanic contractions, suggesting increased excitability compared to the chronic phase of spinal cord injury. Muscle fatigue time also improved rapidly, supporting the role of early stimulation in preserving muscle tissue. Future studies with imaging methods like MRI could help quantify muscle preservation and optimize stimulation parameters.

Acknowledgements

I would like to express my gratitude to Lilla Botzheim and Mariann Mravcsik for additional supervision of my research. This research was supported by the National Research, Development and Innovation Fund, Hungary, Grant number: 2024-2.1.2-EKÖP-KDP-2024-00004

References

[1] S. Chandrasekaran, J. Davis, I. Bersch, G. Goldberg, and A. S. Gorgey, "Electrical stimulation and denervated muscles after spinal cord injury," 2020.

[2] M. Alberty, W. Mayr, and I. Bersch, "Electrical stimulation for preventing skin injuries in denervated gluteal muscles—promising perspectives from a case series and narrative review," *Diagnostics*, vol. 13, 1 2023.

[3] H. Kern, C. Hofer, M. Mödlin, C. Forstner, D. Raschka-Högler, W. Mayr, and H. Stöhr, "Denervated muscles in humans: Limitations and problems of currently used functional electrical stimulation training protocols," *Artificial Organs*, vol. 26, pp. 216–218, 3 2002.

A. FODOR, "Flaccid muscle stimulation training for spinal cord injured patients – Preliminary study" in *PhD Proceedings – Annual Issues of the Doctoral School, Faculty of Information Technology and Bionics, Pázmány Péter Catholic University – 2025.* G. Prószéky, G. Szederkényi Eds. Budapest: Pázmány University ePress, 2025, pp. 23–23.

In silico modeling of the Hes1 autoregulatory network

Bence Tamás GAIZER
(Supervisors: Attila CSIKÁSZ-NAGY, János JUHÁSZ)
Pázmány Péter Catholic University, Faculty of Information Technology and Bionics
50/a Práter street, 1083 Budapest, Hungary
gaizer.bence.tamas@itk.ppke.hu

***Abstract*—The Hes1 (Hairy and enhancer of split-1) gene plays a crucial role in the regulation of cellular differentiation and developmental timing, functioning as a key component of the Notch signaling pathway. In our work, we developed an *in silico* model for both deterministic and stochastic simulation of this gene regulatory network (GRN).**

***Keywords*-Hes1; Gene regulatory network; Reaction network modeling**

I. Introduction

The Hes1 gene regulatory network is defined by autoregulatory behaviour, driving its temporal oscillation. This periodic expression is critical, among others, to cell fate determination, stem cell maintenance, and cell cycle progression.
Since a simple negative autoregulatory loop is mathematically insufficient to produce a limit cycle, there are several different approaches for *in silico* modeling of this network:

1) Boareto et al. [1] used a time delay to introduce oscillations. In our approach, we wanted to avoid using time delays to avoid complications in numerical modeling of the system.
2) The spatiotemporal model of Sturrock et al. [2] produced the required time delay emergent from the meshed domain simulation, although this solution would have been computationally heavy for our application.
3) In order to establish stable limit cycles, Hirata et al. [3] introduced an additional molecule, which they referred to as Interacting Factor (IF), and also applied two second-degree Hill-type elements in their mathematical model. The role of IF was to suppress Hes1 expression. Being negatively regulated by Hes1, its presence led to a positive feedback loop, facilitating a stable limit cycle.

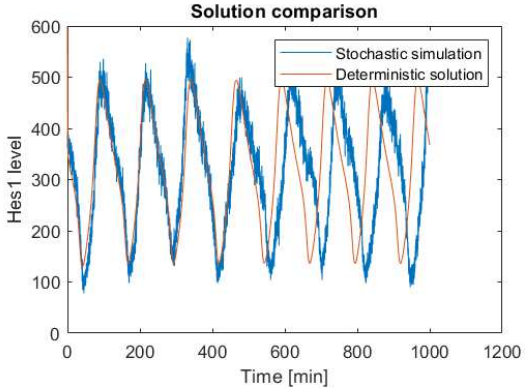

Fig. 1. Comparison between deterministic solution and stochastic simulation.

II. Methods

Our goal was to construct a mathematical model that can be solved deterministically for rapid parameter search, or simulated stochastically to reproduce emergent experimental phenomena.

Following the model of Hirata et al. [3] we assumed the presence of IF but added three new variables to the dynamic system, namely the number of Hes1 dimers and the number of free promoters of the expression of hes1 and IF. This approach replaces both second-degree Hill-type equations with multi-step reactions.

After these considerations, we used the following mathematical model, with variables x_1 - Hes1 protein, x_2 - hes1 mRNA, x_3 - IF, x_4 - free hes1 promoters, x_5 - free IF promoters, x_6 - Hes1 dimers:

$$\frac{\partial x_1}{\partial t} = -\delta_H \cdot x_1 - a \cdot x_1 \cdot x_3 + \beta \cdot x_2 - 2 \cdot k_{dim} \cdot x_1^2 \quad (1)$$

$$\frac{\partial x_2}{\partial t} = -\delta_h \cdot x_2 + \alpha_h \cdot x_4 + \frac{\alpha_h}{\gamma_h} \cdot (N_H - x_4) \quad (2)$$

$$\frac{\partial x_3}{\partial t} = -\delta_{IF} \cdot x_3 + a \cdot x_1 \cdot x_3 + \alpha_{IF} \cdot x_5 + \frac{\alpha_{IF}}{\gamma_{IF}} \cdot (N_{IF} - x_4) \quad (3)$$

$$\frac{\partial x_4}{\partial t} = -\lambda_h \cdot x_4 \cdot x_6 + \mu_h \cdot (N_H - x_4) \quad (4)$$

$$\frac{\partial x_5}{\partial t} = -\lambda_{IF} \cdot x_5 \cdot x_6 + \mu_{IF} \cdot (N_{IF} - x_5) \quad (5)$$

$$\frac{\partial x_6}{\partial t} = -\delta_D \cdot x_6 + k_{dim} \cdot x_1^2 - \lambda_h \cdot x_4 \cdot x_6 - \lambda_{IF} \cdot x_5 \cdot x_6 \quad (6)$$

III. Results

As Figure 1 shows, both deterministic and stochastic models were able to reach stable limit cycles, and their results show similar dynamics.

Acknowledgements

This research is supported by the Hungarian National Research, Development and Innovation Office through Thematic Excellence Programme grant no. TKP2021-EGA-42. Special thanks to Associate Professor Christian Hong for this collaboration.

References

[1] Marcelo Boareto *et al.*, Differential interactions between Notch and ID factors control neurogenesis by modulating Hes factor autoregulation, *Development*, 2017.
[2] Marc Sturrock *et al.*, The Role of Dimerisation and Nuclear Transport in the Hes1 Gene Regulatory Network, *Bull Math Biol.*, 2014.
[3] Hiromi Hirata *et al.*, Oscillatory Expression of the bHLH Factor Hes1 Regulated by a Negative Feedback Loop, *Science*, 2002.

B. GAIZER, "In silico modeling of the Hes1 autoregulatory network" in *PhD Proceedings – Annual Issues of the Doctoral School, Faculty of Information Technology and Bionics, Pázmány Péter Catholic University – 2025.* G. Prószéky, G. Szederkényi Eds. Budapest: Pázmány University ePress, 2025, pp. 24–24.

Quantifying the role of phenotypic variables in inducing delayed cell-cycle re-entry following stress-induced cell-cycle arrest

Valentina GUARINO
(Supervisor: Andrea CILIBERTO)
Pázmány Péter Catholic University, Faculty of Information Technology and Bionics
50/a Práter street, 1083 Budapest, Hungary
guarino.valentina@itk.ppke.hu

***Abstract*—Cell-cycle progression is closely coupled to cell growth, defined by increases in mass and volume. Prolonged G1 arrest leads to excessive volume growth and cytoplasmic dilution [1], disrupting density homeostasis and impairing cell-cycle re-entry [2], [3]. This dysregulation, also seen in senescent cells —a hallmark of cancer [4], [5]— may underlie long-term dormancy. To investigate this, we analyzed mass, volume, and density dynamics during G1 arrest and release in budding yeast, revealing a dependence of cell-cycle re-entry timing on arrest duration. We developed a data-driven model that captures these dynamics and can be applied to understand cancer cell reactivation.**

***Keywords*-Yeast; cell-cycle arrest; mathematical model**

I. Introduction

Osmotic balance and biosynthesis coordinate cell mass and volume to maintain growth homeostasis. Recent studies[2] highlight how cell size and dry mass become dysregulated during cell-cycle arrest, impairing recovery. However, the phenotypic drivers of re-awakening timing remain unclear. To address this, I investigated how cell growth and cell-cycle progression interact during arrest and release by varying their durations and measuring key biophysical parameters—such as volume and protein mass— over time. My results replicate known arrest dynamics[2] and uncover new features of the release phase. Building on these findings, I developed a phenomenological model that captures growth dysregulation and re-entry dynamics, and is generalizable to other systems, including arrested cancer cells

II. Results

I employed a temperature-sensitive budding yeast mutant to induce a G1 arrest via temperature shift. I set up the quantitative framework by assuming different evolving phenotypes. During an *arrested* cell-cycle state cells can be described by a cycling or arrested phenotype. During the arrest *release* regime there are two more intermediate phenotypes, the re-entered one –marking G1/S transition– and the divided one –marking S/G2M transition-. For each phenotype, the model predicts the dynamical behavior of the number of cells, volume and mass both on a cellular level and on a population level by integrating deterministic ODEs.

Acknowledgements

I would like to express my gratitude to Prof. Marco Cosentino-Lagomarsino for the invaluable guidance and support provided throughout my research endeavor.

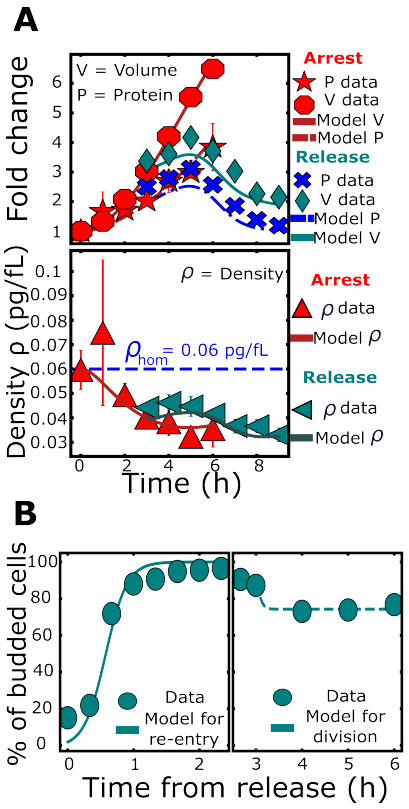

Fig. 1. A) Minimal model with volume/mass scaling during arrest and release, validated in yeast (Data for release after 3 hour arrest). During arrest, volume and mass decoupled growth leads to density decrease. During release, after an initial transient phase –marking G1/S transition– protein mass decreases faster than volume, leading to an uninterrupted density disruption. B) Reactivation follows two sequential and independent transitions, the G1/S and S/G2M ones, modeled by two Poisson processes.

References

[1] J. J. et al., "Coordination of growth with cell division in the yeast Saccharomyces cerevisiae," *Experimental Cell Research*, vol. 105, no. 1, pp. 79–98, 1977.
[2] N. G. et al., "Excessive cell growth causes cytoplasm dilution and contributes to senescence," *Cell*, vol. 176, no. 5, pp. 1083–1097, 2019.
[3] L. M. et al., "Increasing cell size remodels the proteome and promotes senescence," *Molecular Cell*, vol. 82, no. 17, pp. 3255–3269, 2022.
[4] H.-S. A. et al., "Hallmarks of cellular senescence," *Trends Cell Biol.*, vol. 28, no. 6, pp. 436–453, 2018.
[5] C. L. et al., "CDK4/6 inhibitor-mediated cell overgrowth triggers osmotic and replication stress to promote senescence," *Molecular Cell*, vol. 83, no. 22, pp. 4062—-4077, 2023.

V. GUARINO, "Quantifying the role of phenotypic variables in inducing delayed cell-cycle re-entry following stress-induced cell-cycle arrest" in *PhD Proceedings – Annual Issues of the Doctoral School, Faculty of Information Technology and Bionics, Pázmány Péter Catholic University – 2025.* G. Prószéky, G. Szederkényi Eds. Budapest: Pázmány University ePress, 2025, pp. 25–25.

Ligand-induced conformational rearrangements in postsynaptic protein domains

Borbála JAKAB
(Supervisor: Zoltán GÁSPÁRI)
Pázmány Péter Catholic University, Faculty of Information Technology and Bionics
50/a Práter street, 1083 Budapest, Hungary
jakab.borbala@itk.ppke.hu

***Abstract*—Underneath the postsynaptic membrane there are millions of proteins that make up the intricate network known as the postsynaptic density (PSD). In this research, I intend to investigate the rearrangements in the conformation concentrating on those conformation changes which were induced by ligand binding. I use the plethora of experimental structural data of postsynaptic protein domains available in the Protein Data Bank. For this research I used dimension reduction methods on conformational ensembles of our domain of interests.**

***Keywords*-PSD, domain, conformation, internal dynamics**

I. Introduction

The postsynaptic density (PSD) of excitatory synapses is a dynamic, well-organized network of both cytoplasmic and membrane proteins [1]. The generally known role of the PSD is regulating the stability of pre- and postsynaptic membranes and postsynaptic receptor organization in the postsynaptic neurons. The PSD contains many scaffolding proteins like PSD-95, Homer, Shank and GKAP. These scaffolding proteins contain many different domains with different functions. The PDZ domain is one of the common characteristics of these scaffolding proteins [2].

PDZ domains are highly conserved in both humans and yeast. PDZ domains are approximately 90 amino acids long globular protein-protein interactions domains frequently acting as scaffolds to connect various ion channels, receptors, and signaling components. Cell adhesion synaptic signaling, protein trafficking, and numerous other cellular functions are all regulated by PDZ domains, which also additionally assist to organize cellular structures and guide signaling complexes to specific regions in the cell. PDZ domains share low primary amino acid sequence similarity, however they exhibit similar folds and a common topological arrangement of important secondary structural elements [3].

PDZ domains have no enzymatic activity, their primary function is to bind C-terminal regions of their interaction partners. In addition to the β1-β2 loop, the hydrophobic cleft between the β2 strand and α2 helix is known as the ligand binding area. In the typical binding mode, the peptide ligand generates an extension to the β2 strand by a mechanism known as beta augmentation, which establishes a link between residues in the β2 sheet and α2 helix (Fig. 1.) [3].

II. Materials and Methods

The study is carried out by gradually increasing the diversity of the structures to be analyzed. With the use of the abundance of experimental data, I create a conformational ensemble of every PDZ domain dataset by performing multiple structural alignments using MAMMOTH-mult [4]. All experimental structural data was obtained from the Protein Data Bank (PDB) [5]. I used dimension reduction methods to analyze the structural ensembles. The analysis was performed with python scripts using different libraries.

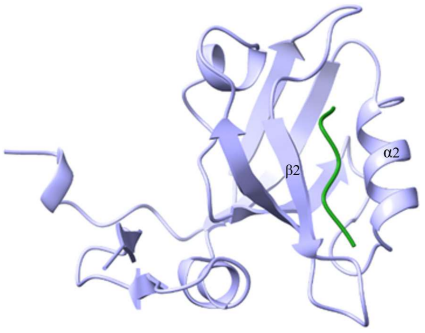

Fig. 1. The structure of the third PDZ domain of PSD-95. Purple is the PDZ domain while the green is the ligand (PDB: 1BE9).

III. Results

In order to describe the rearrangements upon ligand binding, this study aimed to utilize the plethora of structural data available for the PDZ domains by performing a comparative analysis on the structures of several PDZ domains determined under different conditions. I am currently expanding the dataset to obtain deeper understanding about the conformational changes.

Acknowledgements

I would like to express my appreciation to Mounaf Al Makhlouf for his help during the course of the analysis.

References

[1] S. Okabe, "Molecular anatomy of the postsynaptic density," *Molecular and Cellular Neuroscience*, vol. 34, no. 4, pp. 503–518, 2007.
[2] A. Dosemeci, R. J. Weinberg, T. S. Reese, and J.-H. Tao-Cheng, "The postsynaptic density: there is more than meets the eye," *Frontiers in synaptic neuroscience*, vol. 8, p. 23, 2016.
[3] D. Dudola, A. Hinsenkamp, and Z. Gáspári, "Ensemble-based analysis of the dynamic allostery in the PSD-95 PDZ3 domain in relation to the general variability of PDZ structures," *International Journal of Molecular Sciences*, vol. 21, no. 21, p. 8348, 2020.
[4] D. Lupyan, A. Leo-Macias, and A. R. Ortiz, "A new progressive-iterative algorithm for multiple structure alignment," *Bioinformatics*, vol. 21, no. 15, pp. 3255–3263, 2005.
[5] H. M. Berman, J. Westbrook, Z. Feng, G. Gilliland, T. N. Bhat, H. Weissig, I. N. Shindyalov, and P. E. Bourne, "The protein data bank," *Nucleic acids research*, vol. 28, no. 1, pp. 235–242, 2000.

B. JAKAB, "Ligand-induced conformational rearrangements in postsynaptic protein domains" in *PhD Proceedings – Annual Issues of the Doctoral School, Faculty of Information Technology and Bionics, Pázmány Péter Catholic University – 2025.* G. Prószéky, G. Szederkényi Eds. Budapest: Pázmány University ePress, 2025, pp. 26–26.

Integrated microfluidic-microwave sensors

Máté KÁLOVICS
(Supervisors: Kristóf IVÁN, Zsolt SZABÓ)
Pázmány Péter Catholic University, Faculty of Information Technology and Bionics
50/a Práter street, 1083 Budapest, Hungary
kalovics.mate@itk.ppke.hu

I. Introduction

The integration of microfluidic devices with microwave sensors represents a promising advancement in the field of lab-on-a-chip technologies. By combining the precise fluid handling capabilities of microfluidics with the high sensitivity and label-free detection features of microwave sensing, these hybrid systems enable rapid, non-invasive analysis of small-volume biological and chemical samples. This synergy opens new pathways for real-time diagnostics, environmental monitoring, and biochemical assays, where miniaturization, speed, and selectivity are critical.

II. Results

Two integrated microfluidic-microwave sensor platforms were developed which can be seen in Fig. 1 to enable *in situ* monitoring of dynamic processes within microfluidic systems. In the first configuration [1], a microfluidic mixer was integrated with a dual-band complementary double split-ring resonator (CDSRR), etched in the ground plane of a microstrip transmission line. The output channel of the mixer was aligned below the resonator's near field, enabling direct interaction between the electromagnetic field and the fluid. Through combined electromagnetic and fluid-dynamic simulations, optimal channel geometries were identified to enhance sensitivity, reduce sample volume. Transmission measurements revealed distinct frequency shifts in the first two resonances during the mixing of saline solutions with varying concentrations, enabling both real-time monitoring and chemical differentiation. The device required less than $8\mu l$ of total fluid and demonstrated the ability to unambiguously identify different chemicals by analyzing the dual-resonance frequency response.

In the second configuration [2], a pressure-sensitive microfluidic reservoir was coupled with a modified H-slot resonator, also patterned into the ground plane of a microstrip line. The microfluidic element featured a circular reservoir with a flexible membrane and tailored inlet/outlet channels. Changes in internal pressure caused membrane deformation, which altered the local electromagnetic environment and produced a measurable shift in the resonance frequency. Simulation-assisted design ensured high sensitivity across different pressure ranges. Experimental validation using distilled water demonstrated accurate pressure sensing from 0 to 2 bar with a chamber radius of 3 mm and a membrane height of 1.76 mm.

Together, these results demonstrate the versatility and effectiveness of integrating tailored microfluidic architectures with microwave resonators for real-time, label-free sensing of both fluidic composition and pressure dynamics in compact, low-volume platforms.

References

[1] M. Kálovics, K. Iván, and Z. Szabó, "Microfluidic mixing device with integrated dual-band microwave sensor," *IEEE Sensors Journal*, vol. 23, no. 14, pp. 15350–15360, 2023.
[2] M. Kálovics, P. Szolgay, K. Iván, and Z. Szabó, "Microwave resonance based lab-on-a-chip local pressure sensing," *IEEE Sensors Journal*, 2024.

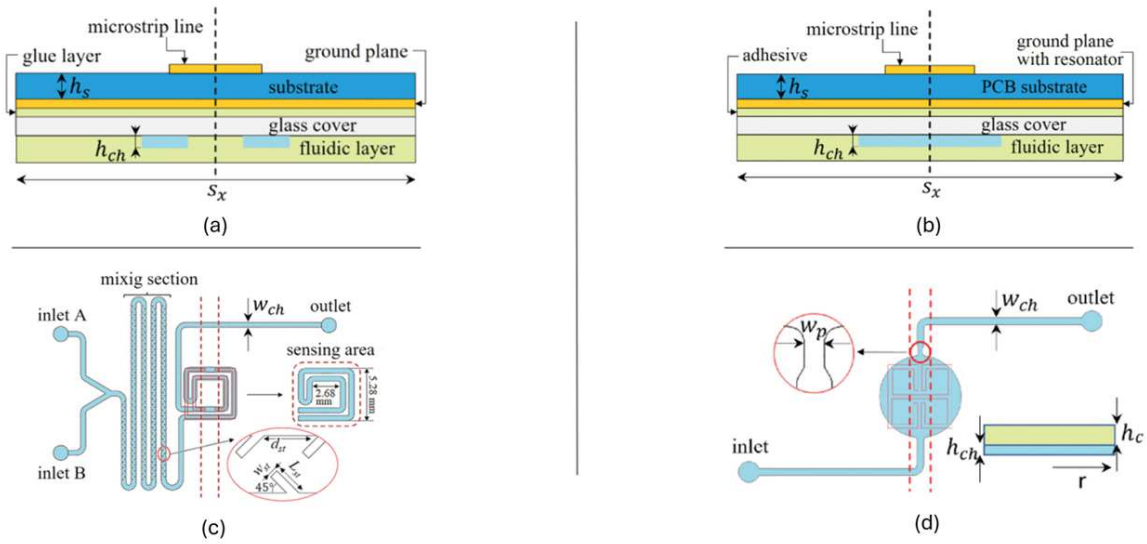

Fig. 1. Geometry of the microfluidic devices with integrated microwave sensors [1], [2]. (a) Schematic cross section of the mixing device and (c) the geometry of the fluidic layer. (b) Schematic cross section of the pressure sensing device and (d) the geometry of the fluidic layer.

M. KÁLOVICS, "Integrated microfluidic-microwave sensors" in *PhD Proceedings – Annual Issues of the Doctoral School, Faculty of Information Technology and Bionics, Pázmány Péter Catholic University – 2025.* G. Prószéky, G. Szederkényi Eds. Budapest: Pázmány University ePress, 2025, pp. 27–27.

Design approach for improving a resistor-based infrared light circuit using a transimpedance amplifier

Réka KISS
(Supervisor: Miklós KOLLER)
Pázmány Péter Catholic University, Faculty of Information Technology and Bionics
50/a Práter street, 1083 Budapest, Hungary
kiss.reka@itk.ppke.hu

***Abstract*—This project focuses on the development and implementation of a circuit designed to amplify photodiode signals using operational amplifiers (op-amps) as an alternative to resistor-based configurations. The objective was to assess the performance differences between these two amplification methods under controlled conditions, with particular emphasis on minimizing noise and ensuring signal stability. The project involved planning, circuit design with op-amp integration, reading out the raw signals using a microcontroller, and PCB design in KiCad 8.0 to design a PCB.**

***Keywords*-Near-Infrared Spectroscopy (NIRS), prosthetics, trans-impedance-amplifier (TIA)**

I. Introduction

Prosthetic control systems rely heavily on accurate and stable signal acquisition to effectively interpret user intentions and translate them into device movements. One potential modality for such systems is the use of near-infrared spectroscopy (NIRS), which can provide valuable data on muscle activity or oxygenation levels. The objective of this project was to refine a circuit design previously developed as a resistor-based system, by incorporating op-amps.

II. Methodology

The previous circuit, developed by a colleague and based on an article [1], faced multiple challenges: high resistance values were required to generate measurable voltage changes, and the ADC range was only partially utilized.

To address these limitations, the design was modified to include an op-amp for signal amplification. Based on literature findings, the photovoltaic configuration was selected [2]. Initial testing focused on evaluating signal output, ranging from oscilloscope readings to ADC microcontroller data acquisition. A testing procedure was also outlined to assess the two circuit versions under consistent conditions. The setup involves placing the circuit in a controlled dark environment, where a robotic arm moves a reflective surface inside a cardboard box reducing the impact of external ambient light.

However, despite these preparations, signal inconsistencies persisted due to wiring inaccuracies and minor ground fluctuations. Even after implementing a calibration procedure to correct for these variations, the ADC readings remained inconsistent, impacting the reliability of the measurements. As a result, the design focus shifted toward stabilizing the circuit through PCB implementation.

In the PCB design, the existing pin headers for the sensor board were retained. The op-amps were connected to standard 2.54 mm 1x2 and 2x2 pin sockets, allowing for adjustable gain settings using interchangeable resistors. Additionally, the transistor circuits controlling the LEDs were also maintained. Due to the single-layer design, multiple ground islands were created, which can later be connected using air wires. The layout was developed in KiCad 8.0 and is now prepared for systematic measurements and analysis.

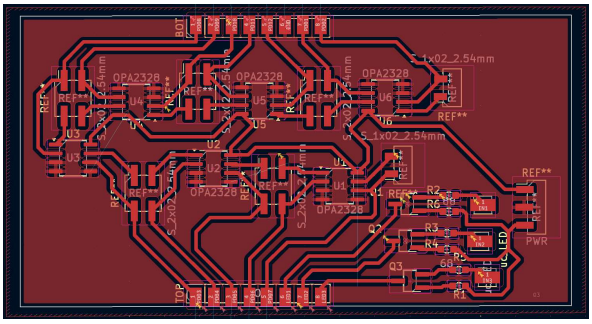

Fig. 1. The designed PCB from the PCB editor of the KiCad 8.0.

Acknowledgements

This work was supported by the Ministry of Culture and Innovation of Hungary from the National Research, Development and Innovation Fund, financed under the TKP2021-NKTA funding scheme (project no. TKP2021- NKTA-66).

The study was funded by the National Research, the Development and Innovation Office in Hungary (RRF-2.3.1-21-2022-00004).

Publications

R. Kiss, S. Földi, A. Répai, Á. Makk, Gy. Cserey, M. Koller, "First steps of creating a simulation environment in OpenSim to design a control method for a novel soft robotic exoskeleton," in 19th IEEE/RAS-EMBS International Conference on Rehabilitation Robotics (ICORR 2025), 2025

References

[1] F. Xie, S. Huang, T. Miao, S. He, Z. Lin, L. Xie, "Development of a Wireless Multichannel Near-Infrared Spectroscopy Sensor System for Monitoring Muscle Activity", IEEE Sensors Journal, vol. 22, no. 23, pp. 22714-22724, 2022

[2] D. Long (1980). Photovoltaic and photoconductive infrared detectors. In: Keyes, R.J. (eds) Optical and Infrared Detectors. Topics in Applied Physics, vol 19. Springer, Berlin, Heidelberg. https://doi.org/10.1007/3540101764_12

R. KISS, "Design approach for improving a resistor-based infrared light circuit using a transimpedance amplifier" in *PhD Proceedings – Annual Issues of the Doctoral School, Faculty of Information Technology and Bionics, Pázmány Péter Catholic University – 2025.* G. Prószéky, G. Szederkényi Eds. Budapest: Pázmány University ePress, 2025, pp. 28–28.

Barrier-on-a-chip devices for monitoring dermal drug delivery

Dorottya KOCSIS
(Supervisor: Franciska ERDŐ)
Pázmány Péter Catholic University, Faculty of Information Technology and Bionics
50/a Práter street, 1083 Budapest, Hungary
kocsis.dorottya@itk.ppke.hu

***Abstract*—Barrier-on-a-chip devices are microfluidic systems that allow the modeling of biological interfaces such as the skin, cornea, or blood-brain barrier. They are cost-effective and have the advantage of ensuring that physiological conditions are maintained through dynamic fluid flow. The smaller sample size also helps to make better use of tissues from experimental animals and to increase the use of cell cultures.**

Our research group participated in the development and validation of a microfluidic diffusion chamber that was optimized to study drug delivery through a main barrier, the skin. We applied the microfluidic devices in a number of experimental setups, such as comparing the healthy dermal barrier of several model animals and artificial in vitro tissue substitutes; studying the impairment of barrier function dermatological pathologies; and determining the transdermal penetration of three newly synthesized cytotoxic aminophosphonates.

***Keywords*-barrier-on-a-chip; transdermal drug delivery**

Summary

In living systems, barriers exist at various levels: a cell membrane, a single-cell layer, or even an entire organ can function as a boundary that separates different compartments and regulates the transport of substances across them.

The skin is the primary physical barrier of the human body, covering a surface area of nearly 2 m². It plays a crucial role in preventing the entry of pathogens and harmful substances. However, it also presents an opportunity for drug delivery. Transdermal drug administration has numerous advantages. The drug bypasses the gastrointestinal tract, thus avoiding the effect of first-pass metabolism in the liver, and can be administered without interference from enzymes, pH, and intestinal bacteria. This also helps minimizing systemic side effects and ensuring sustained release. Thanks to non-invasive delivery, self-administration is possible, leading to greater patient compliance, less pain, and elimination of possible infections. Although this route is beneficial, it is challenging due to effective barrier function, and only approximately 20 systemic medications have been approved for transdermal use.

In order to develop new transdermal formulations, drug penetration studies are needed, which involve three key elements: the device itself with the appropriate parameters and experimental conditions; the skin model used for the penetration study; and the formulation containing the active ingredient (Figure 1). The first part of this study focused on the first aspect. Biological validation of the newly developed skin-on-a-chip microfluidic diffusion chambers and optimization of the flow rate were performed [1]. The emphasis then shifted to the next aspect: the barrier model. Healthy native skin was examined in mouse strains commonly used as disease models in dermatology (namely, C57BL/6J and SKH1 mice), as such control data were not previously available in the literature [2].

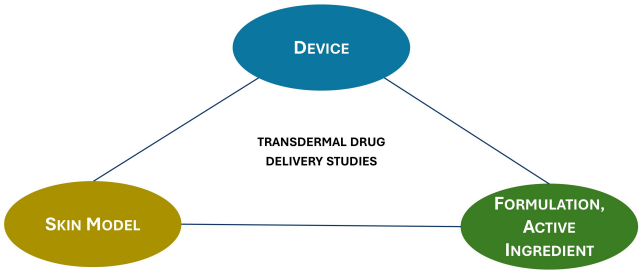

Fig. 1. The key elements in transdermal drug delivery studies.

As a step toward better translation, the comparison of ex vivo human skin samples and artificial human epidermis was performed [3]. After studying healthy conditions, attention turned to disease models and weakening of barrier function was studied in mouse models of two prevalent inflammatory skin diseases, psoriasis and allergic contact dermatitis [4], [5]. Finally, the third crucial element was considered: the active substance. Evaluation of the absorption characteristics of three recently developed aminophosphonates, was carried out, which showed cytostatic effects on tumour cell lines [6].

In conclusion, the skin-on-a-chip device has enhanced our understanding of dermatological pharmacokinetics and expanded our repertoire of reliable test methods.

References

[1] D. Kocsis, S. Dhinakaran, D. Pandey, A. J. Laki, M. Laki, D. Sztankovics, M. Lengyel, J. Vrábel, M. B. Naszlady, A. Sebestyén, J. Ponmozhi, I. Antal, F. Erdő, *Fluid dynamics optimization of microfluidic diffusion systems for assessment of transdermal drug delivery—An experimental and simulation study*, Scientia Pharmaceutica, 92:2, p. 35, 2024.

[2] D. Kocsis, F. E. Kreis, A. Fülöp, C. Pongor, A. Báthory-Fülöp, B. Bánfi, M. B. Naszlady, K. Lőrincz, R. Csépányi-Kömi, F. Erdő, *Multiparametric analysis of the skin barrier of C57BL/6J hairy and SKH1 hairless mice*, Journal of Veterinary Science and Animal Husbandry, 12:2, 2024.

[3] D. Kocsis, H. Kichou, K. Döme, Z. Varga-Medveczky, Z. Révész, I. Antal, F. Erdő, *Structural and functional analysis of excised skins and human reconstructed epidermis with confocal Raman spectroscopy and in microfluidic diffusion chambers*, Pharmaceutics, 14:8, p. 1689, 2022.

[4] D. Kocsis, S. Horváth, Á. Kemény, Z. Varga-Medveczky, C. Pongor, R. Molnár, A. Mihály, D. Farkas, B. M. Naszlady, A. Fülöp, A. Horváth, B. Rózsa, E. Pintér, R. Gyulai, F. Erdő, *Drug delivery through the psoriatic epidermal barrier—A 'skin-on-a-chip' permeability study and ex vivo optical imaging*, International Journal of Molecular Sciences, 23:8, p. 4237, 2022.

[5] G. Szederkényi, D. Kocsis, M. A. Vághy, D. Czárán, P. Sasvári, M. Lengyel, M. B. Naszlady, F. Kreis, I. Antal, R. Csépányi-Kömi, F. Erdő, *Measurement and modeling of transdermal delivery of topical drug formulations in a dynamic microfluidic diffusion chamber in health and disease*, PLOS One, 19:4, p. e0299501, 2024.

[6] D. Kocsis, P. R. Varga, R. Keshwan, M. Nader, M. Lengyel, P. Szabó, I. Antal, K. Kánai, G. Keglevich, F. Erdő, *Transdermal delivery of α-aminophosphonates as semisolid formulations—An in vitro-ex vivo study*, Pharmaceutics, 15:5, p. 1464, 2023.

D. KOCSIS, "Barrier-on-a-chip devices for monitoring dermal drug delivery" in *PhD Proceedings – Annual Issues of the Doctoral School, Faculty of Information Technology and Bionics, Pázmány Péter Catholic University – 2025.* G. Prószéky, G. Szederkényi Eds. Budapest: Pázmány University ePress, 2025, pp. 29–29.

Towards unravelling cellular regulation on the structural level: Reactome as a valuable resource for event-driven agent-based modeling of interaction networks

Szabolcs Cselgő KOVÁCS
Supervisors: Erzsébet FICHÓ, István Zoltán REGULY
Pázmány Péter Catholic University, Faculty of Information Technology and Bionics
50/a Práter street, 1083 Budapest, Hungary
kovacs.szabolcs.cselgo@itk.ppke.hu

***Abstract*—We present a processing pipeline to convert BioPAX Level-3 Reactome pathways into explicit list of cellular component interactions. Reactome organises functional redundancies into abstract entities, efficiently compressing alternative interaction scenarios into a single well-structured entity prone to combinatorial explosions in deeply nested cases. Such entities were addressed to get uncompressed and filtered by the policy of generating a comprehensive dataset of a non-perturbed, healthy cell. As a proof of concept, the MAPK cascades pathway was converted: 939 initial particles and 140 interactions populated 21794 alternative particles manifesting 21274 explicit complexes, and 15439 explicit interactions. Scaling to the whole-human cell covering data, 1127 lowest-level human pathways across 19 superpathways achieved successful conversion for 68% of pathways.**

This workflow leverages Reactome as a seed dataset for Event-Driven Agent-Based Modeling in the CYTOCAST DIGITAL TWIN Cell™ simulator, enabling genome-scale, structurally detailed simulations of cellular regulation.

***Keywords*-Agent-Based Modeling, Reactome, BioPAX, Protein-Protein Interactions, PTMs, Systems Biology**

I. Summary

The intrinsic behavior of cells is embedded in a dynamic interaction network of cellular components, which translate stimuli into cellular responses. The atomic interaction steps of a cellular response are orchestrated via regulatory events like post-translational modifications (PTM), catalytic reactions, complex formation, and degradation [1]. Modeling such cellular response scenarios presents a twofold challenge. First, appropriate mathematical models are required to effectively simulate the nonlinear interactions between cellular components. Second, a comprehensive dataset is essential that describes the qualitative and quantitative properties of the interactions between cellular components. One of the most comprehensive databases is the Reactome Knowledgebase [2], which provides a detailed description of cellular pathways and reactions in a standard file format. However, this file format stores protein complex structures in a recursively nested manner, where a complex component can be an abstract entity, grouping a pool of explicit cellular entities that can individually fulfill the same function within that context (Fig1).

Here, we propose a three-step approach to extract the functionally compressed complexes into a list of explicit complex and re-build the Reactome provided cellular regulatory interactions to a list of explicit alternative interactions. We successfully applied the conversion pipeline to 68% of 1198 lowest-level hierarchical pathways, while the remaining 32% were excluded for several reasons, including irrelevance, memory overflow, an infeasible conversion time window, or imbalanced reactions implying unhandled edge cases.

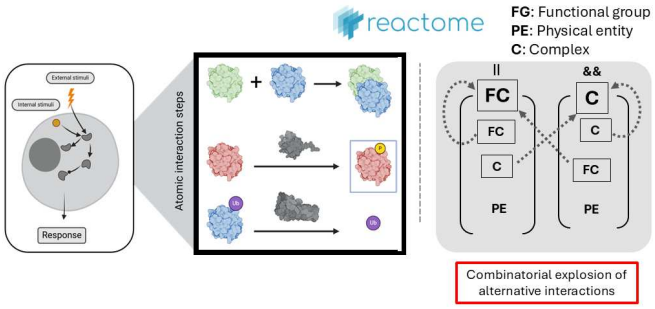

Fig. 1. To predict cellular responses upon stimuli, an annotation rich explicit list of atomic cellular interactions is required. The general concept is to recursively unpack deeply nested structures, where members within functional groups serve as an 'OR' logic and member within complexes serve as an 'AND' logic. Deeply nested structures can make some interactions prone to combinatorial explosions.

With further improvement of the conversion pipeline by leaving specific cellular components (e.g ligands, nucleotide elements) compressed can potentially serve as a valuable input dataset for Cytocast Digital Twin Cell™

Acknowledgment

This research was supported by grant number EKÖP-KDP-2024-PPKE-2 of the Ministry of Culture and Innovation through the National Research, Development, and Innovation Fund under the EKÖP-KDP program. This work was carried out using the resources of Cytocast Hungary Kft.

References

[1] P. Rangamani and R. Iyengar, "Modelling cellular signalling systems," *Essays in Biochemistry*, vol. 45, pp. 83–94, Sep. 2008.

[2] M. Milacic, D. Beavers, P. Conley, C. Gong, M. Gillespie, J. Griss, R. Haw, B. Jassal, L. Matthews, B. May, R. Petryszak, E. Ragueneau, K. Rothfels, C. Sevilla, V. Shamovsky, R. Stephan, K. Tiwari, T. Varusai, J. Weiser, A. Wright, G. Wu, L. Stein, H. Hermjakob, and P. D'Eustachio, "The Reactome Pathway Knowledgebase 2024," *Nucleic Acids Research*, vol. 52, no. D1, pp. D672–D678, Jan. 2024.

Sz. KOVÁCS, "Towards unravelling cellular regulation on the structural level: Reactome as a valuable resource for event-driven agent-based modeling of interaction networks" in *PhD Proceedings – Annual Issues of the Doctoral School, Faculty of Information Technology and Bionics, Pázmány Péter Catholic University – 2025.* G. Prószéky, G. Szederkényi Eds. Budapest: Pázmány University ePress, 2025, pp. 30–30.

Current results and challenges of high-density EMG measurements

Áron Boldizsár KÖVES
(Supervisor: Miklós KOLLER)
Pázmány Péter Catholic University, Faculty of Information Technology and Bionics
50/a Práter street, 1083 Budapest, Hungary
koves.aron.boldizsar@itk.ppke.hu

***Abstract*—Understanding the neuromuscular processes underlying human movements has long been a central issue in clinical diagnostics, as well as in movement rehabilitation and robotic applications. With the advent of high-density electromyography (HD-EMG), complex signal processing on large amounts of recorded data has made it possible to obtain detailed information about muscle function without invasive tools.**

Tensor-based signal processing can be an efficient solution for HD-EMG measurements, as it naturally fits to gridded data carrying temporal and spatial patterns. Such approaches not only allow for source separation, but also for the creation of new, meaningful representations. The question is how reliable, stable and biologically relevant these methods are in decomposing the measured signals.

***Keywords*-Electromyography, Tensor decomposition**

I. High density electromyography

HD-EMG can be seen as an extension of conventional sEMG. The large number of channels allows for spatial and temporal investigation of muscle function through electrode arrays placed on the surface. Over the last decades, the method has undergone significant developments: the number of electrodes has increased, and the accuracy of signal processing has improved. The rise of artificial intelligence has opened the door to the potential of learning-based signal processing in this field. HD-EMG enables the extraction of motor unit-level activation patterns by decomposing the signals recorded on the surface without the use of invasive needle electrodes, thus greatly contributing to the functional mapping of muscle groups and the study of neural control [1].

Of course, like all techniques, HD-EMG has limitations. The large number of channels requires complex data processing, high computational capacity, and precise electrode placement. In addition, noise sensitivity of the signals, electrical crosstalk between muscles, and variability due to individual anatomy remain significant challenges. Future research should aim to improve the portability and real-time processing of acquisition systems and increase the reliability of source separation algorithms.

II. Measurements

During the semester, the 64-channel EMG measuring device I designed and assembled during my MSc was tested (Fig. 1). The data from the measurements were used to test how the source separation algorithm I had previously implemented performed with this amount of data.

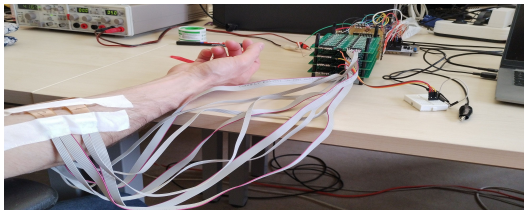

Fig. 1. EMG test measurement using the device I made

III. Tensor decomposition

Tensors are multidimensional data structures that can naturally represent complex measurement data. Tensor decomposition aims to reveal the hidden structures behind the data along some meaningful components, similar to matrix-based methods (e.g., PCA or ICA), but can also capture higher-order relations [2].

In the case of HD-EMG, tensor decomposition can be applied to separate muscle activation patterns, to separate different muscle groups, or even to identify temporal-structural features of motor control. One of the most promising applications is source separation, in which we try to reconstruct the muscle sources that underlying complex activation patterns from surface signals. The method also allows for the reduction of multidimensional redundancy, which is particularly important for large channel numbers and large sample sizes. Challenges include appropriate model selection (e.g., CANDECOMP or Tucker), stability of the fit, and interpretability of the results, especially from a biological point of view.

IV. Acknowledgements

The author would like to thank Borbála Hunyadi, Associate Professor at the Technical University of Delft, and the Signal Processing Sysem group there for their help in learning tensor decomposition algorithms.

This work was supported by the Ministry of Culture and Innovation of Hungary from the National Research, Development and Innovation Fund, financed under the TKP2021-NKTA funding scheme (project no. TKP2021-NKTA-66).

V. Publications

Á. B. Köves and M. Koller, "Development of an HD-sEMG System With Source Separation Algorithm," 2024 31st IEEE International Conference on Electronics, Circuits and Systems (ICECS), Nancy, France, 2024, pp. 1-2, doi: 10.1109/ICECS61496.2024.10848729.

References

[1] Stegeman Dick F., Kleine Bert U., Lapatki Bernd G., Van Dijk Johannes P. (2012). High-density Surface EMG: Techniques and Applications at a Motor Unit Level. Biocybernetics and Biomedical Engineering, 32(3), 3-27.

[2] Cichocki, A., Lee, N., Oseledets, I., Phan, A.H., Zhao, Q., Mandic, D. (2016). Tensor Networks for Dimensionality Reduction and Large-scale Optimization: Part 1 Low-Rank Tensor Decompositions. Foundations and Trends® in Machine Learning, 9(4–5), 249–429.

Á. KÖVES, "Current results and challenges of high-density EMG measurements" in *PhD Proceedings – Annual Issues of the Doctoral School, Faculty of Information Technology and Bionics, Pázmány Péter Catholic University – 2025.* G. Prószéky, G. Szederkényi Eds. Budapest: Pázmány University ePress, 2025, pp. 31–31.

Phage sequence identification benchmarking in a high-performance computing cluster environment

Dániel KRIZSÁN
(Supervisor: Balázs LIGETI)
Pázmány Péter Catholic University, Faculty of Information Technology and Bionics
50/a Práter street, 1083 Budapest, Hungary
krizsan.daniel@itk.ppke.hu

***Abstract*—Accurate in silico identification of bacteriophage sequences is critical for metagenomic studies and therapeutic discovery, yet the rapidly growing volume of data demands methods that scale efficiently on high-performance computing (HPC) clusters. Here, we benchmarked seven widely used "traditional" phage-detection tools (MetaPhinder, PPR-Meta, DeepVirFinder, VIBRANT, Seeker, VirSorter2, GeNomad) on a 1m contig dataset spanning soil, seawater, and human gut samples. We evaluated classification accuracy (ROC-AUC, accuracy, sensitivity, specificity, precision) across four length-categories (1.5–2kb to 10–50kb) and measured end-to-end resource consumption on an NVIDIA A100–equipped cluster. GeNomad consistently achieved the highest ROC-AUC and completed the full dataset in just over one hour on four CPU cores (12 GB RAM), underscoring that even the best current tools incur substantial computational cost—highlighting the need for next-generation, resource-efficient approaches (e.g., genomic language models or hardware-accelerated pipelines) to support truly large-scale metagenomic screening.**

***Keywords*-bacteriophages; high performance computing; benchmarking; metagenomics**

I. Introduction

The microbiome, including both human-associated and environmental microorganisms such as bacteria, fungi, and viruses, plays a pivotal role in health and disease outcomes while simultaneously driving crucial ecological processes in habitats ranging from the human gut to soil and deep-sea environments. These communities influence physiological processes, disease resistance, nutrient cycling, and ecosystem sustainability, highlighting their significance across biological and environmental sciences. Bacteriophages, integral to the virome, target bacteria within the microbiota, influencing its composition and impacting host health. These phages play crucial roles in the pathogenesis of various diseases, including inflammatory bowel disease, where phage-mediated changes in bacterial communities may exacerbate inflammatory responses.

II. Methods

In this study, we benchmarked several established tools, MetaPhinder, PPR-Meta, DeepVirFinder, Seeker, VIBRANT, VirSorter2 and Genomad, evaluating their scalability and computational efficiency in large-scale metagenomic analysis. The real-world test dataset comprised approximately 1 million metagenomic sequences from tomato soil, Antarctic seawater, and the human gut [1].

III. Conclusion

In this study, we have systematically evaluated seven established phage-detection tools on a one-million contig metagenomic dataset within a production-grade HPC environment.

TABLE I
Evaluation results for all tools. (Two methods discarded input sequences based on homology search. Rows for methods evaluated with unclassified sequences are marked with an asterisk (*)).

Accuracy	Specificity	Sensitivity	Method
0.79	0.98	0.44	VirSorter2*
0.70	0.54	0.72	VirSorter2
0.82	0.81	**0.85**	PPR-Meta
0.79	0.82	0.74	DeepVirFinder
0.56	0.51	0.64	Seeker
0.79	0.98	0.46	geNomad
0.66	0.80	0.41	MetaPhinder
0.75	**0.99**	0.32	VIBRANT*
0.67	0.95	0.57	VIBRANT
0.50	0.57	0.37	baseline

Our results confirm that all classifiers benefit substantially from longer input fragments, with modern CNN-based and hybrid methods (GeNomad, PPR-Meta, DeepVirFinder) achieving ROC-AUC values above 0.90 for contigs of length ≥ 5 kb, whereas purely homology-driven or LSTM-based approaches (MetaPhinder, Seeker) require much greater sequence length to approach comparable accuracy. We also demonstrated that deployment and resource efficiency vary dramatically: lightweight native executables such as GeNomad, VIBRANT and MetaPhinder complete analyses in under four hours on modest CPU and memory allocations, while containerized methods dependent on outdated GPU libraries incur extended runtimes, high RAM usage, and complex batch-submission overheads. Taken together, our benchmarks underline the importance of both algorithmic innovation and practical deployability when selecting phage-detection software for large-scale metagenomic screening.

Acknowledgements

I acknowledge the Digital Government Development and Project Management Ltd. for awarding us access to the Komondor HPC facility based in Hungary.

The project was supported by the National Fund for Development, Research and Innovation (NKFIH), OTKA PD (138055) and 2020-1.2.3-EUREKA-2022-00023; Ministry of Innovation and Technology, NRDI Office within the framework of the National Laboratory for Artificial Intelligence (RRF-2.3.1-21-2022-00004).

DK was supported by the National Laboratory for Artificial Intelligence Research Grant (RRF-2.3.1-21-2022-00004).

References

[1] L.-Y. Wu, Y. Wijesekara, G. J. Piedade, N. Pappas, C. P. D. Brussaard, and B. E. Dutilh, "Benchmarking bioinformatic virus identification tools using real-world metagenomic data across biomes," *Genome Biology*, vol. 25, Apr. 2024.

D. KRIZSÁN, "Phage sequence identification benchmarking in a high-performance computing cluster environment" in *PhD Proceedings – Annual Issues of the Doctoral School, Faculty of Information Technology and Bionics, Pázmány Péter Catholic University – 2025.* G. Prószéky, G. Szederkényi Eds. Budapest: Pázmány University ePress, 2025, pp. 32–32.

Investigation of the structure of mixed yeast colonies

Valentina MADÁR
(Supervisor: Attila CSIKÁSZ-NAGY)
Pázmány Péter Catholic University, Faculty of Information Technology and Bionics
50/a Práter street, 1083 Budapest, Hungary
madar.valentina@itk.ppke.hu

***Abstract*—Microbial colonies grown in solid media are structured, spatially heterogeneous communities where environmental gradients, particularly those of nutrients and oxygen, give rise to distinct ecological niches. In yeast *Saccharomyces cerevisiae* colonies, these gradients lead to pronounced metabolic stratification and cellular differentiation between different regions of the colony. This spatial organisation significantly influences cell physiology, including proliferation, respiration, autophagy, and stress responses.**

In this study, we want to explore these interactions between multiple yeast strains in a single colony. Despite their similar morphology and phenotype, these strains exhibit distinct growth dynamics depending on their position within the colony. To distinguish these strains from each other, we use a genome-integrated fluorescent tag that does not modify the natural functioning of the cells. While top-down imaging revealed the overall spatial patterns, cross-sectional analysis was necessary to resolve interactions occurring in internal and basal regions of the colony.

Even though we are experimenting with one species, our results show that different strains behave differently within the colony and this may be due to genetic differences between strains.

***Keywords*-yeast; interaction; differentiation;**

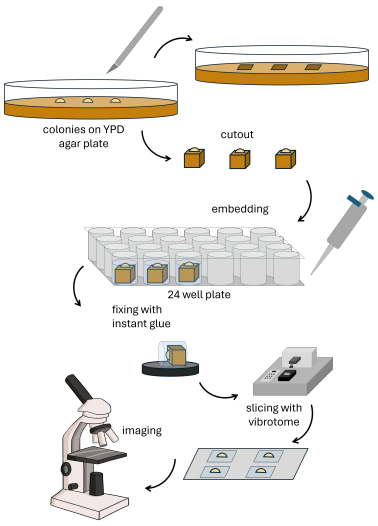

Fig. 1. Sequence of experimental methods

I. Introduction

Microbial colonies on solid substrates exhibit complex spatial organization driven by diffusion-limited gradients of nutrients and oxygen [1]. In Saccharomyces cerevisiae, this leads to the formation of distinct ecological niches within the colony, resulting in clustered cell populations with divergent metabolic activities and physiological states [2]. Lower cell layers typically experience nutrient abundance but oxygen limitation, leading to enhanced respiratory activity and ROS accumulation, whereas apical cells benefit from greater oxygen availability but limited carbon sources, resulting in elevated autophagy and localized proliferation [3].

In colonies composed of multiple yeast strains, spatial heterogeneity becomes even more pronounced. Despite similar morphology, strains may occupy distinct niches and engage in spatially resolved competition or cooperation, influenced by their metabolic capabilities, oxygen utilization, or stress tolerance [4]. However, traditional colony imaging is not able to reveal these interactions in every cases.

To observe this different strains and cell clusters, we employed a fluorescent protein-based labelling method using genomically integrated yellow fluorescent protein (YFP) and red fluorescent protein (RFP), allowing for non-invasive, strain-specific visualization during colony growth [5]. To capture vertical organization, colonies grown on YPD agar were embedded in fixing material, and transverse sections were prepared using a vibrating microtome (vibrotome). These sections were then analyzed with a fluorescence microscope, enabling precise mapping of strain localisation inside the colony (Figure 1).

Acknowledgements

The research has been supported by grant EKÖP-24-3-I-PPKE-81 of the University Research Scholarship Program of the Ministry for Culture and Innovation from the source of the National Research, Development and Innovation Fund and by grants OTKA-K20-134489 and ADVANCED-149463 of the Hungarian Scientific Research Fund.

References

[1] H. Tronnolone, A. Tam, Z. Szenczi, J. E. F. Green, S. Balasuriya, E. L. Tek, J. M. Gardner, J. F. Sundstrom, V. Jiranek, S. G. Oliver, and B. J. Binder, "Diffusion-Limited Growth of Microbial Colonies," *Scientific Reports*, vol. 8, p. 5992, Apr. 2018.

[2] M. Čáp, L. Štěpánek, K. Harant, L. Váchová, and Z. Palková, "Cell Differentiation within a Yeast Colony: Metabolic and Regulatory Parallels with a Tumor-Affected Organism," *Molecular Cell*, vol. 46, pp. 436–448, May 2012.

[3] L. Váchová and Z. Palková, "How structured yeast multicellular communities live, age and die?," *FEMS Yeast Research*, vol. 18, p. foy033, June 2018.

[4] J. A. Granek and P. M. Magwene, "Environmental and Genetic Determinants of Colony Morphology in Yeast," *PLOS Genetics*, vol. 6, p. e1000823, Jan. 2010. Publisher: Public Library of Science.

[5] W. P. Voth, J. D. Richards, J. M. Shaw, and D. J. Stillman, "Yeast vectors for integration at the HO locus," *Nucleic Acids Research*, vol. 29, p. e59, June 2001.

V. MADÁR, "Investigation of the structure of mixed yeast colonies" in *PhD Proceedings – Annual Issues of the Doctoral School, Faculty of Information Technology and Bionics, Pázmány Péter Catholic University – 2025.* G. Prószéky, G. Szederkényi Eds. Budapest: Pázmány University ePress, 2025, pp. 33–33.

A machine learning framework for evaluation of brain MRI harmonization performance

Vilmos MADARAS
(Consultant: Béla WEISS, Supervisor: Csaba BENEDEK)
Pázmány Péter Catholic University, Faculty of Information Technology and Bionics
50/a Práter street, 1083 Budapest, Hungary
madaras.vilmos@itk.ppke.hu

***Abstract*—This study systematically evaluates ComBat, CovBat, and ComBat-GAM harmonization of structural brain MRIs through a machine learning framework. Our findings reveal that harmonization effectiveness declines with multi-site data from diverse populations or when coupled with nonlinear analyses. Accordingly, they emphasize the importance of careful covariate selection and highlight the need for improved harmonization methods that address both linear and nonlinear site effects while preserving biologically relevant variation. Additionally, the proposed framework enables systematic evaluation and extension to other harmonization strategies.**

***Keywords*-Magnetic resonance imaging; Harmonization; Image quality**

I. Introduction

Multi-site data collection enables the assembly of large, diverse datasets, which are essential for developing robust machine learning models in the field of brain research. Several harmonization techniques have been developed to address site-related variations present in multi-site magnetic resonance imaging (MRI) data while also preserving biologically relevant information. However, little is known about how different methods and covariates influence harmonization effectiveness and downstream analysis.

II. Methods

We present a machine learning framework (Figure 1) to evaluate harmonization methods by comparing classifier performance on predicting the original data site of the samples using unharmonized and harmonized image quality and structural segmentation metrics derived from structural brain MRI (sMRI) measurements. We evaluated ComBat, CovBat, and ComBat-GAM, with and without covariates (age and sex, image quality label, or all three), using linear and quadratic discriminant analysis, logistic regression, support vector machines (with linear and radial basis function kernels), random forest, and extreme gradient boosting classifiers. To statistically validate the differences between the results Cohen's Kappa [1], Mcnemar [2], DeLong [3], Venkatraman [4] tests were conducted on the confusion matrices or the ROC curves.

III. Results

Using this framework, we demonstrate and statistically prove that harmonization of sMRI data significantly diminishes site classification accuracy for linear models, whereas nonlinear classifiers retain discriminative performance, regardless of the harmonization method. This indicates that nonlinear biases remain in the harmonized data. Furthermore, our results also show that incorporating biological covariates into the harmonization models reduces harmonization efficiency of sites with different demographic distributions. Taken together, our findings reveal that harmonization effectiveness may be significantly reduced in multi-site data from different populations, or when coupled with nonlinear subsequent analyses, and accordingly, emphasise the importance of careful covariate selection and highlight the need for continued development of harmonization approaches that can effectively account for both linear and nonlinear site effects without compromising biologically meaningful variations. The implemented framework provides a robust basis for systematically evaluating the performance of harmonization models and can be extended to test additional parameters, such as varying covariate configurations or novel harmonization techniques.

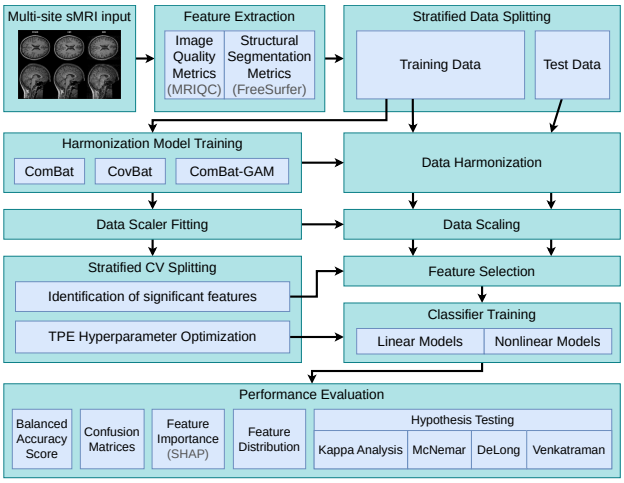

Fig. 1. The proposed machine learning framework for statistical comparison of different harmonization approaches.

Acknowledgements

The author is grateful to HUN-REN SZTAKI and HUN-REN TTK Brain Imaging Centre, particularly to Béla Weiss and Csaba Benedek for the opportunity to work on this project.

References

[1] Congalton, R.G., 1991. A review of assessing the accuracy of classifications of remotely sensed data. Remote sensing of environment, 37(1), pp.35-46.
[2] McNemar, Q., 1947. Note on the sampling error of the difference between correlated proportions or percentages. Psychometrika, 12(2), pp.153-157.
[3] DeLong, E.R., DeLong, D.M. and Clarke-Pearson, D.L., 1988. Comparing the areas under two or more correlated receiver operating characteristic curves: a nonparametric approach. Biometrics, pp.837-845.
[4] Venkatraman, E.S. and Begg, C.B., 1996. A distribution-free procedure for comparing receiver operating characteristic curves from a paired experiment. Biometrika, 83(4), pp.835-848.

V. MADARAS, "A machine learning framework for evaluation of brain MRI harmonization performance" in *PhD Proceedings – Annual Issues of the Doctoral School, Faculty of Information Technology and Bionics, Pázmány Péter Catholic University – 2025.* G. Prószéky, G. Szederkényi Eds. Budapest: Pázmány University ePress, 2025, pp. 34–34.

Comparison of optimization algorithms for finding best invariant sets in decoupled oscillatory power grid models

Gyula MOLNÁR
(Supervisors: Gábor SZEDERKÉNYI, Mihály KOVÁCS)
Pázmány Péter Catholic University, Faculty of Information Technology and Bionics
50/a Práter street, 1083 Budapest, Hungary
molnar.gyula@itk.ppke.hu

***Abstract*—This work is concerned with transient rotor angle stability of power grids: it compares optimization algorithms for determining feasible and optimal sets of angular constraints of generator nodes resulting in valid and maximal invariant sets in decoupled oscillatory power grid models.**

***Keywords*-Modeling, Electrical power systems, Stability of nonlinear systems**

I. Introduction

Renewable forms of power generation are prone to environmental uncertainties, and are less stable in general. This is because regenerative energy production means are controlled by power electronics in place of mechanical variables such as moment of inertia or friction. These are associated with less damping, hence falling behind in stability. Transient rotor angle stability is concerned with whether a power system can maintain synchronism after a major disturbance. We build on a set-based stability assessment method, which is a robust approach ensuring that if a system's state remains within a precomputed invariant set, stability is formally guaranteed.

II. Methods

The power system is modeled as interconnected second-order oscillators, the dynamics $\dot{\boldsymbol{x}} = [\dot{\delta}_i \;\; \dot{\omega}_i]$ of which are governed by the swing equations each [2]. Using the Effective Network model [3], the effect of generator interactions are captured into an oscillatory graph, which is then decomposed into smaller subsystems, treating interactions with neighboring subsystems as bounded disturbance inputs. Then, following [4], invariant sets are determined for each subsystem. For this, we rely on the theory of barriers from [4, S. 3.1], [5, S. 4], and [6].

III. Optimization Problem

We choose $\boldsymbol{z} := [\boldsymbol{\delta}_{\min}\, \boldsymbol{\delta}_{\max}]^T$ as the design variable vector, and define the goal function $f(\boldsymbol{z})$ so that it returns $(-\infty, -1]$ if $\boldsymbol{z}$ is feasible and $(-1, 0]$ otherwise, where $\boldsymbol{z}$ is considered feasible if z_i constitutes valid MRPI barriers for all non-reference generators. The optimization problem is then formulated as $\boldsymbol{z}^* = \operatorname{argmin}_{\boldsymbol{z}\in\mathbb{R}^n} f(\boldsymbol{z})$ subject to some design constraints. As for the concrete implementation of the goal function, we are considering goal functions that reward invariant set size. Two approaches to implementing such a goal function has been considered: the set area method's main metric is the resulting invariant set size, whereas the span method's is the distance between the set barrier candidates' $\omega = 0$ axis intersections. Because neither of these approaches result in a continuous objective function, we rely on gradient-free algorithms and metaheuristics such as the Nelder-Mead simplex algorithm, the pattern search method, surrogate optimization, the particle swarm approach, a genetic algorithm, and simulated annealing.

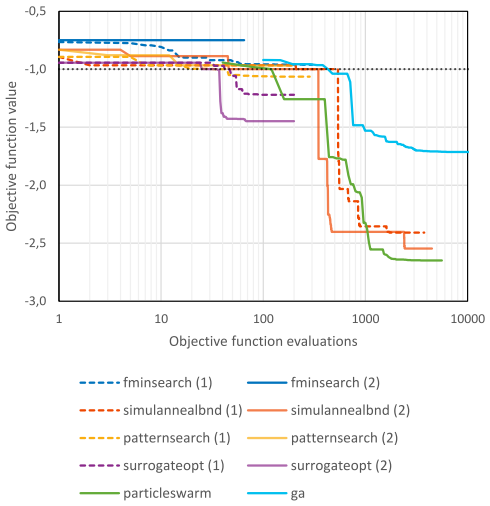

Fig. 1: Optimization performance of different solvers with the span objective function.

Acknowledgement

We would like to thank Willem ESTERHUIZEN and Tim ASCHENBRUCK of Chemnitz University of Technology, Faculty of Electrical Engineering for their contribution.

References

[1] Gy. Molnár, T. Aschenbruck, G. Szederkényi, S. Streif, "Utilizing Barrier Phases in Set-Based Transient Power Grid Stability Analysis", submitted to ICSTCC 2025.
[2] T. Nishikawa, A. E. Motter, "Comparative analysis of existing models for power-grid synchronization", *New Journal of Physics.* vol. 17 (2015).
[3] A. E. Motter, S. A. Myers, M. Anghel, T. Nishikawa, "Spontaneous synchrony in power-grid networks", *Nature Physics*, vol. 9 no. 3 (2013).
[4] T. Aschenbruck, W. Esterhuizen, S. Streif, "Transient Stability Analysis of Power Grids with Admissible and Maximal Robust Positively Invariant Sets", *Automatisierungstechnik*, vol. 68, no. 12 (2020).
[5] W. Esterhuizen, T. Aschenbruck, S. Streif, "On maximal robust positively invariant sets in constrained nonlinear systems", *Automatica*, vol. 119 (2020).
[6] J. A. Doná, J. Lévine, "On barriers in state and input constrained nonlinear systems", *SIAM Journal on Control and Optimization*, vol. 51 no. 4 (2013).

Gy. MOLNÁR, "Comparison of optimization algorithms for finding best invariant sets in decoupled oscillatory power grid models" in *PhD Proceedings – Annual Issues of the Doctoral School, Faculty of Information Technology and Bionics, Pázmány Péter Catholic University – 2025.* G. Prószéky, G. Szederkényi Eds. Budapest: Pázmány University ePress, 2025, pp. 35–35.

The influence of pretraining bias on saliency in medical image segmentation

Zsófia MOLNÁR
(Supervisor: András HORVÁTH)
Pázmány Péter Catholic University, Faculty of Information Technology and Bionics
50/a Práter street, 1083 Budapest, Hungary
molnar.zsofia@itk.ppke.hu

***Abstract*—The use of pre-trained models for 2D-stacked data in 3D-like applications, particularly in microscopy and image segmentation, has raised concerns about the potential introduction of bias into the network's predictions. A major factor influencing this bias is the reliance on pretrained models, which are often designed using large-scale image datasets like ImageNet. These models, trained primarily on natural images, may not be fully adapted to the specific needs of scientific applications such as biomedical imaging. As a result, the color channels and features learned from these generic datasets may not adequately represent the unique characteristics present in microscopy images.**

I. Introduction

In this context, the saliency map analysis plays a crucial role in identifying the areas within an image that contribute most to the model's predictions. Saliency maps highlight regions where the model focuses its attention and can reveal potential biases introduced by the pre-training process. In the case of microscopy images, the saliency map could show a preference for certain features that are not relevant to the desired biological structures. These artifacts may lead to overfitting or misclassification, where the model learns spurious patterns that do not generalize well to new data.

II. Background

The extent of this bias is particularly concerning because it can affect network performance, especially when dealing with rare or unseen patterns. For example, a pre-trained model might incorrectly weigh certain visual features that are common in natural images, such as edges or gradients, as more important than the fine details in the scientific images. This could result in poor segmentation quality, especially when the input data comes from specialized fields like tissue microscopy, where the structures and textures are vastly different from those found in natural images.

To address this issue, one potential solution is to explore non-pretrained networks that are specifically trained on domain-relevant datasets. These networks can be trained from scratch, allowing them to learn features that are more aligned with the task at hand. Additionally, approaches like fine-tuning pre-trained models on smaller, domain-specific datasets can also reduce the impact of pre-existing biases, ensuring that the network's learned features are more representative of the target data.

Another promising avenue for improvement is the use of advanced regularization techniques and data augmentation strategies that focus on mitigating the over-reliance on irrelevant features. For example, introducing noise or distortions that mimic the imperfections found in scientific imaging could help the model become more robust to these biases. Furthermore, the implementation of attention mechanisms or layer-wise analysis could enable more targeted learning, focusing on biologically relevant features while minimizing interference from irrelevant image components.

III. Discussion and Conclusion

Ultimately, understanding the bias introduced by pre-trained models is essential for improving the accuracy and reliability of 2D-stacked data applications in 3D-like contexts. By recognizing the potential issues with saliency maps and implementing solutions that either fine-tune or train networks specifically for these tasks, researchers can ensure better segmentation performance and more accurate predictions in specialized fields such as microscopy.

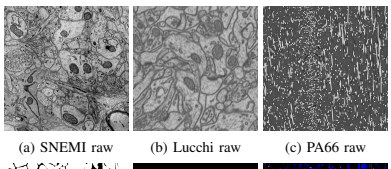

(a) SNEMI raw (b) Lucchi raw (c) PA66 raw

(d) SNEMI mask (e) Lucchi mask (f) PA66 mask

Fig. 1: Example images from three different datasets. The top row contains raw input images, while the bottom row shows their corresponding segmentation masks.

References

[1] Deng, Jia, Dong, Wei, Socher, Richard, Li, Li-Jia, Li, Kai, and Fei-Fei, Li. "ImageNet: A large-scale hierarchical image database." In *2009 IEEE Conference on Computer Vision and Pattern Recognition*, pp. 248-255. IEEE, 2009.

[2] Arganda-Carreras, Ignacio, Seung, H. Sebastian, Vishwanathan, Ashwin, and Berger, Daniel R. "SNEMI3D: 3D Segmentation of neurites in EM images." Zenodo, 2013.

[3] Lucchi, Aurélien, Smith, Kevin, Achanta, Radhakrishna, Knott, Graham, and Fua, Pascal. "Supervoxel-based segmentation of mitochondria in em image stacks with learned shape features." *IEEE Transactions on Medical Imaging* 31, no. 2 (2011): 474-486.

[4] Bertoldo, João P. C., Decencière, Etienne, Ryckelynck, David, and Proudhon, Henry. "A Modular U-Net for Automated Segmentation of X-Ray Tomography Images in Composite Materials." *Frontiers in Materials* 8 (2021): 761229. https://doi.org/10.3389/fmats.2021.761229.

[5] Zhang, Yichi, Liao, Qingcheng, Ding, Le, and Zhang, Jicong. "Bridging 2D and 3D segmentation networks for computation-efficient volumetric medical image segmentation: An empirical study of 2.5 D solutions." *Computerized Medical Imaging and Graphics* 99 (2022): 102088.

[6] Zhuang, Fuzhen, Qi, Zhiyuan, Duan, Keyu, Xi, Dongbo, Zhu, Yongchun, Zhu, Hengshu, Xiong, Hui, and He, Qing. "A comprehensive survey on transfer learning." *Proceedings of the IEEE* 109, no. 1 (2020): 43-76.

[7] Mokuwe, Mamuku, Burke, Michael, and Bosman, Anna Sergeevna. "Black-box saliency map generation using bayesian optimisation." In *2020 International Joint Conference on Neural Networks (IJCNN)*, pp. 1-8. IEEE, 2020.

Zs. MOLNÁR, "The influence of pretraining bias on saliency in medical image segmentation" in *PhD Proceedings – Annual Issues of the Doctoral School, Faculty of Information Technology and Bionics, Pázmány Péter Catholic University – 2025.* G. Prószéky, G. Szederkényi Eds. Budapest: Pázmány University ePress, 2025, pp. 36–36.

Applied deep learning techniques in fetal phonocardiography

Kristóf MÜLLER
(Supervisor: Miklós KOLLER)
Pázmány Péter Catholic University, Faculty of Information Technology and Bionics
50/a Práter street, 1083 Budapest, Hungary
muller.kristof@itk.ppke.hu

***Abstract*—Heart sound segmentation from phonocardiogram signals can be done in multiple ways, but in recent years machine learning models have shown the best robustness and accuracy. The state-of-the art is always changing, however, neural networks are the current leaders. These models are usually trained and tested on non-fetal data, but with this project we aim to show their merit to be used with fetal data. We trained a preexisting model and evaluated it on fetal data. It achieved 10.8 ms and 19.3 ms mean absolute error, 98.7% and 87.9% F1-score for the first and the second heart sounds, respectively. In the future this model can be extended with more sophisticated temporal models and trained on a larger dataset.**

I. Introduction

Segmenting the heart cycle in phonocardiograms (PCG) into heart sounds (S1-S2) and the systole-diastole regions is still under research even after the publication of the currently most widely used method of Springer *et al.* [1]. In recent years neural networks have been used to improve this method, either by replacing it completely or by extending it. Renna *et al.* in 2019 [2] published a convolutional neural network (CNN) model based on the U-net architecture which achieved better results than the previous best model. We applied their model for fetal PCG segmentation using an open source reimplementation [3].

II. Methods

The CNN architecture was realized as 4 stages of encoding blocks and 4 stages of decoding blocks, with skip connections between the encoding and decoding feature maps of the same level. Each block contained 3 convolutional layers with one-dimensional filters, ReLU activations and max-pooling. The final layer uses a softmax activation to output probabilities of a given time point being in a certain heart cycle state (S1, systole, S2, diastole). The model was trained on the CirCor DigiScope dataset, and fine-tuned for a smaller fetal dataset with a smaller learning rate. These values can be used to model the heart state and segment the heart sounds from the signal, either by taking the maximum probability or passing it into a more complex temporal modelling solution.

III. Results

On Figure 1, an example output of the model is shown superimposed on the input signal. By visual inspection these can be considered accurate, but quantitative measurement is needed. By taking the state with the maximal probability for each sample, and taking the temporal center of the heart sound segments, a mean absolute error (MAE) to the manual labels can be calculated. For our fetal dataset this method showed a 10.8±6.4 ms MAE for S1 and 19.3±12.4 ms MAE for S2. With the introduction of a tolerance parameter commonly used classification accuracy methods can be used, such as F1-score [4]. Using a 30 ms tolerance interval the F1-score of the CNN was 98.7% for S1 and 87.9% for S2.

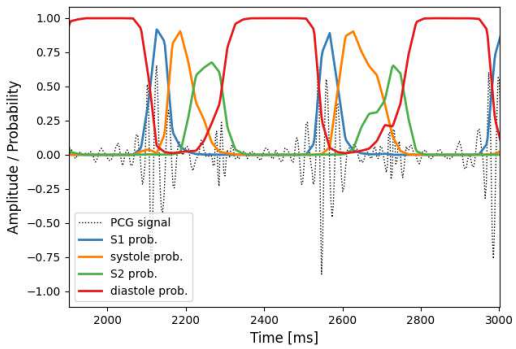

Fig. 1. Outputs of the CNN compared to a sample PCG signal

IV. Conclusions

Based on these results this CNN based segmentation, even by training on a non-fetal dataset, shows great potential. In the future training on a larger fetal dataset is planned, as well as experimenting with other temporal models, such as specialized hidden Markov models [5]. Experimenting with other neural network architectures, such as transformers, are also under consideration.

Acknowledgments

Project no. TKP2021-NVA-27 has been implemented with the support provided by the Ministry of Culture and Innovation of Hungary, financed under the TKP2021 funding scheme and from the National Research, the Development and Innovation Office in Hungary (RRF-2.3.1-21-2022-00004). I would like to express my gratitude towards Janka Hatvani and Márton Áron Goda for their extensive help during the development of this work.

References

[1] D. B. Springer, L. Tarassenko, and G. D. Clifford, "Logistic regression-HSMM-based heart sound segmentation," *IEEE Transactions on Biomedical Engineering*, vol. 63, no. 4, pp. 822–832, 2016.

[2] F. Renna, J. Oliveira, and M. T. Coimbra, "Deep convolutional neural networks for heart sound segmentation," *IEEE Journal of Biomedical and Health Informatics*, vol. 23, no. 6, pp. 2435–2445, 2019.

[3] D. Enériz, A. J. Rodriguez-Almeida, H. Fabelo, S. Ortega, F. J. Balea-Fernandez, G. M. Callico, N. Medrano, and B. Calvo, "Low-cost FPGA implementation of deep learning-based heart sound segmentation for real-time CVDs screening," *IEEE Transactions on Instrumentation and Measurement*, pp. 1–1, 2024.

[4] K. Müller, J. Hatvani, M. Koller, and M. Á. Goda, "pyPCG: a Python toolbox specialized for phonocardiography analysis," *Physiological Measurement*, vol. 45, p. 125007, dec 2024.

[5] J. Oliveira, F. Renna, T. Mantadelis, and M. Coimbra, "Adaptive sojourn time HSMM for heart sound segmentation," *IEEE Journal of Biomedical and Health Informatics*, vol. 23, no. 2, pp. 642–649, 2019.

K. MÜLLER, "Applied deep learning techniques in fetal phonocardiography" in *PhD Proceedings – Annual Issues of the Doctoral School, Faculty of Information Technology and Bionics, Pázmány Péter Catholic University – 2025.* G. Prószéky, G. Szederkényi Eds. Budapest: Pázmány University ePress, 2025, pp. 37–37.

Machine learning-based stroke segmentation in kayaking using integrated IMU and EMG data

Gábor NAGY
(Supervisors: György CSEREY, László GRAND)
Pázmány Péter Catholic University, Faculty of Information Technology and Bionics
50/a Práter street, 1083 Budapest, Hungary
nagy.gabor@itk.ppke.hu

***Abstract*—This study presents a machine learning approach to classify left and right kayak paddle strokes using combined surface electromyography (EMG) and inertial measurement unit (IMU) data. Six skilled right-handed kayakers performed on-water paddling trials across a range of stroke rates. EMG sensors recorded activity from key muscles involved in paddling, while IMUs and accelerometers mounted on the paddle and boat provided kinematic data and ground truth for stroke segmentation. A Gradient Boosted Decision Tree (GBDT) model was developed to segment stroke phases and classify stroke side with high temporal precision.**

***Keywords*-EMG sensors, IMU sensor, accelerometer, kayak stroke segmentation, time series segmentation**

I. Introduction

Wearable technologies like IMUs and EMG have revolutionized biomechanical analysis in sports, enabling detailed monitoring of complex movements such as kayaking [2]. IMUs track body segment motion with portability, and EMG reveals muscle activation patterns, together offering comprehensive insights into paddling technique [1]. Accurate classification of paddle strokes by side is critical for detecting asymmetries, optimizing performance, and reducing injury risk. This work aims to leverage these sensor modalities to segment kayak stroke phases and classify strokes in near real-time.

II. Methods

Six right-handed male kayakers participated, performing paddling sessions at controlled stroke rates from 80 to 120 strokes per minute (SPM). EMG data were recorded from seven muscles following SENIAM guidelines and normalized using on-land maximal voluntary contractions. IMU data were captured at 60 Hz using an Xsens system, with additional accelerometers on the paddle and boat to identify stroke timing and side. Data preprocessing involved filtering EMG signals [3], smoothing accelerometer data, and removing outlier strokes based on stroke timing parameters, resulting in 1384 valid strokes from 24 runs after excluding low-quality data. Stroke phases were segmented using paddle and boat accelerometer signals to determine propulsion and recovery periods. Two classifiers were compared: a baseline Gaussian Naive Bayes and a Gradient Boosted Decision Tree (GBDT) model, trained and validated via grouped cross-validation to prevent data leakage and ensure generalizability across athletes and intensities.

III. Results

The Gradient Boosted Decision Tree (GBDT) classifier outperformed the Gaussian Naive Bayes baseline, achieving a test accuracy of 95.14% compared to 92.86%. This improvement was statistically significant according to McNemar's test ($p = 0.00$), confirming the robustness of the more complex model in classifying left and right kayak strokes on a per-sample basis. The use of grouped cross-validation ensured that data from the same run were kept separate between training and validation, enhancing the reliability of the performance estimates and demonstrating generalizability across different athletes and stroke intensities. Per-subject results showed variability: the GBDT improved accuracy by 2–4.5% over Naive Bayes for four athletes, but for two, differences were minimal or favored Naive Bayes 1. This suggests GBDT better captures individual stroke nuances, though simpler models may suffice for some. Both classifiers performed best between 20–80% of the stroke cycle, where movements are more consistent. Accuracy dropped sharply near stroke start, down to 35%, highlighting the challenge of classifying early stroke phases and the potential need for enhanced features or sensors. Temporal precision was assessed by comparing predicted stroke onsets to the ground truth onsets. The GBDT model achieved a median onset error of 21 ms, with 90% of predictions within 64 ms, supporting its use in real-time feedback like coaching systems. It tended to predict stroke onset slightly late in about 69% of cases, reflecting a conservative bias. Subject-level accuracy varied, with the best athlete averaging an 8.5 ms error and the worst at 54.7 ms. This suggests personalized models could improve performance. Overall, the GBDT classifier reliably segments kayak strokes with high accuracy and temporal precision, making it suitable for performance monitoring and technique analysis where timely detection is critical.

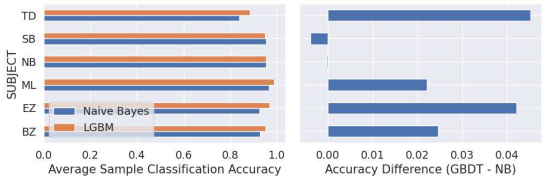

Fig. 1. Sample classification accuracy among the 6 subjects and difference between Naive Bayes classifier and Gradient Boosting Decision Trees

References

[1] L. Liu, H. Wang, S. Qiu, Y. Zhang, and Z.-D. Hao, *Paddle Stroke Analysis for Kayakers Using Wearable Technologies* Sensors, vol. 21, no. 3, 2021.
[2] McDevitt, S., Hernandez, H., Hicks, J., Lowell, R., Bentahaikt, H., Burch, R., Ball, J., Chander, H., Freeman, C., Taylor, C., Anderson, B. *Wearables for Biomechanical Performance Optimization and Risk Assessment in Industrial and Sports Applications* Bioengineering (Basel, Switzerland), 9(1), 33. (2022)
[3] Reaz M.B.I., Hussain M.S., Mohd-Yasin F. *Techniques of EMG signal analysis: detection, processing, classification and applications* Biological Procedures Online volume 8, 11–35 (2006).

G. NAGY, "Machine learning-based stroke segmentation in kayaking using integrated IMU and EMG data" in *PhD Proceedings – Annual Issues of the Doctoral School, Faculty of Information Technology and Bionics, Pázmány Péter Catholic University – 2025.* G. Prószéky, G. Szederkényi Eds. Budapest: Pázmány University ePress, 2025, pp. 38–38.

The role of extracellular vesicles in BRAF and MEK inhibitor resistance

Afrodité NÉMETH
(Supervisor: Tamás Márton GARAY)
Pázmány Péter Catholic University, Faculty of Information Technology and Bionics
50/a Práter street, 1083 Budapest, Hungary
nemeth.afrodite@itk.ppke.hu

***Abstract*—Extracellular vesicles (EVs) are nanosized, lipid bilayer-enclosed particles secreted by basically all cell types under both physiological and pathological conditions. They play pivotal role in intercellular communication and are increasingly recognized as key modulators of cancer progression. Based on our previous findings, EVs can enhance melanoma cell migration even under BRAF inhibitor (BRAFi) treatment. However, this effect appears attenuated when BRAF and MEK inhibitors are administered in combination. A limitation of the previous model was the absence of MEK inhibitor resistance. In this study, we established a melanoma cell line resistant to both encorafenib (BRAFi) and binimetinib (MEKi) and examined the contribution of EVs to therapy resistance in this novel model system. The resistant clone exhibited phenotypic alterations consistent with epithelial-to-mesenchymal transition (EMT), including a more elongated morphology and reduced circularity. Compared to the parental line, resistant cells displayed decraseased proliferative and migratory capacity, while EV production—particularly lipid content—was markedly increased. Although direct transfer of resistance via EVs could not be demonstrated in proliferation assays, pretreatment with EVs prior to BRAFi-MEKi administration led to enhanced cell migration. These findings suggest that EVs may mediate therapy resistance not solely by encapsulating drugs or drug efflux transporters, but by transferring complex, time-dependent molecular signals to drug-sensitive cells.**

***Keywords*-extracellular vesicles, melanoma, vemurafenib, dabrafenib, trametinib, single cell migration**

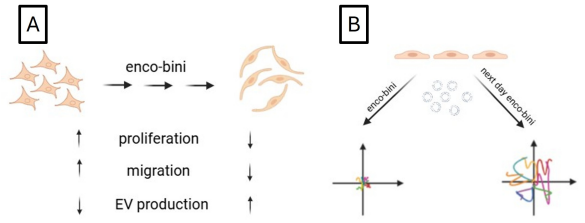

Fig. 1. Graphical Abstract. A) Comparison of parental and enco–bini–resistant cell line characteristics. Resistant clones display an elongated morphology, reduced proliferation and migration capacities, and increased extracellular vesicle (EV) production.; B) Simultaneous treatment with EVs and BRAF–MEK inhibitors did not enhance migration, whereas EV pretreatment prior to drug exposure partially restored migratory capacity.

I. Introduction

Melanoma is the most aggressive form of skin cancer, with a five-year survival rate dropping from over 90% in localized disease to around 16% in metastatic cases. Activating BRAF mutations occur in approximately 50% of melanomas and are targeted by selective inhibitors such as vemurafenib, dabrafenib, or encorafenib, often combined with MEK inhibitors like binimetinib to delay resistance. Despite improved outcomes with dual therapy, resistance inevitably develops [1]. Extracellular vesicles (EVs) have been implicated in tumor progression and drug resistance [2]. Here, we investigated whether EVs from resistant melanoma cells promote therapy resistance in a model generated through long-term dual BRAF–MEK inhibition.

II. Methods

The characteristics of enco–bini–resistant clones, including proliferation, migration, cell size, and morphology, were assessed. EVs isolated from parental and resistant cells were quantified for protein, lipid, and particle content using Qubit fluorometry, SPV assay, and NTA. To evaluate EV function in therapy resistance, cells were either co-treated with EVs and drugs or pretreated with EVs before drug exposure. Proliferation and migration assays were performed to determine whether EVs enhanced survival or motility under drug pressure.

III. Results and Summary

The encorafenib-binimetinib-resistant clone exhibited distinct phenotypic alterations, including elongated morphology accompanied by decreased cell proliferation and migration, and elevated EV production. While EV-mediated transfer of resistance was not evident in proliferation-based assays, pretreatment with EVs prior to dual inhibitor administration led to a marked increase in cell migration. These findings indicate that EVs may contribute to resistance through mechanisms that extend beyond passive drug sequestration. Instead, EVs may convey biologically active molecules that prime sensitive cells for a resistant phenotype, though this requires time for uptake and downstream signaling.

IV. Acknowledgements

This research was supported by the EKÖP-24-3-II-PPKE-85 grant.

References

[1] L. Skudalski, R. Waldman, P. E. Kerr, and J. M. Grant-Kels, "Melanoma: An update on systemic therapies," *Journal of the American Academy of Dermatology*, 2022.

[2] A. Németh, G. L. Bányai, N. K. Dobos, T. Kós, A. Gaál, Z. Varga, E. I. Buzás, D. Khamari, M. Dank, I. Takács, A. M. Szász, and T. Garay, "Extracellular vesicles promote migration despite BRAF inhibitor treatment in malignant melanoma cells," *Cell communication and signaling*, 2024.

A. NÉMETH, "The role of extracellular vesicles in BRAF and MEK inhibitor resistance" in *PhD Proceedings – Annual Issues of the Doctoral School, Faculty of Information Technology and Bionics, Pázmány Péter Catholic University – 2025.* G. Prószéky, G. Szederkényi Eds. Budapest: Pázmány University ePress, 2025, pp. 39–39.

Comparative evaluation of hemispheric cerebral blood flow using MR perfusion and phase contrast MRI in ischemic stroke patients

Bence NÉMETH
(Supervisor: András HORVÁTH)
Pázmány Péter Catholic University, Faculty of Information Technology and Bionics
50/a Práter street, 1083 Budapest, Hungary
nemeth.bencze@itk.ppke.hu

***Abstract*—This study evaluates the correlation between hemispheric cerebral blood flow (CBF) derived from dynamic susceptibility contrast (DSC) perfusion MRI and phase contrast (PC) MRI using NOVA. Eighteen patients with ischemic stroke underwent both modalities. CBF maps were processed using oSVD deconvolution and FreeSurfer-based hemisphere segmentation. NOVA-derived flow values were calculated in ACA, MCA, and PCA arteries per hemisphere.**

Perfusion-based CBF averaged 218 mL/min, while NOVA values averaged 273 mL/min. A moderate but significant correlation was observed (Pearson $r = 0.546$, $p < 0.0001$). Results suggest that although NOVA overestimates CBF and shows greater variability, it provides complementary macrocirculatory information. The combination of microvascular (DSC) and macrovascular (PC-MRI) techniques may improve cerebrovascular assessment.

***Keywords*-phase contrast MRI, MR perfusion imaging, , quantitative MRI, NOVA, ischemic stroke, cerebral blood flow**

I. Introduction

Accurate cerebral blood flow (CBF) assessment is critical in stroke. DSC perfusion estimates microvascular flow, while PC-MRI with NOVA measures arterial flow macroscopically. This study compares hemispheric CBF from both methods in stroke patients.

II. Methods

Eighteen stroke patients underwent 3T MRI with both DSC perfusion and PC-MRI. Perfusion maps were processed using oSVD (Olea Sphere), and hemispheric ROIs were extracted via FreeSurfer segmentation.

PC-MRI was acquired using NOVA (VasSol Inc.), which uses ECG-gated 2D phase contrast sequences aligned to TOF angiograms. Flow was measured in ACA, MCA, and PCA segments per hemisphere. Total hemispheric flow was computed by summing these values. CBF maps were coregistered to anatomical space for voxel-wise analysis. Pearson correlation was used to compare perfusion- and NOVA-derived hemispheric CBF.

III. Results

Of the 18 enrolled patients, 16 provided usable datasets. Mean perfusion CBF was 218 mL/min (SD: 106), and NOVA-derived CBF was 273 mL/min (SD: 162). Pearson correlation between the methods was moderate but significant ($r = 0.546$, $p < 0.0001$), indicating a physiological relationship between micro- and macrovascular flow.

NOVA values were higher in all patients but varied individually. The difference appeared greater on infarcted sides.

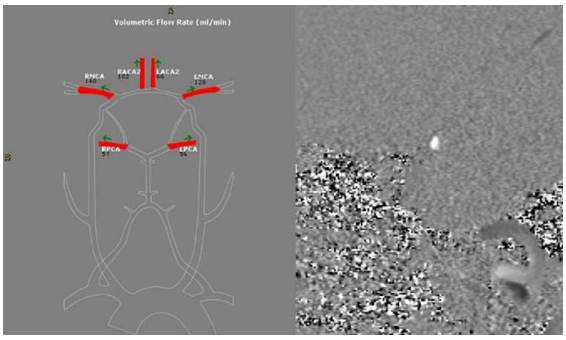

Fig. 1. Left: Flow measurements in major intracranial arteries. Right: Phase contrast image.

Notably, in cases with large infarcts, both modalities showed reduced ipsilateral flow, while smaller infarcts showed symmetry.

Intra-individual comparison between infarcted and contralateral hemispheres revealed high symmetry in perfusion-derived CBF (Pearson $r = 0.956$), but only moderate correlation in NOVA (Pearson $r = 0.587$), suggesting greater variability in large-vessel flow, particularly after stroke.

IV. Conclusion

PC-MRI using NOVA moderately correlates with DSC-derived CBF and offers a contrast-free option for assessing cerebral hemodynamics. Complementary use is recommended.

V. Discussion

These findings suggest that NOVA may be particularly useful in cases where contrast administration is contraindicated or longitudinal non-invasive monitoring is needed. Additionally, inter-hemispheric asymmetries in NOVA-derived flow may serve as a surrogate marker for large-vessel pathology, warranting further investigation in chronic stroke and vascular dementia populations.

VI. Acknowledgements

Support from the Department of Neuroradiology at the University Hospital Zürich and the Clinical Neuroscience Center is gratefully acknowledged.

References

[1] Shakur, S.F., Amin-Hanjani, S., Bednarski, C., Du, X., Aletich, V.A., Charbel, F.T., Alaraj, A., *Intracranial blood flow changes after extracranial carotid artery stenting*, Neurosurgery, vol. 76, no. 3, pp. 330–336, 2015.

B. NÉMETH, "Comparative evaluation of hemispheric cerebral blood flow using MR perfusion and phase contrast MRI in ischemic stroke patients" in *PhD Proceedings – Annual Issues of the Doctoral School, Faculty of Information Technology and Bionics, Pázmány Péter Catholic University – 2025.* G. Prószéky, G. Szederkényi Eds. Budapest: Pázmány University ePress, 2025, pp. 40–40.

Estimating visual acuity in cat visual cortex

Ábel PETIK
(Supervisors: Dániel HILLIER, István ULBERT)
Pázmány Péter Catholic University, Faculty of Information Technology and Bionics
50/a Práter street, 1083 Budapest, Hungary
petik.abel@itk.ppke.hu

***Abstract*—Visual acuity is a fundamental measure of visual system function, yet traditional assessment methods are limited in scope and applicability, especially in non-verbal subjects. Here, I use functional ultrasound imaging (fUSI) to map spatial frequency tuning across early visual cortex in the anesthetized cat, providing high-resolution, cortical-level acuity profiles. My results reveal a systematic reduction in cortical activation with increasing spatial frequency, offering a novel approach to assess both central and peripheral visual processing.**

***Keywords*-functional ultrasound imaging; visual acuity**

I. Introduction

Visual acuity, the spatial resolution of the visual system, is a key indicator of visual health. As such, its measurement is a fundamental tool in the diagnosis and monitoring of conditions affecting vision. The standard approach for assessing acuity in humans involves the Snellen chart, a method favored for its simplicity and widespread availability. However, its reliance on verbal or symbolic responses limits its applicability in non-verbal populations, such as young children and animals. In these cases, visual evoked potentials (VEPs) offer an alternative, as they do not depend on active subject participation.

While traditional measures focus on the highest spatial frequency discernible by the visual system, often corresponding to foveal acuity, they provide limited insight into the broader spatial resolution profile across the visual cortex. A more comprehensive approach would involve mapping visual acuity across cortical areas, enabling assessment of peripheral as well as central visual processing.

I apply functional ultrasound imaging (fUSI) to map visual acuity in early visual cortex of the cat at high resolution [1].

II. Methods

The functional mapping experiment was carried out using fUSI in an anesthetised cat. In preparation for the imaging experiment, a cranial window was created in the animal's skull to aid the propagation of the ultrasound waves to the target brain tissue. A 12 MHz ultrasound transducer was mounted on the head of the animal using a custom motorized holder. Imaging framerate was 2 Hz throughout the experiment.

Visual stimuli were presented on a large screen in front of the animal. They consisted of a flickering checkerboard pattern with different spatial frequencies, as illustrated in Figure 1, inverting at 5 Hz. Each spatial frequency was presented 10 times, with each repetition consisting of a 5 second pre-baseline period, when the screen was grey, then 4 seconds of stimulation, lastly 10 seconds of post-baseline.

The analysis steps of the created recording are the following. First, a baseline correction is applied on each repetition, then the 5 second periods before and after stimulation onset are sampled, and a Mann-Whitney U test is used to determine significant activation for a given pixel.

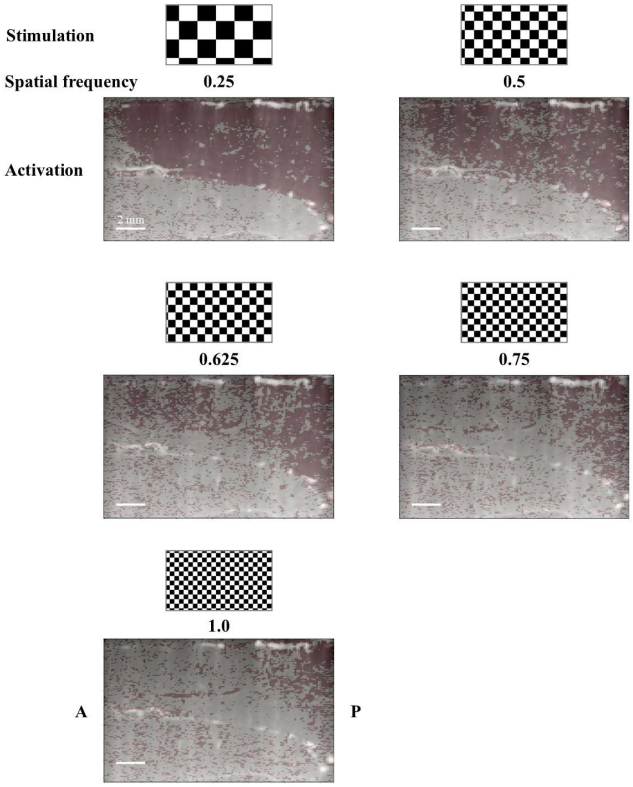

Fig. 1. Activation of the visual cortex to flickering checkerboards with different spatial frequencies given in cycles/visual degrees. Scale bars 2 mm. A: Anterior, P: Posterior

III. Results and Discussion

The data presented in Figure 1 shows that as the spatial frequency of the stimulation increases, the activated area of the visual cortex becomes smaller. As expected, the activation recedes toward the posterior edge of the field of view, which corresponds to the area centralis in the visual field, based on our retinotopy mapping data (not shown).

The mapping of visual acuity throughout the visual cortex will help in understanding the effects of visual conditions.

Acknowledgements

Supported by grants 2019-2.1.7-ERA-NET-2021-00047, ELKH-POC-2021-026, the Lendület ("Momentum") Programme of the Hungarian Academy of Sciences to Daniel Hillier.

References

[1] E. Macé, G. Montaldo, I. Cohen, M. Baulac, M. Fink, and M. Tanter, "Functional ultrasound imaging of the brain," *Nature Methods*, vol. 8, pp. 662–664, Aug. 2011.

Á. PETIK, "Estimating visual acuity in cat visual cortex" in *PhD Proceedings – Annual Issues of the Doctoral School, Faculty of Information Technology and Bionics, Pázmány Péter Catholic University – 2025.* G. Prószéky, G. Szederkényi Eds. Budapest: Pázmány University ePress, 2025, pp. 41–41.

Characterization of electromyogram regularity by entropy-based approach

Balázs RADELECZKI
(Supervisor: József LACZKÓ)
Pázmány Péter Catholic University, Faculty of Information Technology and Bionics
50/a Práter street, 1083 Budapest, Hungary
radeleczki.balazs@itk.ppke.hu

This study explores the use of Sample Entropy (SampEn) as a scalar metric to quantify the regularity of surface electromyography (EMG) signals, aiming to assess muscle activation quality during gait rehabilitation. The outcomes are compared with clinical measures. The novelty of the work lies in applying SampEn to EMG data from two individuals with incomplete spinal cord injury (iSCI) who underwent conventional gait rehabilitation combined with a hybrid Functional Electrical Stimulation (FES) cycling training.

The two participats, P3 and P7 (ages P3: 63 and P7: 46) received 2 × 30-minute hybrid FES cycling sessions per week in addition to standard therapy. Five lower limb muscles: *Rectus Femoris* (RF), *Vastus Lateralis* (VL), *Vastus Medialis* (VM), *Semitendinosus* (Smt), *Biceps Femoris* (BF) were recorded by electromyogrphy and processed through standard filtering, rectification, and smoothing techniques. Gait cycles were identified using heel marker data from a VICON motion capture system. SampEn was computed on time-normalized EMG envelopes using optimized parameters (m = 2, r = 0.4).

Clinical assessments (ASIA, SCIM III, WISCI, and 10-meter walk test) showed substantial functional improvement in P3, including a transition from walker-assisted to independent walking. P7 had a better baseline condition, exhibited moderate gains, primarily in walking speed. See Table I. These outcomes were reflected in the SampEn results: P3 showed a consistent decrease in entropy values, indicating improved regularity in muscle activation. See Fig. 1. In contrast, P7's entropy values remained low and stable, with no clear trend. See Fig. 2.

This case study supports the feasibility of using Sample Entropy as a biomechanical marker for muscle activation regularity in SCI rehabilitation. While promising, further research with larger cohorts and control groups is needed to validate its clinical utility.

TABLE I
CLINICAL SCORES AND VALUES OF CLINICAL TESTS BEFORE AND AFTER THE HYBRID FES CYCLING TRAINING

	P3		P7	
Clinical Assessments	week 0.	week 12.	week 0.	week 12.
ASIA	C	D	D	D
SCIM III.	9	20	20	20
WISCI	25	39	39	40
10-m walking [cm]	15	103	90	136
Supplementary tool	walker	none	none	none

ACKNOWLEDGMENTS

I would like to express my gratitude to the HUN-REN Wigner Research Centre for Physics, National Institute for Medical Rehabilitation, and University of Pécs for providing me the instrumental and professional support and knowledge to my studies.

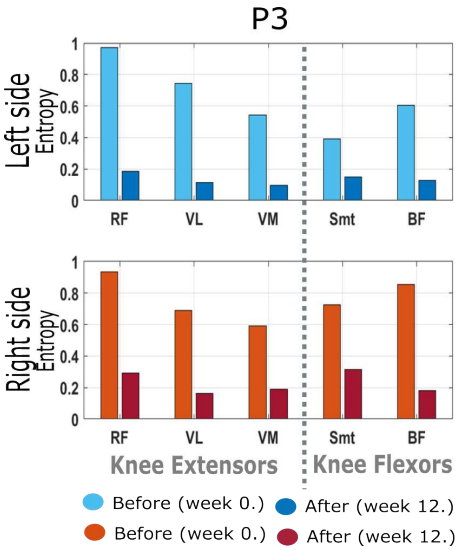

Fig. 1. Sample Entropy values of P3 participants before and after the training. For each muscle, the entropy of the average EMG envelopes decreased, so the regularity of the signals increased.

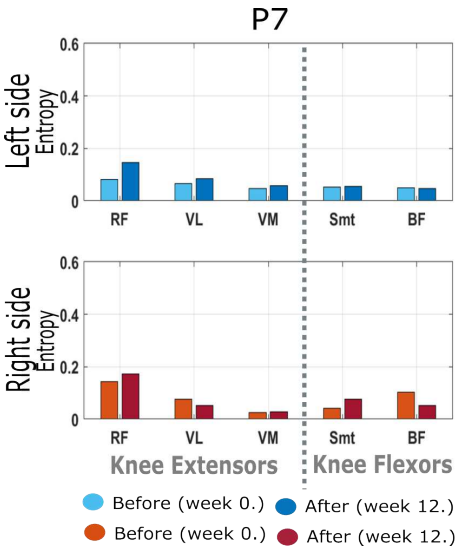

Fig. 2. Sample Entropy values of P7 participants before and after the training. There was not any general trend in his sample entropy values. Its must to note, that his entropy values stayed low during the whole training.

B. RADELECZKI, "Characterization of electromyogram regularity by entropy-based approach" in *PhD Proceedings – Annual Issues of the Doctoral School, Faculty of Information Technology and Bionics, Pázmány Péter Catholic University – 2025.* G. Prószéky, G. Szederkényi Eds. Budapest: Pázmány University ePress, 2025, pp. 42–42.

Preliminary case study: comparing psychophysiological responses of a borderline and an OCD patient during the Rorschach inkblot test

Péter SZABÓ
(Supervisors: Katalin CSIGÓ, György CSEREY)
Pázmány Péter Catholic University, Faculty of Information Technology and Bionics
50/a Práter street, 1083 Budapest, Hungary
szabo.peter@itk.ppke.hu

***Abstract*—This preliminary report compares psychophysiological responses during the Rorschach inkblot test between two patients: one with Borderline Personality Disorder (BPD), and one with Obsessive-Compulsive Disorder (OCD). Skin conductance (GSR) and eye-tracking (ET) were recorded during testing. The findings reveal distinct patterns of physiological and attentional responses between the two diagnostic groups.**

***Keywords*-Rorschach test; skin conductance; eye tracking**

I. Introduction

The Rorschach inkblot test has long been used to explore underlying cognitive and emotional processes in psychiatric populations. Despite ongoing debates about its diagnostic validity, recent advances in psychophysiological tools offer new ways to quantify subjective responses [1] [2] [3] [4]. This study explores how two distinct psychiatric profiles - Borderline Personality Disorder (BPD) and Obsessive-Compulsive Disorder (OCD) - differ in their physiological and attentional engagement during the Rorschach test.

II. Methods

Two female patients were assessed: BPD (30 y/o) and OCD (23 y/o). The Rorschach test was digitally administered while GSR (Shimmer 3 GSR+) and ET (SmartEye AI-X) data were collected via iMotions 10.1. Baseline and recovery rest periods bracketed the test. Due to small ample, only descriptive statistics could stated.

III. Results

GSR: BPD showed markedly elevated electrodermal activity across all phases (e.g., avg. amplitude: 0.23 vs. 0.04 OCD, measured in microsiemens). Even in rest phases, BPD patient displayed higher arousal (e.g., Rest 1: 0.16 BPD vs. 0.02 OCD, measured in microsiemens).

Eye Tracking: OCD patient made more fixations and saccades per minute, consistent with over-controlled scanning. BPD showed fewer but longer fixations on chromatic (emotionally charged) cards, reflecting sustained emotional attention.

Rorschach Content: BPD provided more color-based and white-space answers, reflecting affective intensity and impulsivity. OCD responses reflected detail-focus and cognitive rigidity.

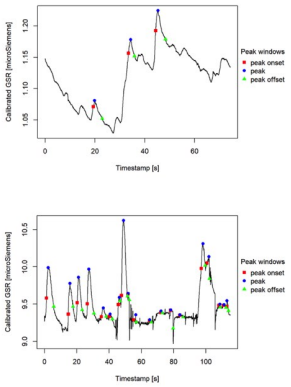

Fig. 1. Figure 1. presents GSR charts for the two participants. The upper image belongs to the patient with OCD, the lower to the patient with BPD.

IV. Discussion

These results align with existing literature: BPD patients exhibit affective hyper-reactivity and heightened autonomic responses, while OCD individuals display hypervigilance with minimal physiological arousal. Eye-tracking data further support attentional divergence—OCD shows fragmented scanning, BPD shows emotional dwell.

Acknowledgements

Project no. TKP2021-NVA-27 has been implemented with the support provided by the Ministry of Culture and Innovation of Hungary from the National Research, Development and Innovation Fund, financed under the TKP2021 funding scheme.

Project RRF-2.3.1-21-2022-00004 has been implemented provided by the Ministry of Culture and Innovation of Hungary from the National Research, Development and Innovation Fund.

References

[1] K. Csigó, "A Rorschach-teszt klinikai alkalmazása," *Medicina Könyvkiadó Zrt*, 2018.
[2] J. E. Exner Jr, *The Rorschach: A comprehensive system: Basic foundations, Vol. 1*. John Wiley & Sons, 1993.
[3] F. Mérei, *A Rorschach-próba*. Medicina Könyvkiadó Zrt, 2002.
[4] J. L. Mihura, G. J. Meyer, N. Dumitrascu, and G. Bombel, "The validity of individual Rorschach variables: systematic reviews and meta-analyses of the comprehensive system.," *Psychological bulletin*, vol. 139, no. 3, p. 548, 2013.

P. SZABÓ, "Preliminary case study: comparing psychophysiological responses of a borderline and an OCD patient during the Rorschach inkblot test" in *PhD Proceedings – Annual Issues of the Doctoral School, Faculty of Information Technology and Bionics, Pázmány Péter Catholic University – 2025.* G. Prószéky, G. Szederkényi Eds. Budapest: Pázmány University ePress, 2025, pp. 43–43.

Protein embeddings for target prediction

János SZALMA

(Supervisors: Attila CSIKÁSZ-NAGY, Erzsébet FICHÓ)
Pázmány Péter Catholic University, Faculty of Information Technology and Bionics
50/a Práter street, 1083 Budapest, Hungary
janos.szalma@itk.ppke.hu

***Abstract*—Accurate prediction of protein–ligand interactions is essential for drug discovery, but traditional simulation-based methods remain too slow and structure-dependent for large-scale applications. Recent advances in protein language models (PLMs) offer an efficient alternative by generating high-dimensional embeddings directly from amino acid sequences. In this study, we compare two such models: ESM-2 (650M parameters) and the newer, more compact ESM-C (600M parameters) to understand how compression affects protein representations. Using a dataset of 7,400 druggable human proteins, we generated sequence embeddings from both models and evaluated their similarity, structure, and variance. Principal component analysis showed that ESM-C compresses the embedding space significantly, concentrating variance in fewer dimensions. These results suggest that ESM-C trades off some of the nuanced structural information captured by ESM-2 in exchange for efficiency, which may be beneficial for broad screening tasks but limiting for fine-grained functional predictions. This comparison highlights the importance of understanding embedding geometry when choosing or deploying PLMs in drug-target prediction pipelines.**

***Keywords*-deep-learning; protein embeddings; drug discovery**

I. Introduction

Predicting how small molecules bind to proteins is a fundamental challenge in drug discovery. Traditional computational methods, such as molecular docking and molecular dynamics, can model protein-ligand interactions in detail but are often limited by their high computational cost and dependency on accurate 3D structures, which are not always available for all targets.

In recent years, deep learning–based approaches have emerged as a powerful alternative. In particular, protein language models (PLMs) trained on massive datasets of protein sequences have shown the ability to learn biologically meaningful representations without the need for structural input.

Among PLMs ESM-2 [1] has become a popular choice due to its strong performance across multiple biological tasks. A more recent variant, ESM-C [1], offers similar capabilities in a more compact model, optimized for speed and resource efficiency. However, it remains unclear to what extent this efficiency affects the quality of the learned embeddings. In this work, we directly compare the embeddings produced by ESM-2 and ESM-C to evaluate their structural complexity and information content.

II. Methods

We analyzed 7,400 proteins from the human druggable proteome, selected to reflect relevant targets in biomedical research. Sequences and protein family information were retrieved from UniProt. We generated fixed-length embeddings for each protein using frozen versions of ESM-2 (650M parameters) and ESM-C (600M parameters), with mean pooling applied over residue-level outputs. To compare the geometric structure of the resulting embedding spaces, we performed principal component analysis (PCA) separately on the ESM-2 and ESM-C embeddings. We then computed the cumulative variance explained by the top 100 components to assess the effective dimensionality of each space.

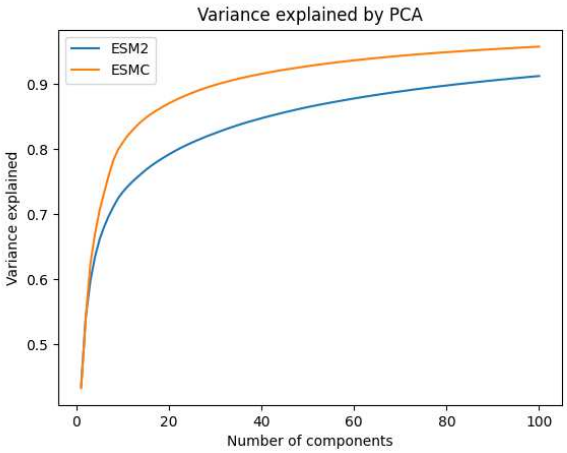

Fig. 1. Cumulative variance explained by the top 100 PCA components.

III. Results

The results indicate a clear difference in how the two models distribute information in embedding space. As shown in Figure 1, ESM-C embeddings concentrate their variance more heavily in fewer components. The first 10 principal components of ESM-C account for approximately 80% of the total variance, while ESM-2's top 10 components explain only around 70%, suggesting that ESM-C creates a more compact, lower-rank representation of proteins. The gap between the two models remains consistent, ESM-2 continues to retain more tail variance, pointing to a richer, more complex representation space.

IV. Discussion

While ESM-C offers a more efficient representation, the higher variance retained by ESM-2 suggests it may be better suited for tasks that rely on fine-grained biological detail.

Acknowledgments

This work was supported by Cytocast Hungary Kft.

References

[1] Lin, Z., Akin, H., Rao, R., Hie, B., Zhu, Z., Lu, W., ... & Sercu, T. (2023). Evolutionary-scale prediction of atomic-level protein structure with a language model. *Science, 379*(6637), 1123–1130.

J. SZALMA, "Protein embeddings for target prediction" in *PhD Proceedings – Annual Issues of the Doctoral School, Faculty of Information Technology and Bionics, Pázmány Péter Catholic University – 2025.* G. Prószéky, G. Szederkényi Eds. Budapest: Pázmány University ePress, 2025, pp. 44–44.

Increasing protein synthesis rates and ribosome content jointly set cell growth in budding yeast

Giorgio TALLARICO
(Supervisors: Andrea CILIBERTO)
Pázmány Péter Catholic University, Faculty of Information Technology and Bionics
50/a Práter street, 1083 Budapest, Hungary
tallarico.giorgio@itk.ppke.hu

***Abstract*—While bacterial models have provided insights in growth physiology and cellular resource allocation, limited research exists for eukaryotic cells. This study proposes a combination of mathematical modelling and experimental approaches for enabling a quantitative description of cellular growth and its regulation. Preliminary results shows that budding yeast sets cell growth by jointly increasing protein synthesis rates and ribosome content and this could be due to the TOR pathway sensing and regulation.**

***Keywords*-Yeast; growth laws**

I. Background

In bacteria, recent work has shown how growth physiology [1], [2] can be described by simple mathematical relationships (sometimes termed "growth laws") which formalize complex emerging principles that connect environmental cues to growth and cell composition. These models are based on a broad description of cells, typically organizing proteins into groups based on their function (e.g., ribosomal proteins grouped as the "R class" or "R sector") or shared regulation [3].

These models have been instrumental in explaining how cells optimize the allocation of cellular resources to physiological processes and pathways, thereby influencing the molecular composition of the cell in response to environmental conditions, such as bacterial response to antibiotics, and how they respond such as to minimize disruption [1].

While there is a wealth of literature on bacterial growth laws [1], [2], [4], the available body of research on eukaryotic cells is comparatively small. However, some seminal studies have shown clear evidence of growth laws in both yeast and cancer cells [5], [6], [7] but at the same time, these studies often lack the experimental data required to validate their quantitative models or are more phenomenologically oriented. My PhD project aim at performing "knowledge transfer" of powerful tools that emerged from previous work in bacteria to eukaryotic cells, in particular using the budding yeast *Saccharomyces cerevisiae* as model system.

One of the major breakthroughs in the field of growth laws was the discovery and mathematical description of the so-called "first growth law" [1]. This empirical relation, demonstrates that the bacterial growth rate is primarily determined by the ribosome content, independently from the specific details of the media in which cells are grown or metabolic network configurations, and budding yeast exhibits a similar linear relationship between ribosome content and growth rate [5]. However, the underlying mechanisms in yeast remain unclear.

Growth laws have been successful in explaining bacterial growth physiology using simple mathematical relationships, and the preliminary findings reported in this manuscript support that these laws and mathematical frameworks could also be applied to eukaryotes. In particular, we have shown that similarly to bacteria, cell growth is jointly set by increasing the translation elongation rate and the ribosome content. The applicability of these mathematical frameworks could be relevant also in a cancer context, particularly a robust quantitative theory that explains how cell growth is controlled and how it's disrupted can uncover key trade-offs useful for developing novel treatments and biomarkers.

Acknowledgment

I gratefully acknowledge additional supervision of my research by Marco Cosentino-Lagomarsino.

References

[1] M. Scott, C. W. Gunderson, E. M. Mateescu, Z. Zhang, and T. Hwa, "Interdependence of cell growth and gene expression: Origins and consequences," *Science*, vol. 330, pp. 1099–1102, Nov. 2010.

[2] X. Dai, M. Zhu, M. Warren, R. Balakrishnan, V. Patsalo, H. Okano, J. R. Williamson, K. Fredrick, Y.-P. Wang, and T. Hwa, "Reduction of translating ribosomes enables escherichia coli to maintain elongation rates during slow growth," *Nature Microbiology*, vol. 2, December 2016.

[3] S. Hui, J. M. Silverman, S. S. Chen, D. W. Erickson, M. Basan, J. Wang, T. Hwa, and J. R. Williamson, "Quantitative proteomic analysis reveals a simple strategy of global resource allocation in bacteria," *Molecular Systems Biology*, vol. 11, Feb. 2015.

[4] C. Wu, R. Balakrishnan, N. Braniff, M. Mori, G. Manzanarez, Z. Zhang, and T. Hwa, "Cellular perception of growth rate and the mechanistic origin of bacterial growth law," *Proceedings of the National Academy of Sciences*, vol. 119, May 2022.

[5] E. Metzl-Raz, M. Kafri, G. Yaakov, I. Soifer, Y. Gurvich, and N. Barkai, "Principles of cellular resource allocation revealed by condition-dependent proteome profiling," *eLife*, vol. 6, Aug. 2017.

[6] K. Kochanowski, T. Sander, H. Link, J. Chang, S. J. Altschuler, and L. F. Wu, "Systematic alteration of in vitro metabolic environments reveals empirical growth relationships in cancer cell phenotypes," *Cell Reports*, vol. 34, p. 108647, Jan. 2021.

[7] Q. Wang and J. Lin, "Environment-specificity and universality of the microbial growth law," *Communications Biology*, vol. 5, Aug. 2022.

G. TALLARICO, "Increasing protein synthesis rates and ribosome content jointly set cell growth in budding yeast" in *PhD Proceedings – Annual Issues of the Doctoral School, Faculty of Information Technology and Bionics, Pázmány Péter Catholic University – 2025.* G. Prószéky, G. Szederkényi Eds. Budapest: Pázmány University ePress, 2025, pp. 45–45.

Preliminary case study: comparing psychophysiological responses of a depressed and a psychotic patient during the Rorschach inkblot test

Brigitta UNGVÁRI
(Supervisors: Katalin CSIGÓ, György CSEREY)
Pázmány Péter Catholic University, Faculty of Information Technology and Bionics
50/a Práter street, 1083 Budapest, Hungary
ungvari.brigitta@itk.ppke.hu

***Abstract*—This preliminary case study examines the integration of psychophysiological and projective methods in the assessment of two individuals with differing psychiatric conditions: one with major depressive disorder (MDD) and the other with schizo-obsessive psychotic features. Galvanic skin response (GSR) and eye-tracking were recorded during the administration of the Rorschach inkblot test to explore patterns of affective and attentional engagement. The goal was to investigate whether physiological and perceptual markers align with clinical observations and projective test responses. Early findings suggest that such multimodal approaches may offer valuable insights into emotional reactivity and perceptual organization across different diagnostic profiles. This case-based approach highlights the potential utility of combining traditional clinical tools with objective measures to support differential diagnosis.**

***Keywords*-visual perception; cognitive functions; eye tracking; pupil dilation; contrast sensitivity; psychiatric disorders, endophenotype**

This preliminary case study explores the use of multimodal assessment—combining projective techniques with psychophysiological and perceptual data—in the evaluation of two patients with differing psychiatric diagnoses: one diagnosed with major depressive disorder (MDD) and the other with obsessive-compulsive disorder accompanied by psychotic features (a schizo-obsessive profile). The aim of the study was to examine whether real-time physiological responses and visual-perceptual patterns elicited during the Rorschach Inkblot Test can reflect underlying emotional and cognitive processes characteristic of these diagnostic categories[1][2].

To this end, galvanic skin response (GSR) and eye-tracking measures were recorded during the administration of the digital Rorschach test. The GSR data were analyzed for stimulus-related reactivity, while the eye-tracking component provided insights into attentional dynamics, including fixations, saccades, and gaze stability. The results suggest contrasts between the two cases which correspond the characteristics of the two psychiatric conditions and also the test results.

Overall, the study illustrates the potential of integrating physiological monitoring and perceptual analysis with projective psychological assessment to yield a richer, more differentiated understanding of individual psychopathology. Although the findings are based on only two cases and cannot be generalized, they support the value of such multimodal approaches in clinical research and highlight promising directions for future investigation into the psychophysiological underpinnings of affective and psychotic disorders.

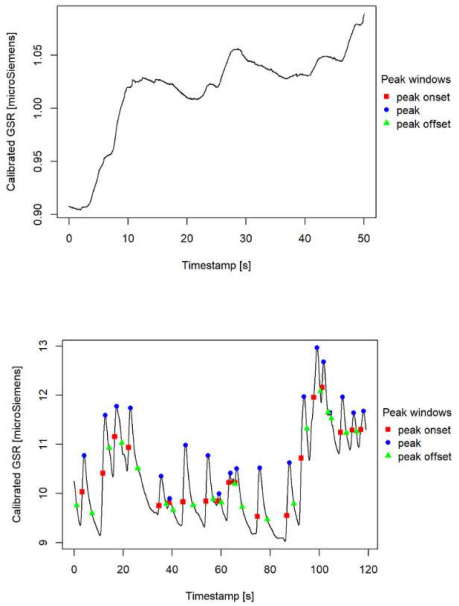

Fig. 1. Comparison of the GSR-pattern of the two patients during the presentation of Card IX. Top: major depression, bottom: schizo-obsessive, psychotic spectrum

ACKNOWLEDGEMENTS

Project no. TKP2021-NVA-27 has been implemented with the support provided by the Ministry of Culture and Innovation of Hungary from the National Research, Development and Innovation Fund, financed under the TKP2021 funding scheme. Project RRF-2.3.1-21-2022-00004 has been implemented provided by the Ministry of Culture and Innovation of Hungary from the National Research, Development and Innovation Fund.

REFERENCES

[1] J. E. Exner Jr, *The Rorschach: A comprehensive system: Basic foundations, Vol. 1*. John Wiley & Sons, 1993.
[2] F. Mérei, *A Rorschach-próba*. Medicina Könyvkiadó Zrt, 2002.

B. UNGVÁRI, "Preliminary case study: comparing psychophysiological responses of a depressed and a psychotic patient during the Rorschach inkblot test" in *PhD Proceedings – Annual Issues of the Doctoral School, Faculty of Information Technology and Bionics, Pázmány Péter Catholic University – 2025.* G. Prószéky, G. Szederkényi Eds. Budapest: Pázmány University ePress, 2025, pp. 46–46.

Domain decomposition methods for PDEs on networks

Mihály András VÁGHY
(Supervisors: Mihály KOVÁCS, Gábor SZEDERKÉNYI)
Pázmány Péter Catholic University, Faculty of Information Technology and Bionics
50/a Práter street, 1083 Budapest, Hungary
vaghy.mihaly.andras@itk.ppke.hu

This progress report is based on [1].

***Abstract*—In this report we develop a Neumann-Neumann type domain decomposition method for elliptic problems on metric graphs. We describe the iteration in the continuous and discrete setting and rewrite the latter as a preconditioner for the Schur complement system. Then we formulate the discrete iteration as an abstract additive Schwarz iteration and prove that it converges to the finite element solution with a rate that is independent of the finite element mesh size. We show that the condition number of the Schur complement is also independent of the finite element mesh size. We provide an implementation and test it on various examples of interest and compare it to other preconditioners.**

***Keywords*-quantum graphs, elliptic partial differential equations, nonoverlapping domain decomposition methods, finite element methods**

I. Introduction

In recent decades differential operators on metric graphs have found a myriad of applications when describing quasi-one-dimensional phenomena in a broad range of fields, such as classical wave propagation in wave guide networks [2], cell differentiation [3].

We consider a quantum graph; that is, a metric graph $\mathsf{G} = (\mathsf{V}, \mathsf{E})$ equipped with an elliptic differential operator on each edge and certain standard vertex conditions. Each edge $\mathsf{e} \in \mathsf{E}$ is assigned a length $\ell_\mathsf{e} \in (0, \infty)$ and a local coordinate $x \in [0, \ell_\mathsf{e}]$. To define the vertex conditions, let us denote by E_v the set of edges incident to the vertex $\mathsf{v} \in \mathsf{V}$, and by $d_\mathsf{v} = |\mathsf{E}_\mathsf{v}|$ the degree of $\mathsf{v} \in \mathsf{V}$. We denote by $\mathrm{int}(\mathsf{G})$ the set of vertices with degree $d_\mathsf{v} > 1$ and by $\partial\mathsf{G}$ the set $\mathsf{V}\backslash\mathrm{int}(\mathsf{G})$. We seek solutions that are continuous on G and satisfy the Neumann-Kirchhoff (often called standard) condition, given as

$$\sum_{\mathsf{e}\in\mathsf{E}_\mathsf{v}} c_\mathsf{e}(\mathsf{v}) u'_\mathsf{e}(\mathsf{v}) = 0, \qquad \mathsf{v} \in \mathsf{V}.$$

We wish to approximate the solution in the finite element framework. In [4] a special finite element is assigned to the vertices that have a star shaped support on the neighbouring edges ensuring the continuity of solutions, and use standard finite elements on the edges. However, the size of the corresponding stiffness matrix can grow quickly and it loses its banded (tridiagonal) nature compared to one-dimensional problems.

To overcome such issues, we investigate a Neumann-Neumann type nonoverlapping domain decomposition method.

II. Neumann-Neumann method

We start by decomposing G into arbitrary disjoint (w.r.t. its edges) subgraphs $\{\mathsf{G}_i = (\mathsf{V}_i, \mathsf{E}_i)\}_{i=1,2,\dots,N}$ with $n_i = |\mathsf{V}_i|$ and $m_i = |\mathsf{E}_i|$. We note that each subgraph is itself a metric graph and that a subgraph may consist of only one edge. The set of vertices that are shared on the boundary of multiple subgraphs will be denoted with Γ and called the interface. The corresponding function values are denoted as $u_\Gamma = \big(u(\mathsf{v})\big)_{\mathsf{v}\in\Gamma}$.

Let us consider the linear equation $A\boldsymbol{u} = \boldsymbol{f}$ arising from the finite element approximation of the quantum graph $\mathsf{G} = (\mathsf{V}, \mathsf{E})$, where A is a symmetric, positive definite matrix. We assume that G is partitioned into two nonoverlapping subgraphs $\{\mathsf{G}_i = (\mathsf{V}_i, \mathsf{E}_i)\}_{i=1,2}$; that is, we have that

$$\mathsf{E} = \mathsf{E}_1 \cup \mathsf{E}_2,\ \mathsf{E}_1 \cap \mathsf{E}_2 = \emptyset,\ \Gamma = \mathsf{V}_1 \cap \mathsf{V}_2.$$

The Neumann-Neumann method can be written as a preconditioned Richardson iteration on the Schur-complement of the stiffness matrix as follows:

$$u_\Gamma^{k+1} - u_\Gamma^k = \theta\Big({S^{(1)}}^{-1} + {S^{(2)}}^{-1}\Big)(g_\Gamma - S u_\Gamma^k).$$

We note that we formulate this Richardson iteration mainly for historical reasons and to avoid the inconvenience of expressing the update of u_Γ in the case of a more sophisticated iteration. However, in practice, one should instead use a preconditioned conjugate gradient (PCG) or minimal residual method. Our main results are as follows.

Theorem 1: The condition number of the Schur complement S is a constant that is independent of $\hat{h}$ and satisfies the bound $\kappa(S) \leq C d_{\max}$.

Theorem 2: The Neumann-Neumann algorithm converges to the finite element solution with a geometric rate that is independent of $\hat{h}$.

Acknowledgements

The authors acknowledge the support of the Hungarian National Research, Development and Innovation Office (NKFIH) through the grant 145934. M.A.V. acknowledges the support of the EKÖP-24-3-II-PPKE-134 University Research Scholarshop Program of the Ministry for Culture and Innovation from the source of the National Research, Development and Innovation Fund.

References

[1] M. Kovács and M. Vághy, "Neumann-Neumann type domain decomposition of elliptic problems on metric graphs," *BIT Numerical Mathematics*, vol. 65, no. 2, 2025.

[2] C. Flesia, R. Johnston, and H. Kunz, "Strong Localization of Classical Waves: A Numerical Study," *Europhysics Letters (EPL)*, vol. 3, no. 4, p. 497–502, 1987.

[3] H. Cho, K. Ayers, L. de Pills, Y.-H. Kuo, J. Park, A. Ranudskaya, and R. Rockne, "Modelling acute myeloid leukaemia in a continuum of differentiation states," *Letters in Biomathematics*, vol. 5, pp. 69–98, 2018.

[4] M. Arioli and M. Benzi, "A finite element method for quantum graphs," *IMA Journal of Numerical Analysis*, vol. 38, no. 3, p. 1119–1163, 2018.

M. VÁGHY, "Domain decomposition methods for PDEs on networks" in *PhD Proceedings – Annual Issues of the Doctoral School, Faculty of Information Technology and Bionics, Pázmány Péter Catholic University – 2025.* G. Prószéky, G. Szederkényi Eds. Budapest: Pázmány University ePress, 2025, pp. 47–47.

Complementary application of NMR and SAXS to study the non-globular regions in the postsynaptic Drebrin protein

Soma VARGA
(Supervisor: Bálint Ferenc PÉTERFIA)
Pázmány Péter Catholic University, Faculty of Information Technology and Bionics
50/a Práter street, 1083 Budapest, Hungary
varga.soma@itk.ppke.hu

***Abstract*—Single alpha-helices (SAHs) are regions in proteins with unique mechanical properties, forming long stable monomeric helical structures in solution. To date, only few naturally occurring SAH regions have been extensively characterized, mostly from myosins, thus, the variability of the structural and dynamical aspects of SAH regions in proteins is largely unexplored. Drebrin (developmentally regulated brain protein) contains a predicted SAH segment with unique sequence characteristics, including the presence of aromatic residues within the SAH region and the strong preference of arginine over lysine residues in its C-terminal half. In this work, using CD and NMR spectroscopy combined with SAXS measurements, we prove that the Drebrin SAH is helical and monomeric in solution. NMR resonance assignment required the use of specific 4D techniques to overcome the severe signal overlap resulting from the low complexity nature of the sequence and its largely helical conformation. To characterize its structural properties in more detail, we have generated a structural ensemble consistent with Ca, Cb chemical shifts and SAXS data. The ensemble reveals that while the structure is primarily extended, its helicity is not uniform along the sequence and it can deviate from the straight helical conformation. Our results suggest that the dynamic rearrangement of salt bridges and the presence of potential transient cation-pi interactions participate in the formation and stabilization of both helical and non-helical local conformational states.**

***Keywords*-SAH, NMR Spectroscopy, SAXS, Molecular dynamics**

I. Introduction

Drebrin modulates and regulates several functions of the nervous system, thereby responsible for a few molecular mechanisms involved in learning and memory [1]. Drebrin (Developmentally Regulated Brain Protein) is an actin-cytoskeleton organizing protein [2], which has key importance in the morphogenesis and organization of the dendritic spine. Earlier studies reported its actin-bundling, actin-binding, and actin-depolymerizing properties, thereby showcasing its importance in the PSD (Postsynaptic Density). [3].

My goal was to corroborate the results yielded by earlier functional investigation of Drebrin, and to extend the available knowledge with structural information. In addition to the expression and experimental investigation of protein segments, my goal was to interpret my results from a holistic perspective and apply bioinformatic methods, to build an integrative model from the Single Alpha-Helix (SAH) in Drebrin [4] that describes the structure and behavior of this non-globular protein segment in as much detail as possible.

II. Methods

After molecular cloning and protein purification, NMR experiments were performed on a 800 MHz Bruker Avance spectrometer equipped with a cryoprobe. SAXS measurements were measured at the EMBL-P12 bioSAXS beam line (DESY, Hamburg Germany).

III. Results

Driven by NMR and SAXS data, further aided by molecular dynamics simulations, I constructed an ensemble-based model of the single alpha-helix, which reflects both the local and global structural parameters revealed by experiments and highlights the formation of a transient network of salt bridges and cation-pi interactions that provide the extraordinary stability of the helical motif.

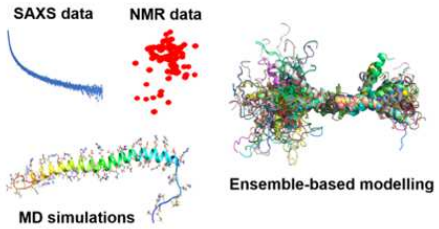

Fig. 1. Simplified representation of the integrative modeling methodology. A model consisting of 60 conformers was created using a selection procedure driven by SAXS and NMR experimental data and aided by MD simulations.

Acknowledgements

I would like to thank my supervisor Dr. Bálint Ferenc Péterfia for his help and guidance with my laboratory work and to Dr. Zoltán Gáspári for his comprehensive help with my research.

References

[1] V. M. Ho, J.-A. Lee, and K. C. Martin, "The cell biology of synaptic plasticity," *Science*, vol. 334, pp. 623–628, Nov. 2011.
[2] M. Pérez-Martínez, M. Gordón-Alonso, J. R. Cabrero, M. Barrero-Villar, M. Rey, M. Mittelbrunn, A. Lamana, G. Morlino, C. Calabia, H. Yamazaki, T. Shirao, J. Vázquez, R. González-Amaro, E. Veiga, and F. Sánchez-Madrid, "F-actin-binding protein drebrin regulates CXCR4 recruitment to the immune synapse," *Journal of Cell Science*, vol. 123, pp. 1160–1170, Apr. 2010.
[3] Y. Hayashi, "Drebrin-Homer interaction at an atomic scale," *Structure*, vol. 27, pp. 3–5, Jan. 2019.
[4] Á. Kovács, D. Dudola, L. Nyitray, G. Tóth, Z. Nagy, and Z. Gáspári, "Detection of single alpha-helices in large protein sequence sets using hardware acceleration," *Journal of Structural Biology*, vol. 204, pp. 109–116, Oct. 2018.

S. VARGA, "Complementary application of NMR and SAXS to study the non-globular regions in the postsynaptic Drebrin protein" in *PhD Proceedings – Annual Issues of the Doctoral School, Faculty of Information Technology and Bionics, Pázmány Péter Catholic University – 2025.* G. Prószéky, G. Szederkényi Eds. Budapest: Pázmány University ePress, 2025, pp. 48–48.

In vitro and *in vivo* characterization of long and flexible, flip chip bonded, polymer neural probes

Levente VÍG
(Supervisor: István ULBERT)
Pázmány Péter Catholic University, Faculty of Information Technology and Bionics
50/a Práter street, 1083 Budapest, Hungary
vig.levente@itk.ppke.hu

***Abstract*—Flexible neural probes are increasingly used in chronic brain implants due to their improved biocompatibility and ability to better match the mechanical properties of neural tissue, which helps minimize long-term signal degradation. However, many current designs lack the structural features needed to access deeper brain regions, limiting their versatility. This work presents a polymer-based neural probe platform that integrates flip chip bonded components to enhance both flexibility and structural integrity. The design enables reliable insertion and stable performance across various brain depths. Validation through *in vitro* testing and *in vivo* recordings in rodents highlights the platform's potential for long-term neural interfacing with consistent signal quality.**

***Keywords*-neural implant; flexible polymer probe; electrophysiology; deep brain recording**

I. Introduction

The high prevalence of neurological disorders such as epilepsy and Parkinson's disease underscores the urgent need for improved diagnostic and therapeutic technologies. In the pursuit of effective interventions, the limitations of traditional rigid micro-electromechanical system (MEMS) electrodes—such as their mechanical mismatch (e.g., Young's modulus) with brain tissue and potential for long-term damage—have prompted interest in alternative approaches [1]. One promising direction is the use of flexible depth electrodes, which offer less invasive means to access subcortical regions with reduced tissue disruption, hence reduced immune response. Exploring the integration of such polymer-metal electrode technologies may open new avenues for both research and clinical applications in neural signal recording and even the modulation of neurons.

II. Methods

Neural probes were fabricated on standard-sized silicon wafers using ordinary cleanroom processes (photolithography, metal deposition etc.), and they consist of multiple polymer-based components assembled through precious metal bonding. The modular design enables the construction of highly elongated (10-30 cm) probes suitable for deep brain access. Each probe features a cone-shaped, flexible shank with linearly arranged microelectrodes composed of Iridium Oxide. Variations in probe architecture include differences in metal layer configurations and electrode placements [2]. *In vitro* characterization of the mentioned probes was conducted using electrochemical impedance spectroscopy in saline solution to assess electrode performance before implantation. Later on, acute *in vivo* implantation (followed by data collection and analysis) of the probes into rat cortical, hippocampal, and thalamic regions under anesthesia was done to refine surgical handling and test recording feasibility. Figure 1 shows an example of this recording, where the channels with low and high impedance magnitude are also marked.

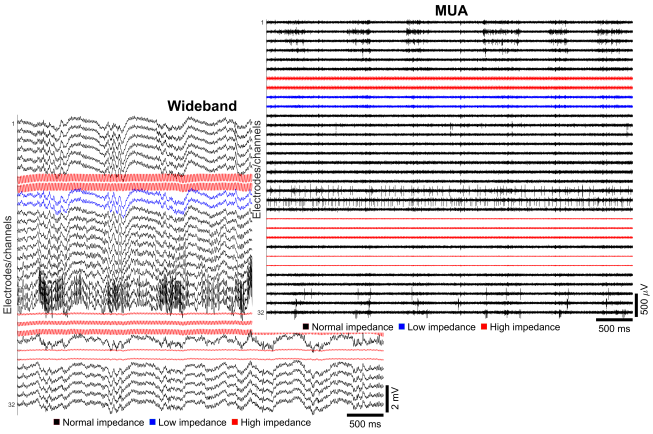

Fig. 1. *In vivo* recording from an anesthetized rat

III. Results and discussion

Impedance measurements revealed that the microelectrodes maintained a stable and acceptable magnitude level, averaging around 200 kΩ at 1 kHz. This indicates proper electrode–electrolyte coupling under physiological conditions. In anesthetized rats, we successfully recorded high-quality local field potentials and robust multi-unit activity from functional microelectrodes (Figure 1), demonstrating the reliability and sensitivity of our data acquisition system in capturing both low- and high-frequency neural signals.

Since the tested extended probes were functional in short term, our future plans include chronic implantation of them in rodents and large animal models (e.g., cats) to evaluate their long-run electrophysiological performance, as well as testing the stimulation capabilities of the devices.

IV. Acknowledgement

The research leading to these results has received funding from the Hungarian Brain Research Program Grant (NAP2022-I-2/2022). The author thanks Richárd Fiáth for his general guidance and research fellow Balázs Barkóczi for his laboratory expertise.

References

[1] Y. Cho, S. Park, J. Lee, and K. J. Yu, "Emerging materials and technologies with applications in flexible neural implants: A comprehensive review of current issues with neural devices," *Advanced Materials*, vol. 33, no. 47, p. 2005786, 2021.

[2] M. Keller, "Neural probes of extended length realized using thermocompression bonding," Master's thesis, University of Freiburg, 2023.

L. VÍG, "In vitro and in vivo characterization of long and flexible, flip chip bonded, polymer neural probes" in *PhD Proceedings – Annual Issues of the Doctoral School, Faculty of Information Technology and Bionics, Pázmány Péter Catholic University – 2025.* G. Prószéky, G. Szederkényi Eds. Budapest: Pázmány University ePress, 2025, pp. 49–49.

Complex predictions using cell simulations

Áron WEBER
(Supervisors: Attila CSIKÁSZ-NAGY, Erzsébet FICHÓ)
Pázmány Péter Catholic University, Faculty of Information Technology and Bionics
50/a Práter street, 1083 Budapest, Hungary
weber.aron@itk.ppke.hu

***Abstract*—Proteins usually function by forming complexes through dynamic interactions with other proteins in the cell. While several databases catalog known protein complexes, these resources remain incomplete due to the labor-intensive nature of in vitro validation. This provides opportunity for *in silico* methods to be employed, either based on cell simulation, machine learning or network-based approach, among others.**
We present a novel approach that employs the CYTOCAST DIGITAL TWIN Cell™, a stochastic spatial simulator driven by multiomics data, to model the complexome of *Saccharomyces cerevisiae*. Predicted complexes were filtered to exclude those resembling known references and were pruned of non-essential, peripheral proteins, to obtain their functional core part.
Several of our predicted complexes closely resembled those generated by ClusterOne on the same interaction network. The spatial structures of predicted complexes were further validated using AlphaFold3, and the pDockQ score for evaluating the fidelity of these structures. If verified in vitro, these predictions could enhance our understanding of cellular processes and uncover new potential drug targets.

***Keywords*-protein complex prediction; complexomics; computational simulation**

SUMMARY

Understanding the functional architecture of the cell requires comprehensive mapping of the complexome—the full set of protein complexes within a cell. While experimental databases like ComplexPortal and CORUM provide valuable insights, they remain incomplete due to the laborious nature of *in vitro* validation. Computational methods, including network-based clustering and machine learning, have emerged to bridge this gap. This study introduces a novel simulation-based approach using the CYTOCAST DIGITAL TWIN Cell™, a stochastic, spatial simulator driven by multiomics data, to predict protein complexes in *Saccharomyces cerevisiae*.

The simulation integrates protein-protein interactions, domain-domain interactions, and protein abundance data to model dynamic complex formation in a 3D cellular environment. Simulations were run 100 times to reduce noise stemming from stochasticity. Predicted complexes were clustered, then pruned, isolating core functional units by removing peripheral, low-importance proteins. Two strategies were employed during clustering. First, we performed an uninformed clustering where no reference data was used. In the second strategy, simulated complexes were first matched to known complexes using cosine similarity, followed by clustering of the unmatched results.

Predicted complexes were compared to those generated by ClusterONE, a gold standard clustering algorithm. Structural validation was performed using AlphaFold3, and complex fidelity was assessed via pDockQ scores. One of the key results we obtained is the prediction of a six-subunit pyridoxal 5'-phosphate synthase complex, matching both ClusterONE predictions and subcomplex dimers present in ComplexPortal. The predicted structure showed biologically plausible pDockQ scores, significantly outperforming random protein sets.

This simulation-based approach demonstrates potential for uncovering novel protein complexes, complementing existing computational and experimental methods. In our future work, we plan on focusing mostly on refining clustering techniques. Additionally, we will also explore the possibility of *in vitro* validation.

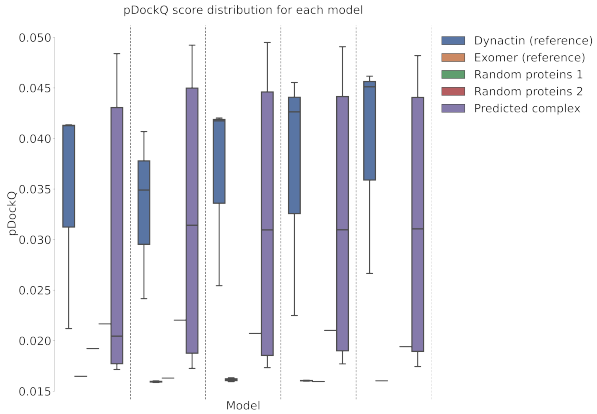

Fig. 1. pDockQ score distributions for the putative six-subunit pyridoxal 5'-phosphate synthase complex, two reference complexes, and two random protein sets

ACKNOWLEDGEMENTS

This work was carried out using the resources of Cytocast Hungary Kft.

REFERENCES

[1] S. Rizzetto, P. Moyseos, B. Baldacci, C. Priami, and A. Csikász-Nagy, "Context-dependent prediction of protein complexes by SiComPre," *npj Systems Biology and Applications 2018 4:1*, vol. 4, pp. 1–9, 1 Sep. 2018, ISSN: 2056-7189. DOI: 10.1038/s41540-018-0073-0. [Online]. Available: https://www.nature.com/articles/s41540-018-0073-0.

[2] T. Nepusz, H. Yu, and A. Paccanaro, "Detecting overlapping protein complexes in protein-protein interaction networks," *Nature Methods 2012 9:5*, vol. 9, pp. 471–472, 5 Mar. 2012, ISSN: 1548-7105. DOI: 10.1038/nmeth.1938. [Online]. Available: https://www.nature.com/articles/nmeth.1938.

Á. WEBER, "Complex predictions using cell simulations" in *PhD Proceedings – Annual Issues of the Doctoral School, Faculty of Information Technology and Bionics, Pázmány Péter Catholic University – 2025.* G. Prószéky, G. Szederkényi Eds. Budapest: Pázmány University ePress, 2025, pp. 50–50.

PROGRAM 2
COMPUTER TECHNOLOGY BASED ON MANY-CORE PROCESSOR CHIPS, VIRTUAL CELLULAR COMPUTERS, SENSORY AND MOTORIC ANALOG COMPUTERS

Head: Péter SZOLGAY

Distant object recognition and tracking methods for UAVs

Lóránt Szabolcs DAUBNER
(Supervisors: Tamás ZSEDROVITS, Kálmán TORNAI)
Pázmány Péter Catholic University, Faculty of Information Technology and Bionics
50/a Práter street, 1083 Budapest, Hungary
daubner.lorant.szabolcs@itk.ppke.hu

I. Introduction

Detect and Avoid (DAA) algorithms are crucial for UAVs (Unmanned Aerial Vehicles) to avoid mid-air and near mid-air collisions. Pilots of medium to large airborne systems are, in most cases, unable to recognize and avoid smaller, non-cooperative aircraft (e.g. drones, balloons, light aircraft). Classical approaches of vision-based DAA include commonly used computer vision techniques with the following steps: frame stabilization, background-foreground separation, filtering, detection, and tracking. A vision-based closed-loop Sense and Avoid System (SAA) was proposed by Zsedrovits et al. in [1]. Modern visual DAA algorithms, such as AirTrack [2] rely on deep neural network-based object detection and tracking methods. The goal of the author is to further develop DAA/SAA methods in the ways detailed later. As a starting point, two modern methods were examined: AirTrack [2] and NEFELI [3].

II. State-of-the-art DAA methods

The detection and tracking module of AirTrack is based on CenterNet [4] and CenterTrack [5]. CenterNet simply extracts a single center point per object without the need for grouping or post-processing. Objects are represented by a single point at their bounding box center. Other properties, such as object size and dimension are then regressed directly from image features at the center location. Object detection becomes a standard keypoint estimation problem this way. CenterTrack is a point-based algorithm for joint detection and tracking. CenterNet detector is adopted to localize center points which are then tracked through time. Specifically, the detector is conditioned on two consecutive frames as well as a heatmap of prior tracklets. This algorithm is end-to-end differentiable and can be trained on static image datasets too [5].

NEFELI is also a vision-only onboard deep learning framework used for object detection and tracking, but its detection module is based on a former version of YOLO (v5) [7]. Detection capabilities were enhanced by a sliced inference method which improves detection accuracy for distant and small objects while maintaining real-time performance [3].

III. Improving the performance of DAA

The improvement is planned using the following techniques (described later in detail and shown in Figure 1.):

- Pre-processing/filtering with additional methods
- Enhanced detection: Using different methods in different steps/situations
- More accurate calculation of Closest Point of Approach (CPA) and tCPA using additional input data (e.g. from IMU)

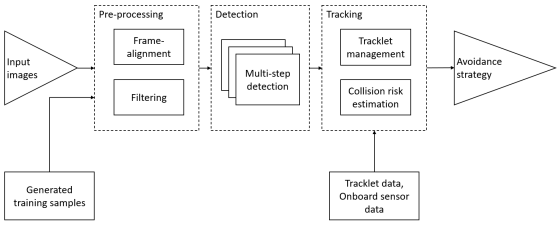

Fig. 1. DAA architecture with the proposed enhancements

- Generating training samples with image captioning to improve closed-set accuracy [6]

The improved DAA algorithm should be built based on the key components described above. The enhancement will include a multi-level detection method and a more accurate and effective CPA/tCPA calculation using additional flight data available. This requires the creation of a new dataset containing images and videos of various airborne objects, captured from a UAV, with available IMU data and range information of aircrafts.

Acknowledgements

Project no. TKP2021-NVA-26 has been implemented with the support provided by the Ministry of Culture and Innovation of Hungary from the National Research, Development and Innovation Fund, financed under the TKP2021 funding scheme.

References

[1] Zsedrovits, T., Bauer, P., Pencz, B., Hiba, A., Gozse, I., Kisantal, M., Nemeth, M., Nagy, Z., Vanek, B., Zarandy, A., Bokor, J., *Onboard Visual Sense and Avoid System for Small Aircraft*. IEEE Aerospace and Electronic Systems Magazine. 31. Pages 18-27, 2016.

[2] S. Ghosh, J. Patrikar, B. Moon, M. M. Hamidi and S. Scherer, *AirTrack: Onboard Deep Learning Framework for Long-Range Aircraft Detection and Tracking*. 2023 IEEE International Conference on Robotics and Automation (ICRA), London, United Kingdom, Pages 1277-1283, 2023.

[3] Anastasios Arsenos, Evangelos Petrongonas, Orfeas Filippopoulos, Christos Skliros, Dimitrios Kollias, Stefanos Kollias, *NEFELI: A deep-learning detection and tracking pipeline for enhancing autonomy in advanced air mobility*. Aerospace Science and Technology, Volume 155, Part 2, ISSN 1270-9638, 2024.

[4] Zhou, Xingyi and Wang, Dequan and Krähenbühl, Philipp, *Objects as Points*. arXiv:1904.07850, 2019.

[5] Zhou, Xingyi and Koltun, Vladlen and Krähenbühl, Philipp, *Tracking Objects as Points*. Computer Vision – ECCV 2020: 16th European Conference, Glasgow, UK, , Proceedings, Part IV, Pages 474 - 490, 2020.

[6] Sagar Vaze and Kai Han and Andrea Vedaldi and Andrew Zisserman, *Open-Set Recognition: a Good Closed-Set Classifier is All You Need?*. arXiv:2110.06207, 2021.

[7] J. Redmon, S. Divvala, R. Girshick and A. Farhadi, *You Only Look Once: Unified, Real-Time Object Detection*. 2016 IEEE Conference on Computer Vision and Pattern Recognition (CVPR), Las Vegas, NV, USA, Pages 779-788, 2016.

L. DAUBNER, "Distant object recognition and tracking methods for UAVs" in *PhD Proceedings – Annual Issues of the Doctoral School, Faculty of Information Technology and Bionics, Pázmány Péter Catholic University – 2025.* G. Prószéky, G. Szederkényi Eds. Budapest: Pázmány University ePress, 2025, pp. 52–52.

Assessing performance and energy efficiency of recent CPU architectures on HPC workloads

Balázs DRÁVAI
(Supervisor: István Zoltán REGULY)
Pázmány Péter Catholic University, Faculty of Information Technology and Bionics
50/a Práter street, 1083 Budapest, Hungary
dravai.balazs@itk.ppke.hu

***Abstract*—We compare recent Intel and AMD x86 processors on representative memory-bound HPC workloads to assess both raw throughput and power efficiency. Our results show that next-generation CPUs deliver notable performance-per-watt gains and that cache-blocking tiling can yield improvements on par with those from hardware upgrades.**

Introduction

HPC workloads increasingly face memory-bound bottlenecks alongside growing power-cost pressures, yet modern x86 CPU generations lack unified performance-per-watt comparisons. This study benchmarks Intel (Sapphire Rapids, Emerald Rapids, Granite Rapids, Sierra Forest) and AMD (Milan, Genoa) processors on representative memory-bound kernels to guide architecture selection.

I. Methods

We describe eight test platforms spanning Intel's Sapphire Rapids (with and without HBM), Emerald Rapids, Granite Rapids, Sierra Forest (96 and 192 core) and AMD's Milan and Genoa CPUs - deployed on the Intel Developer Cloud, the Komondor supercomputer, and a Google Cloud VM.

We evaluated seven proxy applications (CloverLeaf[1], OpenSBLI[2], RTM, Acoustic[3], MG-CFD[4], Volna[5], miniBUDE[6]) implemented in the OPS[7] and OP2[8] DSLs, running in pure MPI and hybrid MPI+OpenMP modes.

Each configuration runs four iterations (first excluded for cache warm-up), reporting average wall clock time and bandwidth (normalized to peak DDR/HBM). RAPL counters (Intel/Milan) and external instrumentation provide power data for perf-per-watt metrics.

II. Results

A. Overall Performance

Figure 1a shows GNR leading at a 2.7× speedup over SPR DDR, with SPR+HBM at 2.4×, SRF 192c at 1.9×, EMR at 1.4×, and SRF 96c at 1.1×. Latency-sensitive kernels saturate nearly 100% of peak bandwidth, while higher-order stencils and unstructured codes achieve only 45–65%, revealing residual memory-latency limits.

B. Energy Efficiency

Figure 1b shows GNR and SRF 192c reach about 1.9× perf-per-watt versus SPR DDR, with EMR at 1.5× and SRF 96c at 1.8×. This demonstrates that both high-bandwidth and many-core designs deliver significant energy savings alongside performance gains.

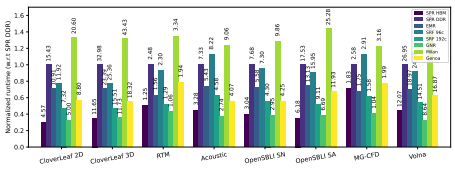

(a) Execution time normalized to SPR DDR.

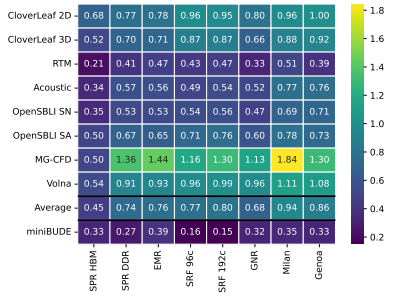

(b) Performance-per-watt relative to SPR DDR.

Fig. 1: (a) Raw performance across architectures. (b) Energy efficiency across architectures.

References

[1] A. Mallinson, D. A. Beckingsale, W. Gaudin, J. Herdman, J. Levesque, and S. A. Jarvis, "Cloverleaf: Preparing hydrodynamics codes for exascale," *The Cray User Group*, vol. 2013, 2013.

[2] C. T. Jacobs, S. P. Jammy, and N. D. Sandham, "OpenSBLI: A framework for the automated derivation and parallel execution of finite difference solvers on a range of computer architectures," *Journal of Computational Science*, vol. 18, pp. 12–23, 2017.

[3] M. Louboutin, M. Lange, F. Luporini, N. Kukreja, P. A. Witte, F. J. Herrmann, P. Velesko, and G. J. Gorman, "Devito (v3. 1.0): an embedded domain-specific language for finite differences and geophysical exploration," *Geoscientific Model Development*, vol. 12, no. 3, pp. 1165–1187, 2019.

[4] A. Owenson, S. A. Wright, R. A. Bunt, Y. Ho, M. J. Street, and S. A. Jarvis, "An unstructured CFD mini-application for the performance prediction of a production CFD code," *Concurrency and Computation: Practice and Experience*, vol. 32, no. 10, p. e5443, 2020.

[5] I. Z. Reguly, D. Giles, D. Gopinathan, L. Quivy, J. H. Beck, M. B. Giles, S. Guillas, and F. Dias, "The VOLNA-OP2 tsunami code (version 1.5)," *Geoscientific Model Development*, vol. 11, no. 11, pp. 4621–4635, 2018.

[6] A. Poenaru, W.-C. Lin, and S. McIntosh-Smith, "A performance analysis of modern parallel programming models using a compute-bound application," in *High Performance Computing*, B. L. Chamberlain, A.-L. Varbanescu, H. Ltaief, and P. Luszczek, Eds. Cham: Springer International Publishing, 2021, pp. 332–350.

[7] I. Z. Reguly, G. R. Mudalige, M. B. Giles, D. Curran, and S. McIntosh-Smith, "The OPS domain specific abstraction for multi-block structured grid computations," in *2014 Fourth International Workshop on Domain-Specific Languages and High-Level Frameworks for High Performance Computing*. IEEE, 2014, pp. 58–67.

[8] I. Reguly, "Op2: An active library framework for solving unstructured mesh-based applications on multi-core and many-core architectures," in *2012 Innovative Parallel Computing (InPar)*. IEEE, 2012, pp. 1–12.

B. DRÁVAI, "Assessing performance and energy efficiency of recent CPU architectures on HPC workloads" in *PhD Proceedings – Annual Issues of the Doctoral School, Faculty of Information Technology and Bionics, Pázmány Péter Catholic University – 2025.* G. Prószéky, G. Szederkényi Eds. Budapest: Pázmány University ePress, 2025, pp. 53–53.

A medical application of ASR and LLM

Imre Gergely JÁNOKI
(Supervisor: Péter FÖLDESY)
Pázmány Péter Catholic University, Faculty of Information Technology and Bionics
50/a Práter street, 1083 Budapest, Hungary
janoki.imre.gergely@itk.ppke.hu

***Abstract*—Due to limited human resources there is a need for automatization of postpartum anamnesis and patient records. The medical terminology, abbreviations and their many pronunciations require a specialized fine-tuning of existing speech-to-text transcription models. In this research, we are heavily enriching the available, very small dataset with synthetic text and synthetic voices for the model training.**

***Keywords*-transcription, TTS, STT, medical, anamnesis**

I. Introduction

The need for automated postpartum anamnesis transcription was identified meeting with doctors from Semmelweis University, Budapest. The requirements for such a system include ease of operation, accurate transcription of spoken postpartum anamnesis and medical records, immediate feedback with the option for correction, and automatic generation of a digital record conforming to a predefined structure and format. While similar tools exist with varying degrees of accuracy [1], the specialized medical terminology of specific fields limits the universal applicability of even high-performing AI-based solutions. These systems typically require separate training or fine-tuning for each field.

II. Methods

OpenAI's Whisper [2] is a state-of-the-art text-to-speech architecture, and it includes a pretrained model for the Hungarian language. Although it was not originally designed for real-time use, Whisper.cpp [3], a fast, community-driven C++ implementation, allowed us to achieve near-real-time continuous transcription of Hungarian speech with acceptable accuracy in everyday language. However, a specialized dataset was needed to fine-tune the model for postpartum anamnesis transcription. We requested a set of anonymized anamneses from doctors at Semmelweis University (SU). The provided text encompassed approximately 3500 words across 20 cases. Due to limited human resources, a significantly larger dataset was not feasible. Therefore, we employed various generative language models to create artificial, synthetic anamnesis texts. These synthetic texts were subsequently reviewed and validated by a medical resident and PhD candidate specializing in the field. Next, we are using the resulting text data to create a corresponding voice dataset. To achieve this, we augmented the text with all the different pronunciations of each critical term and abbreviation. This approach may guide the AI during fine-tuning, enabling it to transcribe different pronunciations to the same written word. Aside from human participants reading this text, we are generating synthetic voice data using text-to-speech (TTS) AI solutions. XTTS-v2 [4], a suitable and convincing model supporting the Hungarian language.

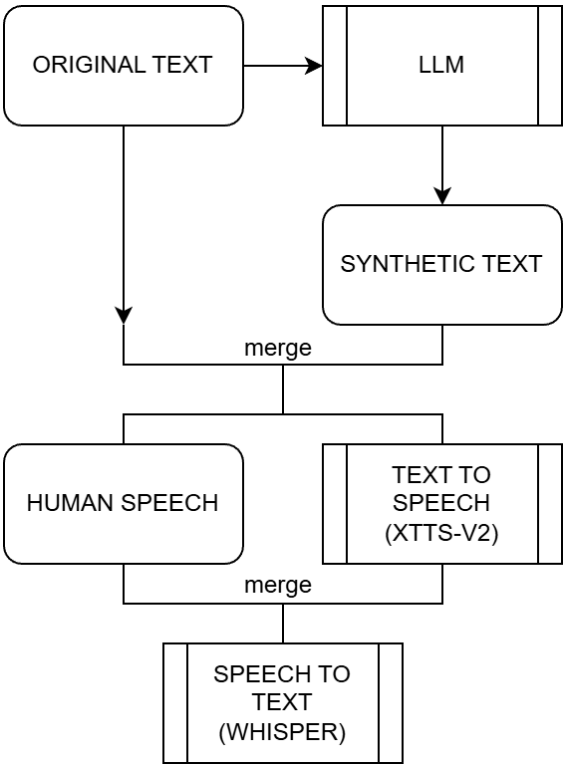

Fig. 1. Flowchart of the database creation and fine-tuning of Whisper for anamnesis transcription at a Hungarian neonatalogy.

Acknowledgements

The author would like to express gratitude to Eszter Zsáry, Ákos Gasparics, Ágnes Jermendy, Péter Mihajlik and Péter Földesy, and to Medicor Elektronika Zrt.

Funding

Project no. 2023-2.1.2-KDP-2023-00011 C2309621 has been implemented with the support provided by the Ministry of Culture and Innovation of Hungary from the National Research, Development and Innovation Fund, financed under the KDP-2023 funding scheme.

References

[1] Speechtex, "SpeechTex jogi beszédleíró," 2018.
[2] A. Radford, J. W. Kim, T. Xu, G. Brockman, C. McLeavey, and I. Sutskever, "Robust speech recognition via large-scale weak supervision," 2022.
[3] ggml org, "GitHub - ggml-org/whisper.cpp: Port of OpenAI's whisper model in C/C++," 2022.
[4] G. Eren and T. C. T. Team, "Coqui TTS," Jan 2021.

I. JÁNOKI, "A medical application of ASR and LLM" in *PhD Proceedings – Annual Issues of the Doctoral School, Faculty of Information Technology and Bionics, Pázmány Péter Catholic University – 2025.* G. Prószéky, G. Szederkényi Eds. Budapest: Pázmány University ePress, 2025, pp. 54–54.

Experimental evaluation of a soft resistive sensor for monitoring respiratory activity

Rizal MAULANA
(Supervisor: György CSEREY)
Pázmány Péter Catholic University, Faculty of Information Technology and Bionics
50/a Práter street, 1083 Budapest, Hungary
rizal.maulana@itk.ppke.hu

***Abstract*—This study aims to develop a soft resistive sensor for continuous noninvasive measurement of respiratory activity. The designed sensor is tested on the abdomen and chest circumferences to detect body movements related to the respiratory process. The measurement results of the designed sensor were evaluated and validated with the results obtained from the OptoForce sensor. The test results demonstrate a high correlation between the measurements from both sensors, as seen by the similar amplitude and frequency characteristics of the signals recorded during various respiratory types.**

***Keywords*-continuous; respiratory signal; wearable device**

I. Summary

The respiratory rate is an essential vital sign that requires continuous monitoring. This continuous monitoring is crucial for preventive efforts aimed at the early detection of serious respiratory diseases, including asthma, sleep apnea, and chronic obstructive pulmonary disease (COPD) [1]. A common symptom of these three conditions is a sudden change in respiratory rate. The normal respiratory rate in a state of rest is between 12 and 20 breaths per minute. Deviations in respiratory rate from this range may indicate a compromised respiratory system.

The traditional methods for evaluating respiratory function are spirometry and lung plethysmography. Spirometry involves utilizing a mouthpiece to measure the volume of air inhaled and exhaled from the lungs, assess airflow speed during respiration, and indirectly evaluate the respiratory rate. Meanwhile, lung plethysmography employs an airtight chamber with a specified air volume, where the variations in gas pressure within the chamber during the testing period are analysed to evaluate respiratory function parameters [2]. Although capable of providing accurate results, these two instruments rely on bulky instruments, and the measurement procedures require supervision by medical staff. Therefore, they are impractical for the continuous and independent monitoring of respiratory activity. These limitations highlight the need for an advanced instrument to monitor respiratory function continuously, especially during daily activities.

Numerous studies have explored the continuous noninvasive measurement of respiratory activity, particularly those employing sensors utilizing capacitive and piezoelectric transduction mechanisms. However, these sensors are highly susceptible to noise in the measurement environment [3]. In this research, we present the implementation of a soft resistive sensor based on resistive yarn for continuous noninvasive measurement of respiratory activity. Resistive yarn is a type of yarn that varies its resistance value when subjected to mechanical stress on its surface. The evaluation of respiratory activity is based on body movements that occurred during the inhalation and exhalation periods of breathing. The test was conducted on the abdomen and chest circumference. To validate the measurement results of the designed sensor, they were compared with the measurement results of the OptoForce sensor. The OptoForce sensor was previously employed by Foldi et al. [4] in their study for the continuous noninvasive measurement of arterial blood pressure waveforms.

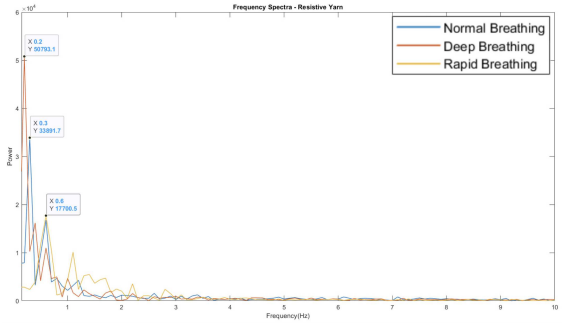

Fig. 1. Frequency spectra of measurement using resistive yarn.

This study conducted respiratory tests on three types of breathing: normal, deep, and rapid. The objective was to evaluate the sensor's ability to detect respiration through a wide range of amplitudes and frequencies. Fig. 1 illustrates the frequency spectra obtained from measurements using resistive yarn on the abdomen for these different respiratory patterns. The dominant frequency captured by the resistive yarn corresponds identically to the measurement obtained from the OptoForce. The thorough signal analysis indicates that the amplitude of the resistive yarns is comparable to that of the OptoForce for all three evaluated respiratory patterns.

Acknowledgements

The author acknowledges Prof. György Cserey and Dr. Sándor Földi for their invaluable guidance in the development of this research.

References

[1] D. Vitazkova, E. Foltan, H. Kosnacova, M. Micjan, M. Donoval, A. Kuzma, M. Kopani, and E. Vavrisnky, "Advances in respiratory monitoring: a comprehensive review of wearable and remote technologies," Biosensors, vol. 14, 2024.

[2] J.C. Quindry, C.G. Ballmann, E.E. Epstein, and J.T. Selsby, "Plethysmography measurements of respiratory function in conscious unrestrained mice," The Journal of Physiological Sciences, vol. 66, pp. 157-164, 2016.

[3] Z. Jia, H. Huth, W.Q. Teoh, S. Xu, B. Wood, and Z.T.H. Tse, "State of the art review of wearable devices for respiratory monitoring," IEEE Access, vol. 13, pp. 18178-18190, 2025.

[4] S. Foldi, T. Horvath, F. Zieger, P. Sotonyi, and G. Cserey, "A novel noninvasive blood pressure waveform measuring system compared to millar applanation tonometry," Journal of Clinical Monitoring and Computing, vol. 32, pp. 717-727, 2018.

R. MAULANA, "Experimental evaluation of a soft resistive sensor for monitoring respiratory activity" in *PhD Proceedings – Annual Issues of the Doctoral School, Faculty of Information Technology and Bionics, Pázmány Péter Catholic University – 2025.* G. Prószéky, G. Szederkényi Eds. Budapest: Pázmány University ePress, 2025, pp. 55–55.

Towards hybrid smart plug systems

Dániel István NÉMETH
(Supervisor: Kálmán TORNAI)
Pázmány Péter Catholic University, Faculty of Information Technology and Bionics
50/a Práter street, 1083 Budapest, Hungary
nemeth.daniel.istvan@itk.ppke.hu

***Abstract*—The literature of Electrical Load Classification is divided into Intrusive and Non-intrusive methods, both having their own benefits and limitations. By combining these approaches, it is possible to create a load classification system that resolves these limitations. We show how a smart plug-based system can be extended to detect multiple electrical loads that are connected to the same plug in parallel. With this capability, the installation cost of a smart plug-based system can be significantly reduced.**

***Keywords*-Electrical Load Classification; Smart Plugs; Home Energy Management**

I. Introduction

With the spread of renewable, non-controllable energy resources, balancing the production and demand-side of the electrical grid becomes even more challenging. To best utilize renewables, grid load composition data and Demand-Side Management are needed.

Electrical Load Classification is generally divided into Non-Intrusive and Intrusive Load Monitoring (NILM and ILM). NILM is an inexpensive way to collect aggregated consumption data utilizing smart meters, but additional disaggregation steps are required to infer appliance-level power consumption. With ILM, each appliance is measured separately using Smart Plugs, which offer accurate, appliance-level consumption data and load control capabilities but at much higher installation costs.

II. Motivation

With smart plugs, it is assumed that at most one load is connected at a time. The system is not prepared for the scenario in which multiple appliances are connected to one plug via an extension cord (Figure 1). The detection algorithm may incorrectly classify a sample as a different load. This presents a serious problem, since incorrect scheduling may be applied to the connected loads.

III. Methodology

Using our previously built smart plug [1], [2], a large dataset of 32000 measurements was collected. A Convolutional Neural Network (CNN) was used to classify the samples. To enable multi-label output in neural networks, we can select the top N neurons with the highest output. By training the neurons to fire if their corresponding electrical load is present in the input, the top N neurons by their output can be considered as the connected loads. To determine N, we opted to use the same CNN. By adding three neurons to the output, these can be trained to recognize one-, two-, and three-load combinations. This way, the output of the CNN is divided into two parts. The first part, each load class has its corresponding neuron, while the second part of the network predicts the number of loads. The output of both parts of the network is normalized separately.

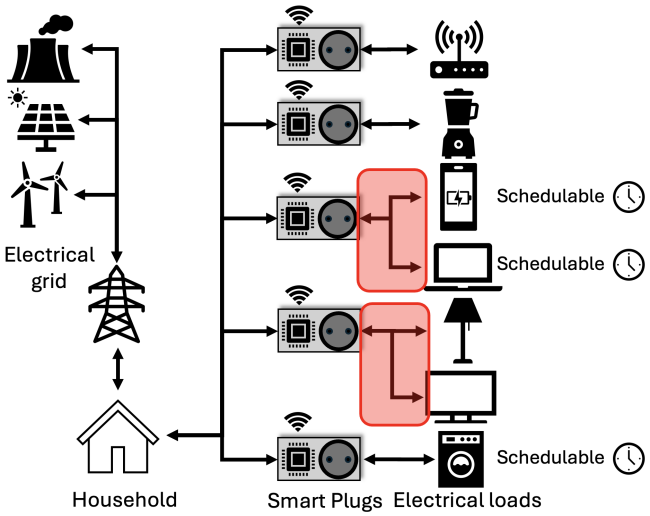

Fig. 1. Smart Plug system with multiple loads connected to one plug

IV. Results

The distribution-part of the network achieved an average of 98.17% accuracy rate, while the load count estimation part achieved 99.13%. Using a combined accuracy measure, the rate was 97.39%.

The scalability of the method was also explored. By reducing the number of training samples for multi-load combinations, we could achieve a 7-fold reduction of measurement time with an accuracy rate of 88.44%.

V. Conclusions

We presented a novel load classification method, enabling a trade-off between the smart plug system's installation cost and the control granularity for the connected appliances, as well as providing a more robust load detection method, capable of correctly detecting multiple electrical loads connected in parallel to the same smart plug.

Acknowledgements

This research was supported by the National Research, Development and Innovation Office (NKFIH) through the grant no. TKP2021-NVA-26

References

[1] D. Németh. and K. Tornai., "SP4LC: A method for recognizing power consumers in a smart plug," in *Proceedings of the 11th International Conference on Smart Cities and Green ICT Systems - SMARTGREENS,*, pp. 69–77, INSTICC, SciTePress, 2022.

[2] D. I. Németh and K. Tornai, "Fast electrical load classification using a dimmer-based smart plug," in *Smart Cities, Green Technologies, and Intelligent Transport Systems* (C. Klein, M. Jarke, J. Ploeg, M. Helfert, K. Berns, and O. Gusikhin, eds.), (Cham), pp. 68–89, Springer Nature Switzerland, 2023.

D. NÉMETH, "Towards hybrid smart plug systems" in *PhD Proceedings – Annual Issues of the Doctoral School, Faculty of Information Technology and Bionics, Pázmány Péter Catholic University – 2025.* G. Prószéky, G. Szederkényi Eds. Budapest: Pázmány University ePress, 2025, pp. 56–56.

Sensor integration and improved control for an fPAM-based soft wrist exosuit

Katalin SCHÄFFER
(Supervisor: Miklós KOLLER)
Pázmány Péter Catholic University, Faculty of Information Technology and Bionics
50/a Práter street, 1083 Budapest, Hungary
schaffer.katalin@itk.ppke.hu

***Abstract*—We present recent sensor integration advancements in a soft wrist exosuit that uses fabric pneumatic artificial muscles (fPAMs) for assistive and rehabilitative applications. Key improvements include higher-accuracy inertial measurement units (IMUs) for joint angle sensing, a force-sensitive resistor (FSR)-based pressure anchoring system for user comfort, and preliminary implementation of electromyography (EMG) sensors for user-intent detection. In preparation for user testing, we developed a graphical user interface (GUI) to streamline interaction. The GUI allows real-time monitoring, trajectory selection, and system control through an intuitive display. These improvements enhance the system's reliability and usability, moving the exosuit closer to clinical readiness.**

***Keywords*-Soft robotics, exosuit, wearable sensors, EMG, IMU, graphical interface, pneumatic actuators.**

I. Overview

Soft exosuits offer a lightweight and compliant alternative to rigid robotic exoskeletons, particularly for applications in stroke rehabilitation and daily activity assistance. Building on our prior design that uses fPAMs [1] to actuate the wrist [2], this work focused on improving the sensing infrastructure and interface usability.

First, we evaluated the sensing accuracy of the BNO085 IMU (inertial measurement unit) against its predecessor, the currently applied BNO055 model, using a hinged test setup. Results indicated significantly improved stability and reduced drift with the newer model, motivating its integration into the wearable system.

Second, we implemented an FSR (force sensitive resistor) sensor in the pneumatic anchoring sleeve's [3] inner layer to monitor surface pressure and regulate inflation through a closed-loop proportional integral feedback controller. This provides a more comfortable and safe user experience, accommodating arm motion and potential air leakage.

Third, we demonstrated intent-based actuation by integrating a reusable EMG (electromiography) sensor. Muscle signals from the forearm were used to trigger real-time inflation and deflation of the corresponding fPAM on a dummy arm. Figure 1 shows an example test with distinguishable signals from short and sustained contractions that triggered actuator response in the exosuit.

Finally, we implemented improvements to the controller and user interface. The current, pressure-based antagonistic feedback controller was updated using our previously derived exosuit torque model. This work includes the refinement of the fPAM force model and testing the controller in simulation.

To support the clinical applicability of the exosuit, a custom GUI (graphical user interface) was created in Processing. It enables live joint angle plots, IMU calibration feedback and data recording control to ensure easy-to-access operation.

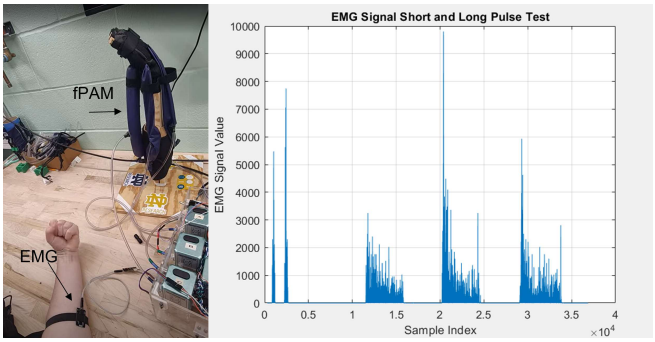

Fig. 1: EMG-triggered exosuit control: muscle activation (right) actuates the corresponding fPAM of the exosuit on the a dummy-hand (left).

II. Conclusion

Sensor integration enhancements and interface development have significantly improved the functionality and usability of our wrist exosuit. These upgrades enable more precise tracking, safe use, and early-stage intention recognition. Future work will focus on embedding these technologies into a compact prototype and conducting pilot user studies to assess performance in clinical contexts.

Acknowledgements

The research was conducted in the IRIS Lab of the University of Notre Dame under the supervision of Prof. Margaret Coad and with the help of undergraduate students Pailyn Groene and Gabriella Shirtcliff. The authors acknowledge the support of the National Research, Development and Innovation Office – NKFIH – through grant no. TKP2021-NKTA-66.

References

[1] N. Naclerio and E. W. Hawkes, "Simple, low-hysteresis, foldable, fabric pneumatic artificial muscle," *IEEE Robotics and Automation Letters*, vol. 5, no. 2, pp. 3406–3413, 2020.

[2] K. Schäffer, Y. Ozkan-Aydin, and M. M. Coad, "Soft wrist exosuit actuated by fabric pneumatic artificial muscles," *IEEE Transactions on Medical Robotics and Bionics*, vol. 6, no. 2, pp. 718–732, 2024.

[3] K. Schäffer, U. Fallon, and M. M. Coad, "Stretchable pneumatic sleeve for adaptable, low-displacement anchoring in exosuits," in *2024 IEEE 7th International Conference on Soft Robotics (RoboSoft)*, 2024, pp. 912–918.

K. SCHÄFFER, "Sensor integration and improved control for an fPAM-based soft wrist exosuit" in *PhD Proceedings – Annual Issues of the Doctoral School, Faculty of Information Technology and Bionics, Pázmány Péter Catholic University – 2025.* G. Prószéky, G. Szederkényi Eds. Budapest: Pázmány University ePress, 2025, pp. 57–57.

Torque control of synchronous motors using feedback linearization

Dávid SOMOGYI
(Supervisor: Gábor SZEDERKÉNYI)
Pázmány Péter Catholic University, Faculty of Information Technology and Bionics
50/a Práter street, 1083 Budapest, Hungary
somogyi.david@itk.ppke.hu

***Abstract*—Actuator dynamics significantly impact mechatronic control systems, especially in cost-optimized industrial setups where motors operate near their limits. The nonlinear behavior of Permanent Magnet Synchronous Motors (PMSMs), particularly at high speeds, can degrade control performance. To address this, a feedback linearization approach is proposed for torque control, using a derived rotor speed reference to maintain linear behavior and handle sudden load changes. Integrated into an electromechanical power steering (EPS) system, this method outperforms standard linear control by improving consistency and stability across the operating range.**

***Keywords*-Feedback linearization, Actuator dynamics, Nonlinear control**

I. Introduction

Permanent Magnet Synchronous Motors (PMSMs) are widely used in mechatronic systems due to their high performance, cost-effectiveness, and adaptability. Standard control methods include Field-Oriented Control (FOC) [1] and Direct Torque Control (DTC) [2]. While FOC uses coordinate transformations to simplify control, it still relies on linear PI controllers, resulting in nonlinear motor behavior across varying operating conditions. Similarly, DTC avoids transformations but still exhibits nonlinear dynamics. These nonlinearities, especially when combined with field-weakening techniques [3], can degrade performance in high-level systems by introducing oscillations or instability.

To address this, nonlinear control strategies such as feedback linearization and Active Disturbance Rejection Control (ADRC) have been explored for PMSMs [4]–[6]. However, actuator control is often treated in isolation rather than as part of an interconnected system.

The main contribution is a feedback linearization method for PMSMs with a torque control objective, capable of handling arbitrary load variations within the limits of estimation bandwidth. This method is embedded into an electromechanical power steering (EPS) system, demonstrating improved linearity and enhanced stability across the operating range.

II. PMSM Control via feedback linearization

For the steering application, the primary control objective is reference tracking, where the actuation signal corresponds to the required motor torque. As a result, the reference input to the motor controller is typically expressed in terms of either torque or current. The role of the controller is therefore to accurately regulate the torque output of the motor.

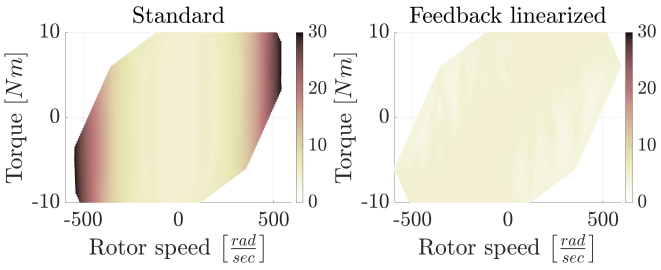

Fig. 1. Time constant of the motor in different operating regions.

Fig. 1 presents the motor's time constant across various operating points as a function of rotor speed and requested torque. A key benefit of the PI-controlled, feedback-linearized motor is its consistent dynamic behavior throughout the entire operating range. In contrast, the conventional PI-controlled motor displays significant variation in its dynamic response. Although both control strategies are tuned to deliver comparable performance under nominal conditions, the feedback linearization approach demonstrates superior performance under extreme operating scenarios.

Acknowledgment

This research was supported by the Hungarian National Research, Development, and Innovation Office through the grant K-145934.

References

[1] F. Amin, E. Sulaiman, and H. Soomro, "Field oriented control principles for synchronous motor," *International Journal of Mechanical Engineering and Robotics Research*, vol. 8, pp. 284–288, 01 2019.

[2] A. Hughes and B. Drury, *Variable Frequency Operation of Induction Motors*, 12 2013, pp. 205–253.

[3] L. Sepulchre, M. Fadel, M. Pietrzak-David, and G. Porte, "Flux-weakening strategy for high speed PMSM for vehicle application," in *2016 International Conference on Electrical Systems for Aircraft, Railway, Ship Propulsion and Road Vehicles & International Transportation Electrification Conference (ESARS-ITEC)*, 2016, pp. 1–7.

[4] Z. Wu, Y. Shen, T. Pan, and Z. Ji, "Feedback linearization control of PMSM based on differential geometry theory," in *2010 5th IEEE Conference on Industrial Electronics and Applications*, 2010, pp. 2047–2051.

[5] C. Lascu, I. Boldea, and F. Blaabjerg, "Direct torque control via feedback linearization for permanent magnet synchronous motor drives," in *2012 13th International Conference on Optimization of Electrical and Electronic Equipment (OPTIM)*, 2012, pp. 338–343.

[6] H. Sira-Ramirez, J. Linares Flores, C. Garcia-Rodriguez, and M. Contreras, "On the control of the permanent magnet synchronous motor: An active disturbance rejection control approach," *IEEE Transactions on Control Systems Technology*, vol. 22, pp. 2056–2063, 06 2014.

D. SOMOGYI, "Torque control of synchronous motors using feedback linearization" in *PhD Proceedings – Annual Issues of the Doctoral School, Faculty of Information Technology and Bionics, Pázmány Péter Catholic University – 2025.* G. Prószéky, G. Szederkényi Eds. Budapest: Pázmány University ePress, 2025, pp. 58–58.

PROGRAM 3
FEASIBILITY OF ELECTRONIC AND OPTICAL DEVICES, MOLECULAR AND NANOTECHNOLOGIES, NANO-ARCHITECTURES, NANOBIONIC DIAGNOSTIC AND THERAPEUTIC TOOLS

Head: Árpád CSURGAY

Spin waves as computational tools for signal processing: convolution

Tamás István KOVÁCS
(Supervisor: György CSABA)
Pázmány Péter Catholic University, Faculty of Information Technology and Bionics
50/a Práter street, 1083 Budapest, Hungary
kovacs.tamas.istvan@itk.ppke.hu

***Abstract*—In recent decades, researchers have explored various physical phenomena for computing and signal processing. One promising path is micromagnetics, spin-wave computing in particular, which offers the potential for reduced device size, low power consumption, and high operational speed. Minimizing size and energy consumption is critical in numerous application domains. A viable approach involves developing hybrid systems, where specialized non-digital technologies replace and outperform specific components of conventional computing architectures.**

The proposed stripe convolver is a spin-wave-based device capable of high-speed convolution of temporal signals, which utilizes the inherent nonlinearities of micromagnetic systems, while consuming a low amount of energy. Possible applications are in the fields of neuromporh computing [1], RF systems, and, in general, any application that uses convolution or cross-correlation operations in any way.

***Keywords*-spin-wave, magnon, signal processing, machine learning**

I. Introduction

The stripe convolver can be introduced as the magnonic cousin of the three-port elastic SAW convolver [2]. This rectangular device measures between a few and a few hundred microns on its sides, is stretched along the wave propagation axis, and usually has a thickness of up to 30 nm. This stripe is made out of yttrium iron garnet and is exposed to a constant, uniform bias field that sets the direction of magnetization and the axis of precession, and two additional time-varying external magnetic fields at the opposite short ends. These input fields are induced by the current flowing in thin wires over the film at the ports. Both current signals are modulated with the frequency of the carrier ω_c. As the waves generated by the external fields propagate in opposite directions, a standing wave will emerge in the region where the waves overlap. Taking the spatial average of the standing wave results in the convolution of the two input signals. The appearance of the frequency $2\omega_c$ is the result of the nonlinear nature of the system 1.

II. Considerations about the stripe convolver

Amplitude Nonlinear waves are a requirement for the convolver to work. However, it is also important to keep the excitation amplitude under control, as magnetization dynamics tend to get chaotic when reaching certain amplitude levels. These amplitude ranges are non-trivial and depend heavily on the device dimension, and geometry of wave propagation. In fact, the relative direction of propagation and bias field dictate the optimal measurement alignment, which is crucial in device design [3].

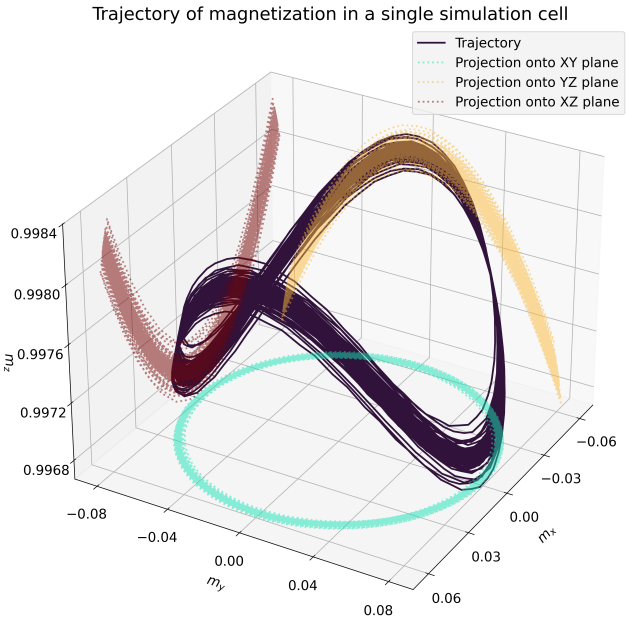

Fig. 1. The source of nonlinear nature of spin waves comes from the non-identical precession in different directions. In linear case, assuming a sinusoidal pulsing external field, and steady-state, the magnetization moves on a circle-like manifold. Here, on the other hand, we can see this saddle-like trajectory. This shape is the reason, why different components have different precession frequencies.

Frequency It is known that the carrier frequency of an amplitude-modulated signal must be substantially higher than the maximum frequency of the baseline signal, which sets some restrictions on the set of possible inputs. In practice, this might not be a serious limitation as very high frequencies can be easily handled by the convolver.

Validity The main limitation of the device is the finite length convolution window. Both signals must be entirely under the readout device; otherwise, the result is truncated.

References

[1] Markovic, Danijela, Alice Mizrahi, Damien Querlioz, and Julie Grollier. "Physics for neuromorphic computing." Nature Reviews Physics (2020): 1-12.
[2] Campbell, Colin. Surface acoustic wave devices and their signal processing applications. Elsevier, 2012.
[3] J. W. Kłos and M. Krawczyk, "Magnonic Crystals: From Simple Models toward Applications," in Magnetic Structures of 2D and 3D Nanoparticles: Properties and Applications, Pan Stanford, Singapore, 2016, p. 283, doi: 10.1201/b19845-9.

T. KOVÁCS, "Spin waves as computational tools for signal processing: convolution" in *PhD Proceedings – Annual Issues of the Doctoral School, Faculty of Information Technology and Bionics, Pázmány Péter Catholic University – 2025.* G. Prószéky, G. Szederkényi Eds. Budapest: Pázmány University ePress, 2025, pp. 60–60.

Spin-wave holography for image processing

Levente MAUCHA
(Supervisors: Ádám PAPP, György CSABA)
Pázmány Péter Catholic University, Faculty of Information Technology and Bionics
50/a Práter street, 1083 Budapest, Hungary
maucha.levente@itk.ppke.hu

***Abstract*—Recently, several publications have emerged in the field of magnonics, presenting machine-learned spin-wave scatterers for wave interference–based neuromorphic computing. Although these devices demonstrate promising computational performance, they often function as black boxes, providing limited insight into the underlying mechanisms of their operation. Here, I present a theoretical investigation to examine the functioning of a spin-wave interference–based network, drawing comparisons with the principles of optical holography. The study reveals the differences between optical and linear spin-wave propagation, and provides an overview of how the linear holographic phenomena capture linear dependencies of the encoded patterns. Furthermore, it introduces machine-learned templates to enhance the performance of holographic image processing.**

***Keywords*-spin-wave, machine-learning, holography**

I. Introduction

Interest in unconventional neuromorphic hardware has surged in recent decade for several reasons. As the fundamental goal of neuromorphic computing is to emulate the brain's approach to perform computations, traditional CMOS-based devices, optimized primarily for Boolean logic operations, are limited in replicating the brain's parallel, analog, and energy-efficient mechanisms [1].

Various physical phenomena have been examined to develop a hardware, capable of efficiently performing such computations. One promising approach is to utilize wave interference. In wave-based systems, each point can interact with every other point of the medium, realizing complex interconnections directly through the physics of the wave propagation, making wave interference an efficient candidate for neuromorphic computing tasks.

The optical implementation of neuromorphic computing is not a novel concept, initial studies in this area appeared during the early stage of neuromorphic research [2]. However, despite the promising results of optical interference based computing, a central challenge of the field is that optical wave propagation is linear, thus passive optical systems does not containing nonlinearity. Neural networks rely strongly on nonlinear activation functions to model complex, nontrivial patterns in the data. However, light waves propagate linearly through conventional optical media, making it difficult to implement the nonlinear transformations that would be a key feature for neuromorphic computations.

Spin-wave interference–based computing has the potential to overcome this challenge. Unlike light, spin-waves can exhibit intrinsic nonlinear behavior, enabling the implementation of nonlinear operations without the need for complex external components. This opens the door to more compact, energy-efficient neuromorphic systems capable of performing both linear and nonlinear operations within the same medium. Papp et al. (2021) [4] published a theoretical study, in which they used an inverse-designed nonlinear spin-wave scatterer to perform vowel recognition. Using their system, they achieved over 90% classification accuracy on 44 vowel sounds from 3 classes. In Kiechle et. al. [5], we designed and experimentally demonstrated a system able to separate two wavelength. In this work, the magnonic index of refraction was modified by Focused Ion Beam Irradiation (FIB) instead of permanent magnets[6], allowed us greater resolution, and more precise control on the magnetic parameters of the YIG.

II. Methods

To gain a deeper understanding of the behavior of spin-wave–based systems, it is useful to draw parallels with optical holography. To simulate the optical phenomena, a two-dimensional finite element discretization was applied based on the Huygens–Fresnel principle:

$$U(P) = -\frac{i}{\lambda} U(r_0) \int_S \frac{e^{ikr}}{r} K(\chi) dS$$

To simulate the magnonic domain, we employed our custom micromagnetic solver, SpinTorch, which numerically solves the Landau–Lifshitz–Gilbert equation:

$$\frac{\partial \vec{\mathbf{M}}}{\partial t} = \overrightarrow{\gamma}_{LL} \frac{1}{1+\alpha^2} (\vec{\mathbf{M}} \times \vec{\mathbf{B}}_{eff} + \frac{\alpha}{M_{sat}} (\vec{\mathbf{M}} \times (\vec{\mathbf{M}} \times \vec{\mathbf{B}}_{eff})))$$

Acknowledgements

The financial funding from M&MEMS project, funded by the EU under the Horizon Europe program (contract number: 101070536), and from MILAB project (RRF-2.3.1-21-2022-00004) is gratefully acknowledged.

References

[1] Markovic, Danijela, Alice Mizrahi, Damien Querlioz, and Julie Grollier. "Physics for neuromorphic computing." Nature Reviews Physics (2020): 1-12.

[2] Fu, T., Zhang, J., Sun, R., Huang, Y., Xu, W., Yang, S., Zhu, Z. and Chen, H., 2024. Optical neural networks: progress and challenges. Light: Science & Applications, 13(1), p.263.

[3] Lin, X., Rivenson, Y., Yardimci, N.T., Veli, M., Luo, Y., Jarrahi, M. and Ozcan, A., 2018. All-optical machine learning using diffractive deep neural networks. Science, 361(6406), pp.1004-1008.

[4] Papp, Á., Porod, W. and Csaba, G., 2021. Nanoscale neural network using non-linear spin-wave interference. Nature communications, 12(1), p.6422.

[5] Kiechle, M., Papp, A., Maucha, L., Mendisch, S., Greil, J., Ahrens, V., Csaba, G. and Becherer, M., 2023, May. Frequency Demultiplexing of Spin Waves by Inverse-designed Magnetization Patterns, Experimentally Realized by FIB Irradiation. In 2023 IEEE International Magnetic Conference-Short Papers (INTERMAG Short Papers) (pp. 1-2). IEEE.

[6] Kiechle, M., Papp, A., Mendisch, S., Ahrens, V., Golibrzuch, M., Bernstein, G.H., Porod, W., Csaba, G. and Becherer, M., 2023. Spin-Wave Optics in YIG Realized by Ion-Beam Irradiation. Small, 19(21), p.2207293.

L. MAUCHA, "Spin-wave holography for image processing" in *PhD Proceedings – Annual Issues of the Doctoral School, Faculty of Information Technology and Bionics, Pázmány Péter Catholic University – 2025.* G. Prószéky, G. Szederkényi Eds. Budapest: Pázmány University ePress, 2025, pp. 61–61.

Pattern classification using competitive oscillator networks

Mitra MOAYED
(Supervisor: György CSABA)
Pázmány Péter Catholic University, Faculty of Information Technology and Bionics
50/a Práter street, 1083 Budapest, Hungary
Mitra.moayed@itk.ppke.hu

***Abstract*—Oscillatory Neural Networks (ONNs) provide a compelling neuromorphic computing approach, leveraging phase relationships of coupled oscillators for low-power, parallel processing. This study investigates a phase-based binary classification model using a single-layer, fully connected ONN to recognize real-world image patterns. The input dataset comprises two distinct 9x9 binary patterns derived from real-world sources, preprocessed into binary vectors and trained via Hebbian learning. Network dynamics, modeled through differential equations, ensure robust pattern recognition via phase synchronization. By optimizing frequency and simulation time, the model generates clear sinusoidal waveforms, validating strong oscillator alignment. Experiments on real-world datasets achieve an exceptional 99% accuracy on test sets. Drawing inspiration from oscillatory Hopfield networks, this work highlights the potential of ONNs for scalable and energy-efficient pattern recognition. The findings position ONNs as ideal for edge computing applications, and pave the way for future research into multi-layer ONN architectures and advanced real-world classification tasks, enhancing their applicability in low-power AI systems.**

***Keywords*—-Classification by ONN, ONN, oscillatory neural networks, oscillator-based computing, VO_2.**

I. Discussion

This study employs a single-layer ONN with VO_2 oscillators to achieve up to 99.66% accuracy in binary classification of 9x9 motion gesture patterns, such as swipe up,swipe right and circle. The network's dynamics are governed by the Kuramoto model, where the phase ϕ_i of each oscillator evolves according to:

$$\frac{d\phi_i}{dt} = 2\pi f + \sum_{j=1}^{n} C_{ij} \sin(\phi_j - \phi_i) \tag{1}$$

Here, f is the uniform natural frequency, and C_{ij} represents the coupling strength between oscillators i and j. The phase differences between oscillators, critical for classification, initially scatter but converge to stable states (e.g., in-phase or anti-phase locking) over time, as visualized in phase difference plots for the 81-oscillator network [1]. figure 1-a show phases aligning horizontally with time, indicating robust pattern recognition driven by Hebbian learning [2]. The synaptic weights C_{ij} are updated using:

$$C_{ij} = \frac{1}{N} \sum_{\mu=1}^{P} \xi_i^\mu \xi_j^\mu \tag{2}$$

where ξ_i^μ and ξ_j^μ are the activities of oscillators i and j for pattern μ, and P is the number of patterns. These equations enable synchronization, mapping input patterns to stable attractors, though complex inputs may extend convergence time. Figure 1-b illustrates the ONN architecture as a Hopfield Neural Network, showing a fully connected network of 81 oscillators, each mapped to a pixel in a 9x9 grid. Nodes represent VO_2 oscillators, and edges denote synaptic weights, capturing the parallel processing that drives energy-efficient computation. The low power consumption of VO_2 oscillators enhances suitability for edge computing [3]. However, the 9x9 resolution limits scalability. Future work should test hardware VO_2 prototypes and multi-class tasks to enhance adaptability, mimicking biological systems.

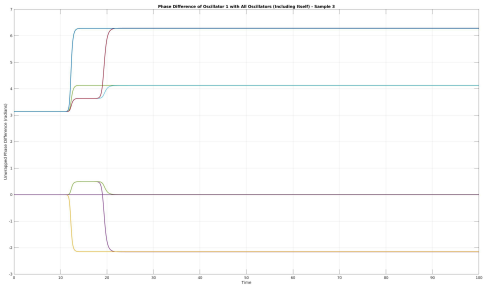

(a) Phase differences model with Hebbian learning rule (81 oscillators)

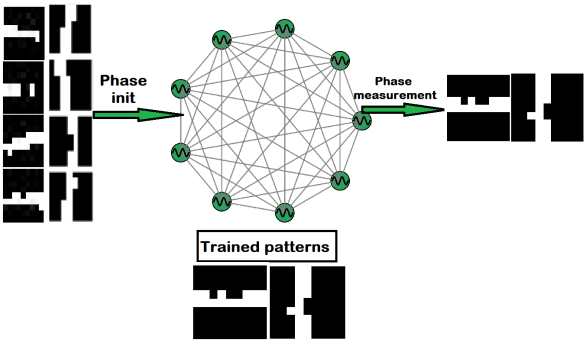

(b) ONN architecture as Hopfield Network

Fig. 1: Network dynamics and architecture. (a) Phase synchronization patterns. (b) Network topology representation.

References

[1] Kuramoto, Y. (1975). Self-entrainment of a population of coupled non-linear oscillators. In: Araki, H. (eds) International Symposium on Mathematical Problems in Theoretical Physics. Lecture Notes in Physics, vol 39. Springer, Berlin, Heidelberg. https://doi.org/10.1007/BFb0013365

[2] J. Hopfield, "Neural networks and physical systems with emergent collective computational abilities," Proceedings of the National Academy of Sciences of the United States of America, vol. 79, pp. 2554–8, 05 1982.

[3] Maffezzoni, P., Daniel, L., Shukla, N., Datta, S., and Raychowdhury, A. (2015). Modeling and simulation of vanadium dioxide relaxation oscillators. IEEE Trans. Circuits Syst. I Regul. Pap. 62, 2207–2215. doi: 10.1109/TCSI.2015. 2452332

M. MOAYED, "Pattern classification using competitive oscillator networks" in *PhD Proceedings – Annual Issues of the Doctoral School, Faculty of Information Technology and Bionics, Pázmány Péter Catholic University – 2025.* G. Prószéky, G. Szederkényi Eds. Budapest: Pázmány University ePress, 2025, pp. 62–62.

PROGRAM 4
HUMAN LANGUAGE TECHNOLOGIES, ARTIFICIAL UNDERSTANDING, TELEPRESENCE, COMMUNICATION

Head: Gábor PRÓSZÉKY

Handshape control in diffusion models for sign language synthesis

Zsolt ROBOTKA
(Supervisors: György CSEREY, Ádám RÁK)
Pázmány Péter Catholic University, Faculty of Information Technology and Bionics
50/a Práter street, 1083 Budapest, Hungary
robotka.zsolt@itk.ppke.hu

***Abstract*—Sign language synthesis requires precise handshapes that carry critical linguistic information. While diffusion models have revolutionized image generation, accurately rendering sign language hand configurations remains challenging. We investigate how region-specific conditioning enhances handshape fidelity in diffusion-based synthesis. Our experiments show that our optimal triple-controller configuration achieves significantly higher acceptance rates than conventional approaches. Our findings provide practical guidance for implementing diffusion-based sign language synthesis with improved handshape fidelity.**

***Keywords*-Diffusion Model, Sign Language, ControlNet**

I. Introduction

Sign language production is crucial for Deaf accessibility, as text-based content creates comprehension barriers [1]. Synthetic sign language videos address this need by providing content in the natural language of Deaf users. Sign language synthesis typically follows a pipeline from text to gloss notation, then to skeletal poses, and finally to visual representation. The final Pose-to-Sign (P2S) stage is challenging due to the importance of precise hand articulations in conveying linguistic meaning. Recent diffusion models [2] offer promising approaches for image generation but still struggle with the accurate rendering of handshapes required for sign language.

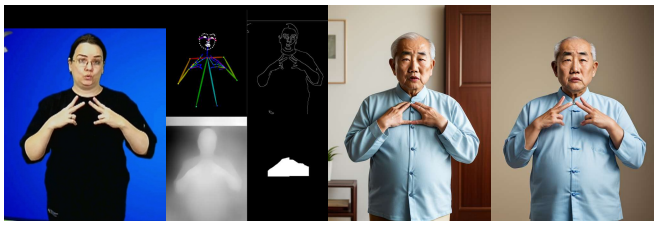

Conditioning Input Image | Extracted Features | Pose-conditioned Output | Multi-conditioned Output

Fig. 1. Pose-only versus multi-controller conditioning for sign language image synthesis. This visual comparison demonstrates how our region-specific multi-conditioning approach achieves superior hand shape fidelity.

II. Methods

We investigate how region-specific conditioning enhances handshape fidelity in diffusion-based sign language synthesis using Stable Diffusion 1.5 [2] with the Cyberrealistic checkpoint. Our approach implements three parallel ControlNet modules [3]: unmasked OpenPose for global constraints, masked edge detection for hand morphology, and masked depth estimation for spatial hand configuration. For evaluation, we used MediaPipe hand landmark detection to calculate RMSE between keypoints in generated and ground truth images, while manual evaluation assessed photorealism, anatomical correctness, and handshape reproduction.

TABLE I
Performance of different ControlNet configurations. P = Pose, D_m = Masked Depth, E_m = Masked Edge; RMSE = HandPose metric, Valid = HandPose valid rate, Accept = Manual acceptance rate.

P	D_m	E_m	RMSE	Valid	Accept
✓			119.30	0.00	0.00
	✓		26.71	0.11	0.02
		✓	**20.78**	**0.43**	**0.15**
✓	✓		37.60	0.18	0.04
✓		✓	22.29	0.49	**0.38**
	✓	✓	**14.34**	**0.54**	0.26
✓	✓	✓	**8.58**	**0.67**	**0.63**

III. Results and Conclusion

We evaluated various controller combinations for sign language image generation, as shown in Table I. The optimal triple-controller configuration achieved (63%) acceptance rate while the baseline pose-only method produced no acceptable outputs, highlighting the limitations of conventional approaches for sign language imagery.

Combining global pose conditioning with targeted edge and depth masking significantly improves handshape fidelity in diffusion-based sign language synthesis. Future work should focus on extending these techniques to video generation and fine-tuning models on sign language datasets.

References

[1] S. Qi et al., "The Role of Phonological Awareness in Reading Comprehension of Deaf and Hard-of-Hearing Children," Journal of Deaf Studies and Deaf Education, 2012.
[2] R. Rombach et al., "High-Resolution Image Synthesis with Latent Diffusion Models," CVPR, 2022.
[3] L. Zhang et al., "Adding Conditional Control to Text-to-Image Diffusion Models," ICCV, 2023.

Zs. ROBOTKA, "Handshape control in diffusion models for sign language synthesis" in *PhD Proceedings – Annual Issues of the Doctoral School, Faculty of Information Technology and Bionics, Pázmány Péter Catholic University – 2025.* G. Prószéky, G. Szederkényi Eds. Budapest: Pázmány University ePress, 2025, pp. 64–64.

PROGRAM 5
ON-BOARD ADVANCED DRIVER ASSISTANCE SYSTEMS

Head: Ákos ZARÁNDY

Extrinsic calibration of multi-modal sensor systems using deep learning

Marcell KÉGL
(Supervisor: Csaba BENEDEK)
Pázmány Péter Catholic University, Faculty of Information Technology and Bionics
50/a Práter street, 1083 Budapest, Hungary
kegl.marcell@itk.ppke.hu

I. Introduction

Modern autonomous systems rely heavily on multi-sensor setups to understand their surroundings accurately and robustly. Cameras, lidars, and radars are among the most widely used sensors, each contributing distinct advantages: cameras capture rich visual detail, lidars provide precise 3D geometry, and radars offer resilience in adverse weather conditions and the ability to measure motion through Doppler data [1]. However, to successfully merge information from these diverse modalities, one must precisely determine the spatial relationships—i.e., the extrinsic parameters—between the sensors.

While traditional target based calibration techniques employ physical targets or markers, these methods can be impractical in dynamic or unstructured environments and may require laborious setup procedures. Consequently, automated targetless calibration methods that do not rely on such targets are gaining importance [2]. Among them, deep learning (DL)-based approaches are particularly promising for their ability to infer complex spatial relationships directly from raw sensor data [3]. Still, accurate calibration—especially involving radar—remains challenging due to its sparse and noisy output, limited spatial resolution, and lack of shared features with vision sensors [4].

In this work, we address the problem of targetless extrinsic calibration involving camera, lidar, and 3D radar sensors. Our approach is designed to generalize across a variety of operating conditions, including both rigid and non-rigid sensor platforms, without the need for manual intervention or handcrafted feature engineering.

II. The proposed method

We propose a novel deep learning framework, for end-to-end extrinsic calibration involving camera, lidar, and radar. The model processes synchronized data from all three sensors and learns to predict the six-degree-of-freedom transformation between them. By projecting radar and lidar point clouds into the depth domain using an equirectangular projection, the network aligns them more effectively with the camera view, since information from the whole point cloud input is considered regardless the large difference in the field of view of the sensor modalities. Feature representations are extracted using modality-specific encoders, fused into a shared latent space, and passed through a regression head to estimate translations and rotations. To improve robustness and consistency, we introduce a joint loop closure loss that enforces alignment across all sensor pairs. Our network also incorporates auxiliary radar information—such as Doppler velocity and RCS—alongside depth cues from monocular images. For rigid sensor setups, a multi-frame variant further enhances accuracy by leveraging temporal consistency. Extensive evaluation on the VoD dataset [1] shows that our approach significantly outperforms state-of-the-art methods, reducing camera - radar calibration errors by more than 50%. An overview of our proposed calibration pipeline is depicted in Figure 1.

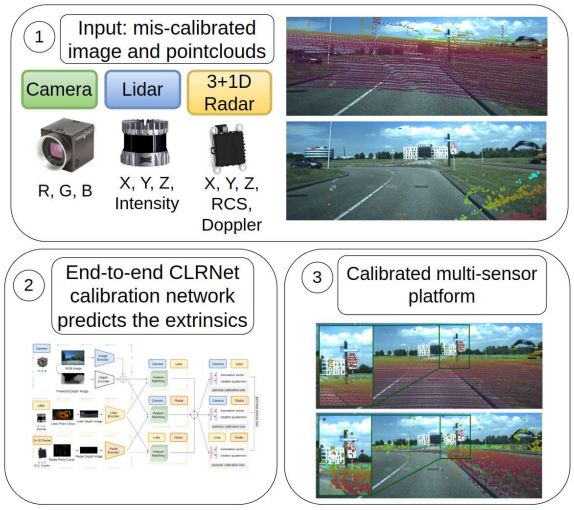

Fig. 1. The proposed work is about the extrinsic calibration of 3 different perception based sensor modalities. The Deep Neural Network get mis-calibrated inputs (data with improper extrinsics) and the end-to-end network predicts the true extrinsic parameters.

References

[1] A. Palffy, E. Pool, S. Baratam, J. F. P. Kooij, and D. M. Gavrila, "Multi-class road user detection with 3+1D radar in the View-of-Delft dataset," *IEEE Robotics and Automation Letters*, vol. 7, no. 2, pp. 4961–4968, 2022.

[2] P. An, J. Ding, S. Quan, J. Yang, Y. Yang, Q. Liu, and J. Ma, "Survey of extrinsic calibration on LiDAR-camera system for intelligent vehicle: Challenges, approaches, and trends," *IEEE Trans. on Intelligent Transportation Systems*, vol. 25, no. 11, pp. 15342–15366, 2024.

[3] X. Lv, B. Wang, Z. Dou, D. Ye, and S. Wang, "LCCNet: LiDAR and Camera Self-Calibration using Cost Volume Network," in *IEEE/CVF Conference on Computer Vision and Pattern Recognition Workshops (CVPRW)*, pp. 2888–2895, 2021.

[4] C. Schöller, M. Schnettler, A. Krämmer, G. Hinz, M. Bakovic, M. Güzet, and A. Knoll, "Targetless rotational auto-calibration of radar and camera for intelligent transportation systems," in *IEEE Intelligent Transport. Systems Conference (ITSC)*, pp. 3934–3941, 2019.

M. KÉGL, "Extrinsic calibration of multi-modal sensor systems using deep learning" in *PhD Proceedings – Annual Issues of the Doctoral School, Faculty of Information Technology and Bionics, Pázmány Péter Catholic University – 2025.* G. Prószéky, G. Szederkényi Eds. Budapest: Pázmány University ePress, 2025, pp. 66–66.

Wireless virtual sensor data acquisition from a UAV digital twin

Viktor KÖRTVÉLYESI
(Supervisors: Antal HIBA, Ákos ZARÁNDY)
Pázmány Péter Catholic University, Faculty of Information Technology and Bionics
50/a Práter street, 1083 Budapest, Hungary
kortvelyesi.viktor@itk.ppke.hu

***Abstract*—Due to their operational efficiency and versatility, UAVs are increasingly integrated into routine workflows across diverse industrial sectors. However, their onboard computational capacity remains limited, making it practical to offload complex processing tasks to high-performance cloud infrastructures. This study explores scalable solutions for remote data processing and management using cloud computing and containerized environments.**

***Keywords*-UAV simulation, cloud computing, validation, wireless network**

I. Introduction

Testing in aviation is both costly and dangerous, this implies the development of simulation-based techniques for validating onboard hardware and software systems. One such method is Vehicle-in-the-Loop (VIL) [1], where the UAV executes real physical movements while simulated sensor data replaces actual mission sensor inputs. Given the limitations in UAV payload and processing capacity, the simulation environment is hosted on a high-performance cloud server. To mitigate the effects of communication latency, the digital twin is temporally advanced using predictive estimation of the UAV's future position and orientation.

II. Cloud and docker

Containerization has become a foundational technology in recent years for the development and deployment of modern applications. Docker, one of the most widely adopted containerization platforms, enables the encapsulation of applications along with their runtime environment, dependencies, and configurations into portable, self-contained units. This approach eliminates inconsistencies across development, testing, and production environments, ensuring reproducible behavior regardless of the underlying infrastructure.

One of the key advantages of containerization is the ability to execute different system components independently, while enabling standardized network communication between them. This architecture facilitates the simulation of interactions between the Carla [2] simulation and a remote drone within a local environment. Through Docker-based containerization, each component of the system operates in isolated containers, communicating via standard network protocols such as TCP and UDP. These connections are established over Docker's virtual network, internal to the host machine. However, certain real-world conditions cannot be fully replicated in this local setup. Network latency is negligible in a local environment, whereas in real deployments, latency can significantly impact real-time performance. On the other hand, data loss does not occur locally, while in actual wireless communication scenarios packet loss is a common issue that can affect system reliability.

These limitations underscore the need for further validation under real-world network conditions to ensure robust system performance.

References

[1] T. Bock, M. Maurer, and G. Farber, "Validation of the vehicle in the loop (VIL); a milestone for the simulation of driver assistance systems," pp. 612 – 617, 07 2007.

[2] A. Dosovitskiy, G. Ros, F. Codevilla, A. Lopez, and V. Koltun, "CARLA: An open urban driving simulator," in *Proceedings of the 1st Annual Conference on Robot Learning*, pp. 1–16, 2017.

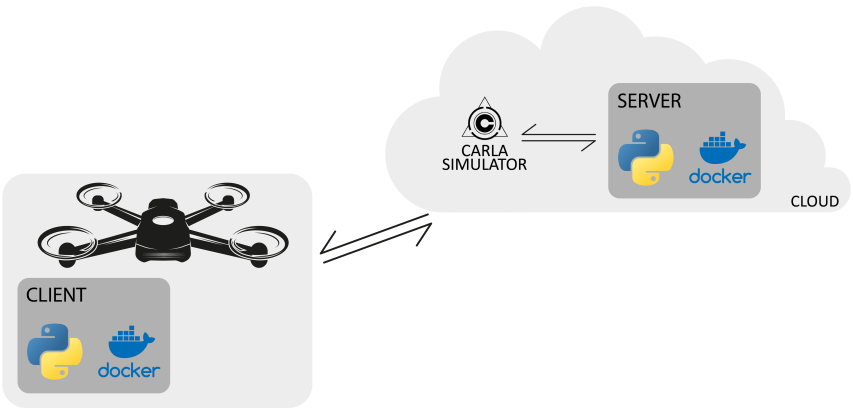

Fig. 1. Vehicle-in-the-loop test setup. A docker container runs onboard in connection with the cloud container and the simulation.

V. KÖRTVÉLYESI, "Wireless virtual sensor data acquisition from a UAV digital twin" in *PhD Proceedings – Annual Issues of the Doctoral School, Faculty of Information Technology and Bionics, Pázmány Péter Catholic University – 2025.* G. Prószéky, G. Szederkényi Eds. Budapest: Pázmány University ePress, 2025, pp. 67–67.

PCD-VAE: a point-cloud variational auto-encoder

József KÖVENDI
(Supervisor: Csaba BENEDEK)
Pázmány Péter Catholic University, Faculty of Information Technology and Bionics
50/a Práter street, 1083 Budapest, Hungary
kovendi.jozsef@itk.ppke.hu

***Abstract*—Generative modeling of uniquely structured set data, such as point clouds, requires capturing local and global geometric features. Utilization of multi-scale frameworks which are based on ordinary, grid-structured structured data is nontrivial. Feature extraction from set-structure demands a process that considers both local and global geometric signatures while accounting for the lack of structure. Motivated by recent progress in irregular and unordered set-encoding we built PCD-VAE, a Point-Cloud Variational Auto-Encoder based on attention and convolution that processes the input set derived from geometric localities within the spatial and the latent domain. Exploiting these modules our generative model learns a smaller, latent representation of the input point cloud. We evaluate our model on point cloud generation tasks and achieve competitive results.**

***Keywords*-Point cloud, variational auto-encoder, deep learning, generative neural network**

I. Introduction

Point clouds are a key 3D shape representation due to their direct acquisition from laser scans, versatility as mesh components, and ease of manipulation via affine transformations. These advantages make them essential in real-world applications like SLAM [1], object detection, building and terrain digitization, and immersive technologies such as AR, VR, XR, and MR. Recently, generative models for set-structured data like point clouds have gained traction in fields from robotics to healthcare . Unlike 2D images with grid-like pixel arrangements, 3D point clouds are unstructured, making conventional CNN-based feature extraction challenging. Given the cost and complexity of acquiring 3D data, there is a strong need for efficient architectures tailored to point cloud generation.

II. Proposed Method

We propose PCD-VAE (Figure 1), which builds on bidirectional inference [2], combining a bottom-up encoder with a top-down generator in a shared hierarchical framework. The encoder merges bottom-up features from input data with top-down priors to form the approximate posterior. It leverages PointConv for capturing local geometry and Induced Set Attention Blocks (ISAB) for modeling global context, enabling effective extraction of both local and global features during encoding.

III. Results

We quantitatively evaluate our model on the ShapeNet airplane category, outperforming previous state-of-the-art methods, as shown in Table I.

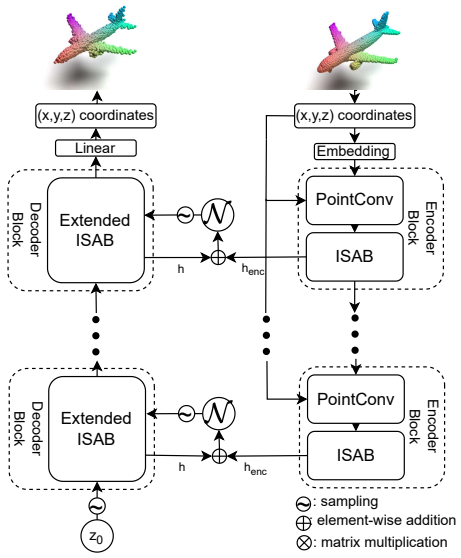

Fig. 1: PCD-VAE network with bidirectional architecture. The right side is the bottom-up encoder and the left side is the top-down decoder

Category	Method	1-NNA(%, → 50%) CD	EMD
Airplane	r-GAN	93.58	99.51
	l-GAN(CD)	86.30	97.28
	l-GAN(EMD)	87.65	**85.68**
	PC-GAN	94.35	92.32
	PCD-VAE (ours)	**81.23**	87.28

TABLE I: Generation results. The closer to 50% the better. Best scores are highlighted in **bold**.

Acknowledgements

The research presented in this paper was supported by the Artificial Intelligence National Laboratory (RRF-2.3.1-21-2022-00004) programs and by the OTKA #143274 project of the Hungarian NRDI Office.

References

[1] Hegde, Deepti, et al. "Relocalization of camera in a 3d map on memory restricted devices." Computer Vision, Pattern Recognition, Image Processing, and Graphics: 7th National Conference, NCVPRIPG 2019, Hubballi, India, December 22–24, 2019, Revised Selected Papers 7. Springer Singapore, 2020.

[2] Vahdat, Arash, and Jan Kautz. "NVAE: A deep hierarchical variational autoencoder." Advances in neural information processing systems 33 (2020): 19667-19679.

J. KÖVENDI, "PCD-VAE: a point-cloud variational auto-encoder" in *PhD Proceedings – Annual Issues of the Doctoral School, Faculty of Information Technology and Bionics, Pázmány Péter Catholic University – 2025.* G. Prószéky, G. Szederkényi Eds. Budapest: Pázmány University ePress, 2025, pp. 68–68.

Environment interpretation from Lidar point clouds

Balázs PÁLFFY
(Supervisor: Csaba BENEDEK)
Pázmány Péter Catholic University, Faculty of Information Technology and Bionics
50/a Práter street, 1083 Budapest, Hungary
palffy.balazs.1@itk.ppke.hu

***Abstract*—Perception systems for robots and vehicles must balance performance with cost, often relying on affordable Lidars that produce sparse data. To address this, MV-DepthFormer is proposed, a single-frame depth completion method for dynamic environments. It reconstructs dense, accurate depth maps from sparse point clouds using a multi-view transformer that processes both camera and bird's-eye views. To align these views, the Linking Map was introduced, a module that enables unified multi-view representation and improves depth estimation. MV-DepthFormer is pre-trained on synthetic data and fine-tuned on real-world datasets for better generalization. Experiments show it outperforms state-of-the-art methods in depth accuracy, point cloud quality, and perceptual similarity.**

I. Introduction

Lidars are highly accurate sensors used in fields like robotics, autonomous driving and 3D mapping. They vary in cost from thousands to hundreds of thousands of dollars. Despite their accuracy, Lidars produce sparse depth maps compared to RGB cameras which affects the efficiency of subsequent algorithms. To address these challenges, purely lidar-based, single-frame depth completion method is proposed tailored for low-cost sensors. The transformer-based network, MV-DepthFormer, uses a dual-branch architecture: one branch processes 2D camera-view data with encoded 3D coordinates, while the other operates in the bird's-eye view using a pillar-based grid. A novel Linking map module aligns these views, enabling an accurate multi-view depth representation. An overview is shown in Figure 1.

II. Proposed method

The approach is pre-trained on synthetic data and fine-tuned on real-world lidar data to improve generalization. The model is tested on both datasets and benchmarked against several state-of-the-art lidar-only methods [1], [2], showing that *MV-DepthFormer* achieves top performance.

- *MV-DepthFormer*, a transformer-based depth completion model is introduced that processes sparse lidar in both camera and bird's-eye views. A novel Linking map module aligns these views via pixel-to-pillar mapping.
- Extensive experiments on a synthetic multi-sensor dataset [3] and the real-world HeLiPR [4] dataset were conducted, demonstrating superior accuracy and robustness over existing methods.

III. Conclusion

With the proposed lidar-based, single-frame, depth image completion method was able to complete incoming lidar data, achieving accurate and dense depth images as output. The model is able to outperform the baseline methods as presented in Table I.

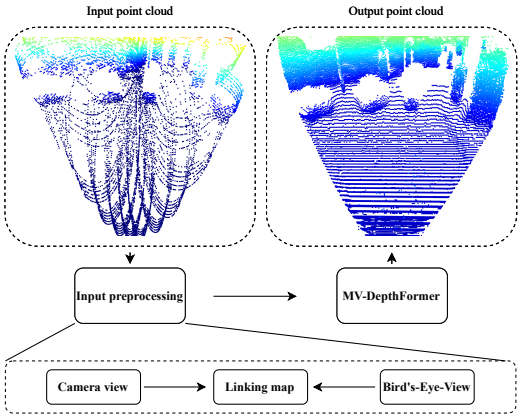

Fig. 1. Overview of the proposed method. The sparse input point cloud is projected onto both the camera view and Bird's-Eye-View to generate complementary, orthogonal representations. The Linking map ensures precise alignment between these perspectives. The high-resolution and accurate depth image output of *MV-DepthFormer* is visualized as reconstructed point cloud.

TABLE I
Results for the Synthetic and Real-life datasets. Let S stand for pre-trained on Synthetic dataset.

	Method	RMSE	MAE	CD	LPIPS	FID
Synthetic		Livox Avia				
	St-DepthNet [1]	7.57	1.81	1.22	0.27	2.82
	Tulip [2]	7.09	1.43	**0.42**	0.25	1.40
	MV-DepthFormer	**6.85**	**1.30**	**0.42**	**0.19**	**1.31**
HeLiPR		Livox Avia				
	St-DepthNet [1]	11.10	2.27	3.05	0.15	4.53
	Tulip [2]	10.58	2.56	2.12	0.14	1.95
	MV-DepthFormer	8.05	1.86	1.07	0.14	1.82
	MV-DepthFormer (S)	**6.38**	**1.18**	**0.95**	**0.12**	**1.67**

IV. Acknowledgements

The author is grateful to HUN-REN SZTAKI, particularly to Csaba Benedek for the opportunity to work on this project.

References

[1] O. Zovathi, B. Palffy, Z. Janko, and C. Benedek, "ST-DepthNet: A Spatio-Temporal Deep Network for Depth Completion Using a Single Non-Repetitive Circular Scanning Lidar," *IEEE Robotics and Automation Letters*, pp. 3270–3277, 2023.

[2] B. Yang, P. Pfreundschuh, R. Siegwart, M. Hutter, P. Moghadam, and V. Patil, "TULIP: Transformer for Upsampling of LiDAR Point Clouds," in *Proceedings of the IEEE/CVF Conference on Computer Vision and Pattern Recognition*, 2024, pp. 15 354–15 364.

[3] A. Dosovitskiy, G. Ros, F. Codevilla, A. Lopez, and V. Koltun, "CARLA: An Open Urban Driving Simulator," in *Proceedings of the 1st Annual Conference on Robot Learning*, 2017, pp. 1–16.

[4] M. Jung, W. Yang, D. Lee, H. Gil, G. Kim, and A. Kim, "HeLiPR: Heterogeneous LiDAR dataset for inter-LiDAR place recognition under spatiotemporal variations," *The International Journal of Robotics Research*, vol. 43, no. 12, pp. 1867–1883, 2024.

B. PÁLFFY, "Environment interpretation from Lidar point clouds" in *PhD Proceedings – Annual Issues of the Doctoral School, Faculty of Information Technology and Bionics, Pázmány Péter Catholic University – 2025.* G. Prószéky, G. Szederkényi Eds. Budapest: Pázmány University ePress, 2025, pp. 69–69.

Image processing with attention mechanisms based on human vision and eye movements

Adrienn RÁCZ
(Supervisor: András HORVÁTH)
Pázmány Péter Catholic University, Faculty of Information Technology and Bionics
50/a Práter street, 1083 Budapest, Hungary
racz.adrienn@itk.ppke.hu

***Abstract*—Despite the complexity of human vision, the eye does not process an image in a single step. Instead, we perform rapid, small eye movements called saccades to scan the visual field. Recurrent neural networks and transformers which use attention mechanisms have achieved promising results when trying to create a neural network that processes images in a way similar to the human eye.**

***Keywords*-Human vision, attention mechanism, deep learning**

I. Introduction

The central fovea is the small part of the retina responsible for sharp central vision. To be able to see all relevant parts of the image sharply, we need to move this spot very rapidly with eye movements are called saccades.

When it comes to image processing with neural networks, the drawbacks of most methods have been high computational complexity, non-scalability and the need for a large amount of training data [1]. Non-convolutional models using self-attention and transformer networks have also been proposed and used for such tasks, with promising results [1][2].

II. Methods for image processing

Vaswani et al.[3] introduced the so-called Transformer network architecture to perform tasks in natural language processing and computer vision. To combat traditional models' finite memory, scaled dot-product self-attention was introduced to the Transformer architecture.

Each word is mapped to three different vectors: **Q**uery, **K**ey-**V**alue pairs. Then, out of these the attention score is computed, which depends on which words in a sentence are relevant to each other.

The use of the model has proven to significantly reduce training costs and the architecture has outperformed all previous models in the WMT 2014 English-to-German and English-to-French translation tasks.

Dosovitskiy et al.[1] have created the Vision Transformer (ViT), which applies the Transformer directly to images. These images are processed in smaller, linearly embedded, fix-sized patches analogous to word-tokens, with positional and class embeddings applied as well.

The inductive bias of the ViT is singificantly less than that of the convolutional networks and the scalability of the network has also proven to be excellent.

The considerable data requirement and the computational complexity are the main drawbacks of the model.

Kumari et al.[2] have experimented with neural networks that process images in a way similar to the human eye.

Their model has an attentional input (part of the image under an attentional window at multiple scales) and and an eye-position input (in the form of a heat map).

The architecture consists of the Classifier Network, the Saccade Network and the Eye-position Network. Their outputs are concatenated and processed to produce the next saccade and the class of the image.

Flip-flop neurons, Elman and Jordan connections serve as the recurrent elements of the model, providing both local and global connections.

The network outperformed state-of-the-art architectures in some cases (e.g. DenseNet's testing accuray is 99.39% for the Medical-MNIST dataset, ViT's 99.54%). The architecture usually needs less steps to correctly classify images and requires less computational resources than RAM.

As for saccadic patterns, most of the time, the attention window is either fixated on the eyes, nose or mouth and the model mostly draws conclusions from these parts of the images, as it can be seen in figure 1.

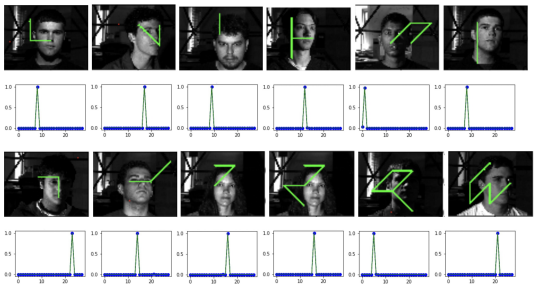

Figure 1. The movement of the attention window during classification (the green line shows the center of the window). The plot below shows the desired (blue) and predicted (green) probabilites for the classes [2].

References

[1] A. Dosovitskiy, L. Beyer, A. Kolesnikov, *et al.*, *An image is worth 16x16 words: Transformers for image recognition at scale*, 2021. arXiv: 2010.11929 [cs.CV]. [Online]. Available: https://arxiv.org/abs/2010.11929.

[2] S. Kumari and V. S. Chakravarthy, "Biologically inspired image classifier based on saccadic eye movement design for convolutional neural networks", *Neurocomputing*, vol. 513, pp. 294–317, 2022, ISSN: 0925-2312. DOI: https://doi.org/10.1016/j.neucom.2022.09.027. [Online]. Available: https://www.sciencedirect.com/science/article/pii/S0925231222011122.

[3] A. Vaswani, N. Shazeer, N. Parmar, *et al.*, "Attention is all you need", *CoRR*, vol. abs/1706.03762, 2017. arXiv: 1706.03762. [Online]. Available: http://arxiv.org/abs/1706.03762.

A. RÁCZ, "Image processing with attention mechanisms based on human vision and eye movements" in *PhD Proceedings – Annual Issues of the Doctoral School, Faculty of Information Technology and Bionics, Pázmány Péter Catholic University – 2025.* G. Prószéky, G. Szederkényi Eds. Budapest: Pázmány University ePress, 2025, pp. 70–70.

APPENDIX

PROGRAM 1: Bionics, Bio-inspired Wave Computers, Neuromorphic Models	
Name	**Supervisor**
Ákos ANTAL	Péter FÖLDESY DSc, Péter MIHAJLIK PhD
Zsófia BALOGH-LANTOS	Kristóf IVÁN PhD, Ágoston Csaba HORVÁTH PhD
Gréta Lilla BÁNYAI	Tamás GARAY PhD
Ramóna BIRÓ-KOVÁCS	Balázs LIGETI PhD, Zsolt ZSÓFI PhD
Eszter BIRTALAN	Miklós KOLLER PhD
Martin János BLAZSEK	Judit MAKARA PhD, Balázs Benedek UJFALUSSY PhD
Balázs Márk BÓDIS	Csaba BENEDEK PhD
Nikolett Kitti DOBOS	Tamás GARAY PhD
Nour ESSAM	Lucia WITTNER MD PhD
Fanni FARKAS	Zoltán GÁSPÁRI PhD
Gábor FARKAS	Szabolcs KÁLI PhD
Bendegúz FILYÓ	Balázs LIGETI PhD
Amelita FODOR	József LACZKÓ PhD
Bence Tamás GAIZER	Attila CSIKÁSZ-NAGY DSc, János JUHÁSZ PhD
Valentina GUARINO	Andrea CILIBERTO PhD
Borbála JAKAB	Zoltán GÁSPÁRI PhD
Máté KÁLOVICS	Kristóf IVÁN PhD, Zsolt SZABÓ DSc
Réka KISS	Miklós KOLLER PhD
Dorottya KOCSIS	Franciska VIDÁNÉ ERDŐ PhD
Szabolcs Cselgő KOVÁCS	Erzsébet FICHÓ PhD, István Zoltán REGULY PhD
Áron Boldizsár KÖVES	Miklós KOLLER PhD
Dániel KRIZSÁN	Balázs LIGETI PhD
Valentina MADÁR	Attila CSIKÁSZ-NAGY DSc
Vilmos MADARAS	Csaba BENEDEK PhD
Gyula MOLNÁR	Mihály KOVÁCS DSc, Gábor SZEDERKÉNYI DSc
Zsófia MOLNÁR	András HORVÁTH PhD
Kristóf MÜLLER	Miklós KOLLER PhD
Gábor NAGY	György CSEREY PhD, László GRAND PhD
Afrodité NÉMETH	Tamás GARAY PhD
Bence NÉMETH	András HORVÁTH PhD
Ábel PETIK	István ULBERT MD DSc, Dániel HILLIER PhD
Balázs RADELECZKI	József LACZKÓ PhD
Péter SZABÓ	György CSEREY PhD, Katalin CSIGÓ PhD
János SZALMA	Attila CSIKÁSZ-NAGY DSc, Erzsébet FICHÓ PhD
Giorgio TALLARICO	Andrea CILIBERTO PhD
Brigitta UNGVÁRI	György CSEREY PhD, Katalin CSIGÓ PhD
Mihály András VÁGHY	Mihály KOVÁCS DSc, Gábor SZEDERKÉNYI DSc
Soma VARGA	Bálint PÉTERFIA PhD
Levente VÍG	István ULBERT MD DSc
Áron WEBER	Attila CSIKÁSZ-NAGY DSc, Erzsébet FICHÓ PhD

PROGRAM 2: Computer Technology Based on Many-core Processor Chips, Virtual Cellular Computers, Sensory and Motoric Analog Computers	
Name	**Supervisor**
Lóránt Szabolcs DAUBNER	Kálmán TORNAI PhD, Tamás ZSEDROVITS PhD
Balázs DRÁVAI	István Zoltán REGULY PhD
Imre Gergely JÁNOKI	Péter FÖLDESY DSc
Rizal MAULANA	György CSEREY PhD
Dániel István NÉMETH	Kálmán TORNAI PhD
Katalin SCHÄFFER	Miklós KOLLER PhD
Dávid SOMOGYI	Gábor SZEDERKÉNYI DSc

PROGRAM 3: Feasibility of Electronic and Optical Devices, Molecular and Nanotechnologies, Nano-architectures, Nanobionic Diagnostic and Therapeutic Tools	
Name	**Supervisor**
Tamás István KOVÁCS	György CSABA PhD
Levente MAUCHA	György CSABA PhD, Ádám PAPP PhD
Mitra MOAYED	György CSABA PhD

PROGRAM 4: Human Language Technologies, Artificial Understanding, Telepresence, Communication	
Name	**Supervisor**
Zsolt ROBOTKA	György CSEREY PhD, Ádám RÁK PhD

PROGRAM 5: On-board Advanced Driver Assistance Systems	
Name	**Supervisor**
Marcell KÉGL	Csaba BENEDEK PhD
Viktor KÖRTVÉLYESI	Ákos ZARÁNDY DSc, Antal HIBA PhD
József KÖVENDI	Csaba BENEDEK PhD
Balázs PÁLFFY	Csaba BENEDEK PhD
Adrienn RÁCZ	András HORVÁTH PhD